Zeitschrift: IABSE reports = Rapports AIPC = IVBH Berichte
Band: 49 (1986)

Rubrik: Theme 2: Light-gauge metal construction and building systems

THEME 2

Light-Gauge Metal Construction and Building Systems

Chairmen:
T. Pekoz, USA, and P.O. Thomasson, Sweden

Leere Seite
Blank page
Page vide

Design of Cold-Formed Steel Purlins

Calcul et conception des pannes en acier formé à froid

Bemessung von Kaltprofilpfetten

J. Michael DAVIES
Prof. of Struct. Eng.
University of Salford
Salford, UK

Professor Davies obtained degrees of Ph.D. and D.Sc. from the University of Manchester for his research into structural steel design. He worked for five years for a firm of consulting engineers before returning to academia. He now specialises in cold-formed steel construction and acts as consultant to several companies.

Graham RAVEN
Techn. Manager
Ward Brothers (Sherburn) Ltd.
Sherburn, Malton, UK

Graham Raven graduated from King's College, London in 1963. After working for thirteen years for consulting engineers he specialised in developments in steel structures. His particular interests are computer-aided detailing and full scale testing of cold-formed and other slender steel structures and cladding.

SUMMARY

The alternative approaches to the design of light gauge steel purlins are reviewed and the reasons why the authors chose to design a new purlin system by testing are outlined. The test facility is described and it is shown how the test results were used as the basis for design expressions.

RÉSUMÉ

Les différentes variantes du calcul et du dimensionnement des pannes en acier formé à froid sont passées en revue. Les raisons pour lesquelles les auteurs ont choisi de concevoir un nouveau système de pannes au moyen d'essais sont soulignées. L'installation d'essais est décrite et il est montré comment les résultats d'essais ont été utilisés comme base des formules de dimensionnement.

ZUSAMMENFASSUNG

Es wird über verschiedene Ansätze zur Bemessung von Kaltprofilpfetten berichtet und begründet, warum die Verfasser für die Bemessung eines neuen Pfettensystems Versuche wählten. Die Versuchseinrichtung wird beschrieben und es wird gezeigt, wie die Versuchsergebnisse für die Bemessung verwendet werden.

1. INTRODUCTION

1.1 Purlin Cross-sections

In the U.K., cold-formed purlins and side rails usually have one of the cross-sections shown in Fig. 1. The conventional lipped Zed (a) has the disadvantage that the principal axis is inclined at about 17^{o} to the web giving rise to significant biaxial bending. The Zeta section (b) is a development which reduces this inclination to about 7^{o} so that on typical roof slopes the principal axis is near vertical. A lipped channel (c) has its shear centre outside the section so that load applied through the flange causes torsion as well as bending. Multibeam, (d) and (e), has a much more favourable position of the shear centre and the additional folds in the web improve its stability. Multibeam MK1 (d) is a well-established profile that has been used for many years. This paper describes some of the considerations which arose during the development of Multibeam MK2 which represents a considerable improvement in terms of performance as well as a more adaptable shape. This development will be described in terms of purlins although the procedures used are equally applicable to side rails and Multibeam MK2 is used for both purposes.

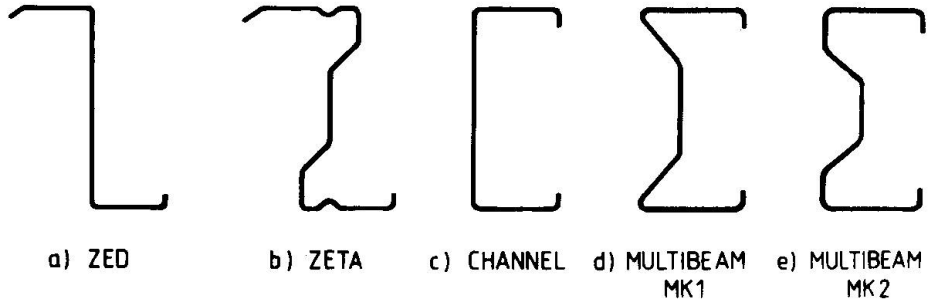

Fig. 1 Typical purlin sections

1.2 Purlin Systems

The above sections are used in the following purlin systems:

- Simple system: double span purlins with single spans in the end bays as necessary.
- Sleeved system: splicing members formed from short lengths of cold formed section at the internal supports provide semi-continuity.
- Overlap system: purlins are overlapped over the internal supports to provide full continuity together with reinforcement in the regions of maximum bending moment.

Despite the theoretical advantages of sleeved and overlap systems for longer spans, simple systems are widely used, particularly for the most common frame spacings of between 6 and 7 metres.

1.3 Design Procedures

Design procedures must take into account the following factors:

- The usual problems of unsymmetrical thin-walled sections, e.g. torsion, biaxial bending, local and lateral-torsional buckling, restrained warping.
- Restraint from the cladding, bearing in mind that the three major types of roof sheeting (namely, profiled steel or aluminium; asbestos cement and its substitutes; standing seam) all require

different treatment and that the behaviour can be further influenced by over-purlin insulation. It should also be noted that the downward load case, where the cladding restrains the compression flange in the span, is fundamentally different from the upward load (wind suction) case when the compression flange is largely unrestrained.

- The influence of anti-sag bars or other restraints within the span.
- The performance of simple systems using two-span purlins is considerably enhanced if advantage is taken of the redistribution of bending moments after first yield at the internal supports. The moment-rotation characteristics of "plastic hinges" forming over the centre supports is critically dependent on the section shape and the cleat detail.
- The moment-rotation characteristic of a sleeve must be determined experimentally.

There are four possible approaches to the design of a purlin system:

- Design by calculation using conventional code of practice procedures for unrestrained light gauge steel beams [1,2,3]. This implies elastic analysis and the neglect of any restraint from the cladding for the wind uplift case.
- Empirical design using safe approximate procedures as given for Zed purlins in many codes of practice e.g. [1,2,3]. This results in rather uneconomical designs.
- Design by calculation using specially derived procedures which take account of the stabilising influence of the cladding. There have been significant developments in recent years and some of these are reviewed in more detail in section 2.
- Design by testing which is the only way to take into account all of the factors listed above.

Design by testing was the authors' choice for the development of the Multi-beam MK2 system shown in Fig. 1(d) because it provided the maximum possible economy for a given level of safety. Testing is, of course, relatively expensive but this was considered to be justified bearing in mind that a system was being developed for a projected production of about 2½ million metres per year for several years. Furthermore, by means of testing economic design can be extended to include systems for which theoretical methods are not currently available.

2. DESIGN BY CALCULATION

A number of simplified analytical approaches are available for the design of purlins restrained by roof sheeting although at the time of writing their relative merits and limits of applicability are not completely clear. These methods are all concerned solely with elastic behaviour and generally concentrate on the more problematical load case of wind uplift. Typically, the part of the cross-section in compression is considered as a column or beam-column restrained by an elastic spring where the spring represents rotational restraint from the sheeting together with an allowance for distortion of the cross-section as shown in Fig. 2. The value of the spring constant varies according to the particular purlin section, sheeting profile and fastener used and is probably best obtained from a simple test as shown in Fig. 3 although it may also be calculated.

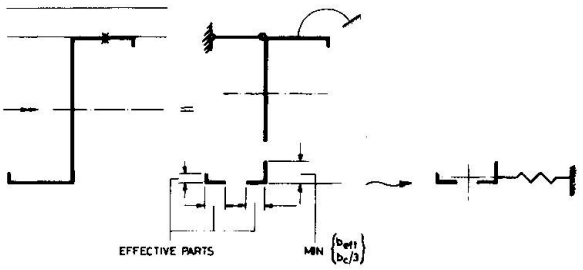

Fig. 2 Equivalent column on an elastic foundation.

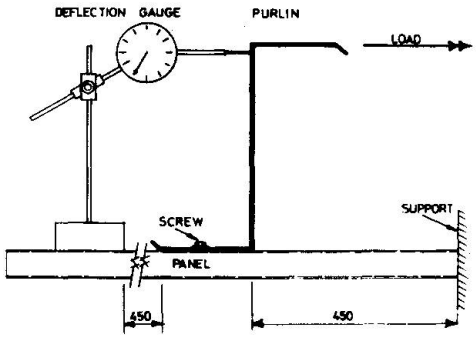

Fig. 3 Simple test for value of spring constant.

A calculation method for Z purlins with lips which is based on an equivalent column on an elastic foundation is included in the draft European Recommendations for the design of light gauge steel members [2]. This method was originally given by Sokol and is based on a calculation of the bifurcation load. It is therefore only strictly valid for sections with an axis of symmetry but appears to give good results for point-symmetrical Z sections. Pekoz and Soroushian [4] have given a procedure for both C and Z purlins which is based on a beam-column model. Thus, twisting of the section is included at all load levels and is not dependent on imperfections. They also include comparison with some test results. Schardt [5] has also described a calculation for Z purlins based on a beam-column assumption. This method is a development of the Pekoz approach which includes an allowance for the reduction in the effective depth of the section as a result of twisting. The latter two methods allow a non-linear load-deflection curve to be determined whereas the Sokol method gives only an estimate of the failure load.

Within the work of ECCS Committee TWG 7.1, the above three methods were compared with the results of 12 tests [4] on simply supported Z purlins subject to wind uplift and with depths in the range 200 to 245mm. The Sokol approach was chosen for inclusion in the European recommendations on the basis of simplicity and consistent safety. However, all three methods gave acceptable results and, bearing in mind the limited nature of the experimental comparisons, there is scope for further investigation. In particular, the extension to sections other than Z, the extension to multi-spans based on lengths between points of contraflecture and a wider range of section depths all appear worthy of more detailed consideration.

Application of the Pekoz method to the authors' test results for single span Multibeam MK2 purlins under wind uplift showed acceptable comparison between theory and test for section depths of 170 and 200mm but rather less good comparison for depths of 140 and 260mm.

A rather different approach has been adopted by Ings and Trahair [6]. Using a modification of the Barsoum and Gallagher finite element analysis [7], they carried out a study of C and Z section purlins restrained laterally but free to rotate at the level of the sheeted flange. The results of this study are presented in the form of non-dimensional design aids which are of more general application and a design procedure based on these aids is described. This procedure was applied to a series of 8 tests on C and Z section purlins with depths of 206 and 230mm. The comparison of theory and test is probably acceptable for practical purposes but does not appear

to be as good as that given by the equivalent column methods considered earlier.

Methods are also available, such as the "generalised beam theory" [8], which are capable of taking account of most of the aspects of the elastic behaviour of purlins restrained by sheeting and giving good agreement with test results. Clearly, accurate design by calculation in the elastic range is becoming a practical possibility but if advantage is to be taken of the plastic redistribution of bending moments, it will continue to be necessary to resort to design on the basis of testing.

3. DESIGN PROCEDURE FOR MULTIBEAM MK2

As the simple system, based on two-span purlins, was crucial to the economy of the design, the design procedure was first established for this case. Design was based on a pseudo-plastic collapse mechanism as shown in Fig. 4 in which M_1 and M_2 are obtained from empirical design expressions deduced from tests on single span purlins as described later. The collapse load W_c may then be predicted using the following expressions.

$$W_c = \frac{2[M_2 L + M_1(L-x)]}{x(L-x)} \qquad \ldots\ldots\ldots\ldots\ldots\ldots(1)$$

$$\frac{x}{L} = \frac{(M_1 + M_2) - [(M_1 + M_2)^2 - M_1(M_1 + M_2)]^{\frac{1}{2}}}{M_1} \qquad \ldots\ldots\ldots(2)$$

Having calculated the collapse load W_c, the plastic hinge rotation θ_p at the centre support at collapse is given by

$$\theta_p = \frac{L}{1.5EI}\left[\frac{W_c L}{8} - M_1\right] \qquad \ldots\ldots\ldots\ldots\ldots\ldots(3)$$

where EI is the flexural rigidity of the purlins.

Investigation over a wide range of purlin sizes and spans as testing proceeded, showed that θ_p was generally in the range 2^o to 3^o and that 3^o represented a reasonable upper limit to the required rotation capacity.

Accordingly, a semi-empirical design expression based on equations (1) and (2) was adopted and this required the following steps:

(a) Determination of an empirical expression for M_1 at a plastic hinge rotation of 3^o using the simulated central support test described later.

(b) Determination of an empirical expression for M_2 based on simply supported purlin tests.

(c) Confirmation of this design procedure by comparison with tests on two-span purlins and the inclusion of a correction factor in order to increase the precision of the method.

The above procedure was first followed for purlins clad with profiled steel sheets and subject to downward load. Consideration of uplift loading and other cladding systems followed later.

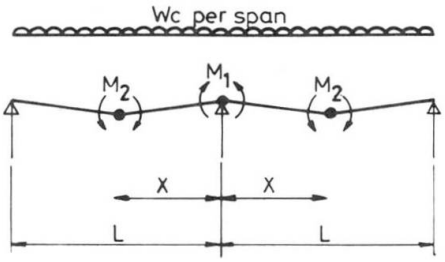

Fig. 4 Collapse mechanism for two-span purlin

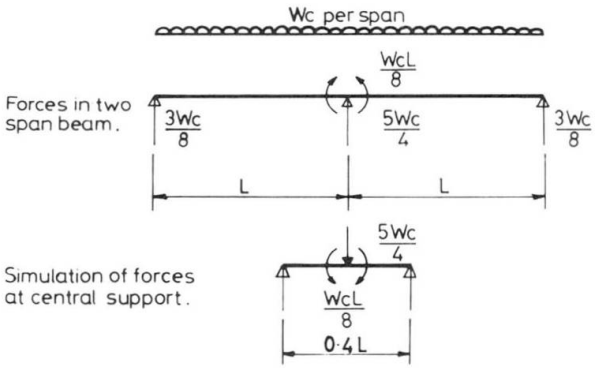

Fig. 5 Simulated central support test

4. DESIGN OF MULTIBEAM MK2 BY TESTING

4.1 Behaviour of Internal Supports

The behaviour at the central support has a great influence on the performance of a two-span purlin and trial profile shapes and their associated support cleats were investigated using the simulated central support test defined in Fig. 5.

The apparatus used is shown in Figs. 6 and 7.

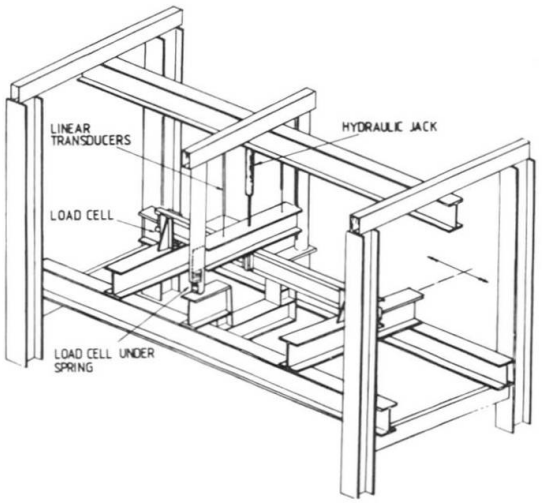

Fig. 6 Central Support test rig.

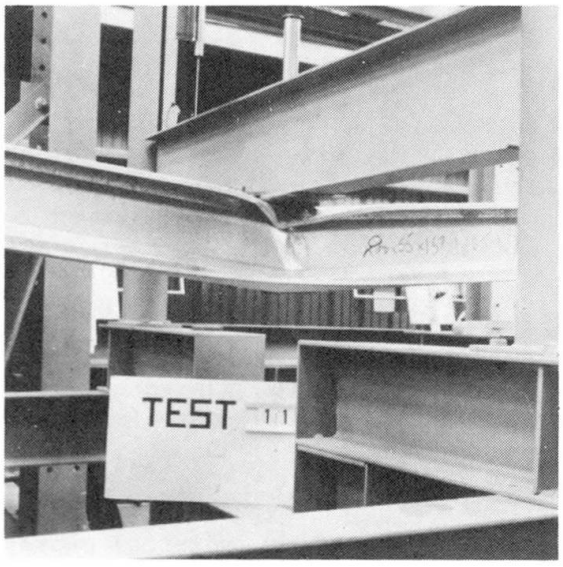

Fig. 7 Central Support testing

In carrying out this test, it was important to be able to determine the load-deflection relationship beyond the maximum load and well into the drooping post-failure region as shown for a typical test in Fig. 8. This can be achieved by loading with a screw jack or, as adopted by the authors, by the incorporation of a spring of suitable stiffness so that a hydraulic jack applies load to both the spring and the purlin and the resulting combination always has positive stiffness.

The cleat arrangement was found to be as important as the shape in ensuring a high maximum bending moment M_1 at the support together with a favourable performance in the post-failure region. A particular advantage of the shape of Multibeam MK2 is that it allows the use of a stiffened cleat with connection to the web at both top and bottom of the section as shown in Fig. 9. The enhanced performance of this detail far outweighs the additional fabrication cost of the cleat. It also has the advantage that it can allow the purlin or side rail to stand off the supporting member if this is required for the installation of insulation etc.

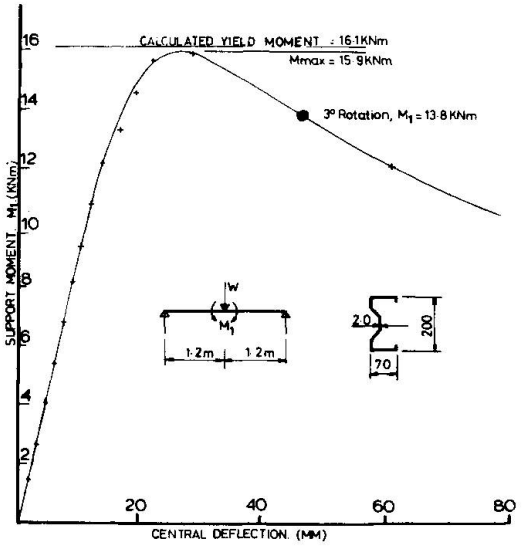

Fig. 8 Typical test result

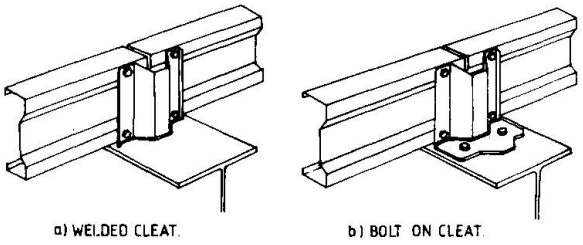

Fig. 9 Cleat details

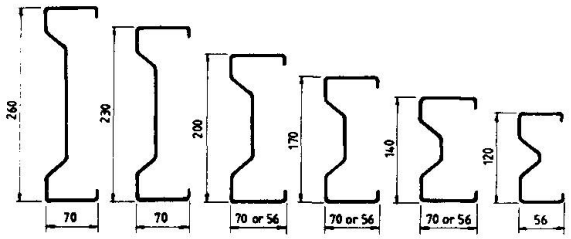

Fig. 10 Multibeam MK2 range

On the basis of the simulated central support tests, the broad details of the section range shown in Fig. 10 were established and a lower bound expression for the support moment M_1 at a plastic hinge rotation of 3^o was derived. In general, the narrower flange widths are used for side rails where stability during erection is less of a problem.

4.2 Vacuum testing and application to downward loading

The remaining tests were carried out using vacuum loading on an assembly of two purlins and a 2 metre width of sheeting in the purpose-built apparatus shown in Figs. 11 and 12. For the first tests in this series, the weakest conventional steel roof sheet in the catalogue was chosen because the performance with metal roofing was considered to be the dominant design factor. Tests with standing seam roof sheets and asbestos-cement substitutes were carried out subsequently. Opportunity was taken to vary the number and type of anti-sag bars but the details used all represented practical arrangements that were under consideration for the final design. Anti-sag bars are required primarily to maintain the lateral stability of the working platform and generally carry only low stresses under downward load as the stability in the clad condition is provided mainly by the sheeting. However, their importance increases under wind uplift and with cladding systems that provide reduced restraint such as standing seam roofing.

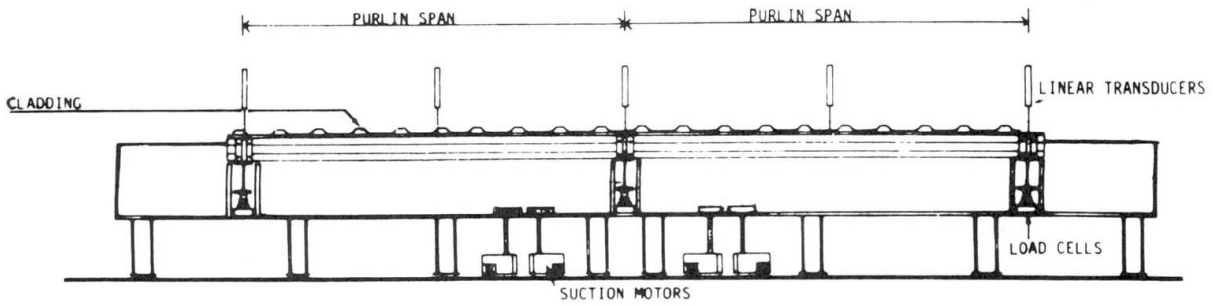

Fig. 11 Longitudinal section through vacuum testing apparatus

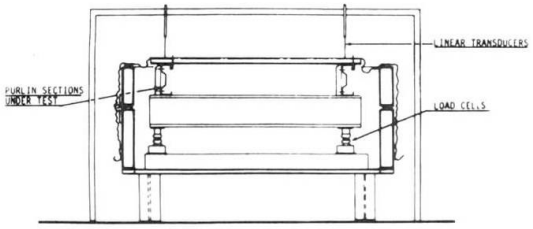

Fig. 12 Transverse section through testing apparatus

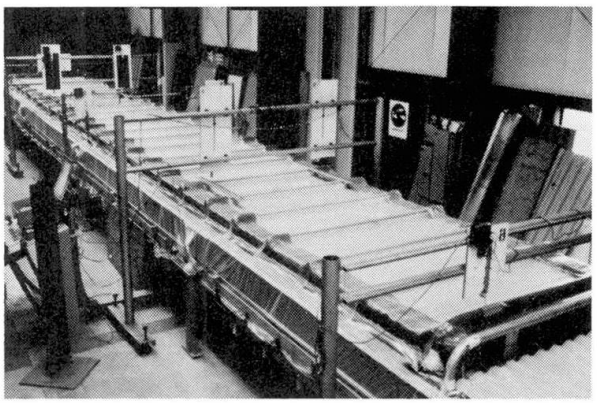

Fig. 13 Purlins under test.

Fig. 13 shows a typical assembly under test in this apparatus which was capable of accommodating single spans and up to two spans of 8 metres. In this way, a lower bound to the span moment M_2 was established on the basis of a series of tests on simply supported beams. The resulting design expression was then confirmed and empirically refined on the basis of 38 tests on pairs of two span purlins. Some refinement was necessary in order to improve the efficiency of the developed theory for purlins of 120 and 140mm depth. However, for purlins of 200mm depth and greater the unmodified theory gave slightly unsafe answers, presumably as a consequence of displacements at the points of contraflecture.

In all of these tests, the flanges of the two purlins faced in the same direction. This had the result of throwing slightly more load onto one of the purlins which usually failed first. The failure loads are therefore the lowest of the four tested spans in a test that is less favourable than the conditions encountered in practice.

The results of this procedure are summarised in Fig. 14. For a total of 30 tests covering the whole range of profile depth, thickness and span which were selected for the final range of sizes, the test results fall within -2% and +14% of the theory.

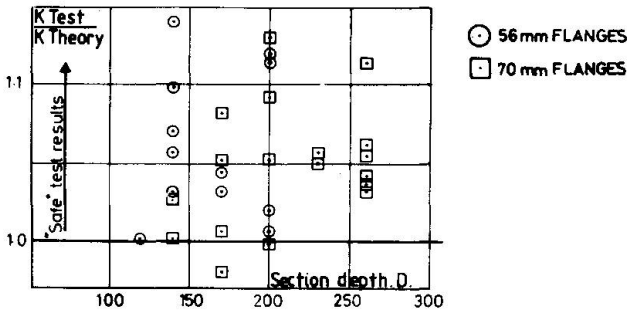

Fig. 14 Gravity load test results compared with theory

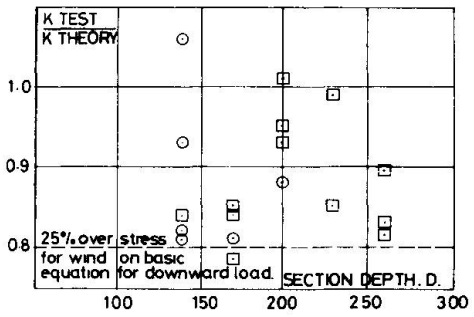

Fig. 15 Uplift test results compared with theory.

4.3 Uplift loading

Under wind uplift, the load capacity is reduced because the compression flange is unrestrained within the span. However, the current British Standard [9] allows a 25% increase of stress or a corresponding decrease to the load factor for wind loading and with steel sheeting fixed with self-tapping screws, it was found to be possible to balance the reduced load capacity against the reduced load factor as shown in Fig. 15. This means that for current U.K. usage, it is possible to use the same safe load tables for both upward and downward level. For other countries, however, different load tables are required.

With asbestos cement or other cladding fixed with hook bolts and for standing seam roofs, greater reductions of strength may occur. The precise reductions depend on the purlin depth, the span and the number and type of anti-sag devices. Values of these reductions based on tests are given in the manufacturer's literature.

4.4 Sleeved purlin system

The program described above was extended in various ways including the development of a sleeved purlin system. However, it is not possible to include a description of this additional work within the scope of this paper.

5. APPROVAL PROCEDURES IN OTHER EUROPEAN COUNTRIES

In the U.K. product approval is in the hands of the local authorities acting under the guidance of the Building Regulations and relevant British Standards. Design by testing is permitted and reputable companies use independent academics to verify their design procedures. The latest British Standard, which has yet to be extended to incorporate cold formed steel members, uses limit state methods with load factors of 1.6 for live loads and 1.4 for dead and wind loads. Deflection limits are at the discretion of the engineer but span/200 is commonly used.

During the course of the development of Multibeam MK2, Ward Brothers extended their interests outside the U.K. with sales outlets in the Netherlands and West Germany and a production facility in France. The building control system, in particular that for light gauge sections, differs in each country although all recognise the use of tests.

In West Germany and the Netherlands, buildings must be checked by a proof

engineer who, in the absence of a codified design method, will ask for a product approval. In West Germany, this is granted by the Institut für Bautechnik on the basis of a report from a recognised independent authority.

In the case of Multibeam this report was prepared by Professor R. Schardt who assessed the test results against his general theory. Working loads are used in design with a factor of safety of 1.71 for both gravity and uplift loads. Deflection limits of span/200 apply. Similar procedures apply in the Netherlands but assessment and approval are provided by the National Building Research Centre, TNO. The factor of safety is 1.5 and the deflection limit is span/250.

In France, the need to insure buildings governs the procedure since, in order to obtain economic premiums, it is necessary to have the designs approved by a recognised Bureau de Controle. For items such as light gauge purlins proved by test, it is beneficial to obtain product approval from a Bureau which will then be accepted by the other COPREC members. SOCATEC were chosen to provide this for Multibeam. A limit state approach is used and the ultimate load is defined from test results as the lesser of 0.7 times collapse load or the load which causes a permanent deflection of 0.075 of the deflection at yield. The load factors are 1.5 for normal live loads, 1.3 for the normal dead loads and 1.0 for extreme loads. The deflection limit is span/200.

6. CONCLUSIONS

Although the design of cold-formed steel purlins and side rails solely on the basis of calculation is becoming an increasingly realistic possibility, good reasons remain for basing the design of any new system on testing. The comprehensive test programme and the semi-empirical design procedure used in the development of Multibeam MK2 for the U.K. market have been described and it has been shown that safe and highly efficient designs have been achieved. Approval of this product has been obtained or is being sought in other countries of Europe and some of the considerations encountered have been outlined.

REFERENCES

1. AISI "Specification for the design of cold-formed structural members" American Iron and Steel Institute, Sept. 1980.

2. ECCS "European recommendations for the design of light gauge steel members" Draft for comment, ECCS-TWG 7.1 - 1985, Sept. 1985.

3. BS 5950 Part 5, Draft British Standard "Code of practice for the design of cold-formed sections" BSI, Sept. 1984.

4. T. PEKOZ and P. SOROUSHIAN "Behaviour of C- and Z- purlins under wind uplift" Proc. 6th International Speciality Conference on cold-formed steel structures, University of Missouri-Rolla, Nov. 16-17 1982, pp 409-429.

5. R. SCHARDT "Z purlins under uplift load" Committee paper, ECCS-TWG 7.1.

6. N.L. INGS and N.S. TRAHAIR "Lateral buckling of restrained roof purlins" Thin-walled structures, Vol. 2, 1984 pp 285-306.

7. R.S. BARSOUM and R.H. GALLAGHER "Finite element analysis of torsional and torsional-flexural stability problems" Int.J.Numr. Methods in Engrg.2, 1970 pp 335-352.

8. R. SCHARDT "The generalised beam theory" Proc. M.R. Horne Conf., Instability and Plastic Collapse of steel structures, Granada, 1983 pp 469-478.

9. ADDENDUM No.1 to BS 449 "Specification for the use of cold-formed steel sections in building" BSI, March 1975.

Torsional Restraint Coefficients of Profiled Sheeting

Coefficient d'encastrement à la torsion dû à la tôle profilée

Drehbettungswerte von Trapezprofilen

Joachim LINDNER
Prof. Dr.
Techn. Univ. Berlin
Berlin

Joachim Lindner, born in 1938, worked in the structural steel fabricating industry and later with an industrial scaffolding company. Since 1974, he has been Professor for steel structures at the Technical University, Berlin. His main research activities centre on the area of stability.

Thomas GREGULL
Dipl.-Ing.
Techn. Univ. Berlin
Berlin

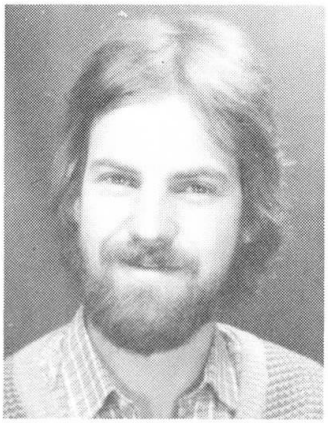

Thomas Gregull, born in 1958, completed his structural engineering studies in 1984 at the Technical University Berlin. Afterwards he joined the scientific staff of the University, structural-steel department, and is involved in research into the stability of struts, and the stabilising of purlins.

SUMMARY

In the dimensioning of steel-purlins it is customary to take into consideration the mitigating action of the roof-skin with respect to lateral torsional buckling. The rotationally flexible restraint is especially achieved by profiled sheeting. The value of the torsional spring under consideration is mainly limited by the flexible connection between purlin and roofing-skin. This report deals with research into the assessment of the torsional bearing assumed in calculations. Different connection-types, with and without thermal insulation between purlin and roofing-skin, are being investigated. An example illustrates application.

RÉSUMÉ

Lors du dimensionnement des pannes, la couverture, surtout celle constituée de tôles trapézoïdales, est très souvent considérée comme un appui latéral contre le déversement. La valeur de ce coefficient d'encastrement à la torsion est fonction de la souplesse de l'assemblage entre panne et couverture. Il est question ici de rechercher le coefficient adéquat à l'aide de plusieurs essais. Sont examinés différents types d'assemblage avec ou sans isolant thermique entre panne et couverture.

ZUSAMMENFASSUNG

Bei der Bemessung von Stahlpfetten wird die Dacheindeckung, insbesondere Trapezbleche, häufig als drehfedernde Stützung beim Nachweis gegen Biegedrillknicken angesetzt. Die Grösse der anzusetzenden Drehfeder wird aber wesentlich durch die weiche Verbindung Pfette-Dachhaus bestimmt. Hier wird über Versuche zur Ermittlung der anzusetzenden Drehbettung berichtet. Es werden unterschiedliche Anschlusskonstruktionen mit und ohne Wärmedämmung zwischen Pfette und Dachhaut untersucht.

1. GENERAL

When dimensioning steel-purlins, it is customary to consider in increasing magnitude the supporting-action of the roofing components as restraint against lateral torsional buckling, the main reason for this being commercial considerations. Depending on the type of roofing-skin being used, the horizontal dislocation of the upper chord is being restrained by the shear stiffness R and/or the twisting of the purlin is being limited by the bending-resistance of the roofing-skin. In the calculations, the bending-resistance of the roofing is being accounted for by the value c_φ of the torsional bearing. Relevant formulae to establish the ideal buckling-moment in consideration of the torsional bearing and the shear stiffness are given for instance in [1], [2], [3], [4].

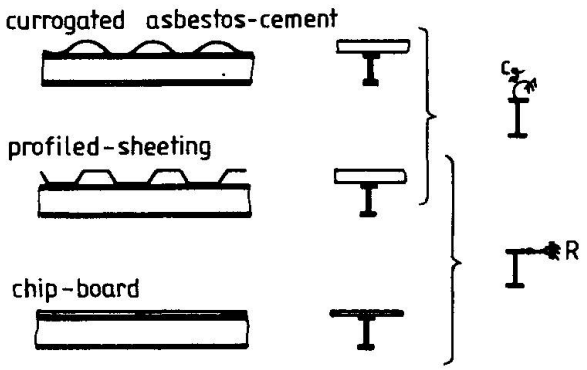

Fig. 1 Stabilizing by adjacent components

This article analyses the value of the applicable torsional restraint coefficient. Assuming an effective areal connection between roofing-skin and purlin, the torsional spring is easily established by way of the flexural stiffness of the roofing-skin. Due to the localised nature of the fastening (i.e. with bolts), additional deformation takes place local to the fixing-points, so that the flexural stiffness may only partly be utilized. The use of thermal insulation between purlin and roof-skin causes, by the compression thereof, further deformation. The tests in [5], [6], in which measurements of the torsional restraint coefficient values were taken on different roof-skin configurations without live-loads, show the deformation local to the connection to have a significant influence on the distorsion of the purlin and to be distinctly more prominent than the deflection of the roof-skin.

A research-project is under way at the Technical University Berlin, in which investigations of the torsional restraint coefficient values under applied live-loads are being carried out [7].

In this, the following parameters are being varied:

- construction of the roofing-skin,
- location and distance of the fixings (ridge, trough, fasteners in every or alternate ridge/trough)
- roofing-construction (with or without intervening thermal insulation, type of thermal insulation used),
- purlin-construction (hot-rolled section, cold formed section).

The following reports on the results of preliminary tests, which preceded the test-programme as laid down in [7].

2. DETAILS OF ROOF-STRUCTURE IN TEST

Representative for hot-rolled sections in the I range, IPE 160 purlins were used in the tests. As roof-sheeting, a profiled steel-sheet 40 x 183 x 0.75 mm in inverted position (see Fig. 2) was chosen. Part of the tests was carried out with a thermal insulation of extruded polystyrol rigid foam panels inserted between purlins and sheeting. The fixing of sheeting and purlins was by way of self-tapping screws ø 6.3 mm. The fixings in the bottom-chord incorporated ø 19 mm washers, in some instances ø 29 mm spreader washers were used instead. Fixings in the top-chord incorporated "Orkan-Calottes" of 0.75 mm thickness.

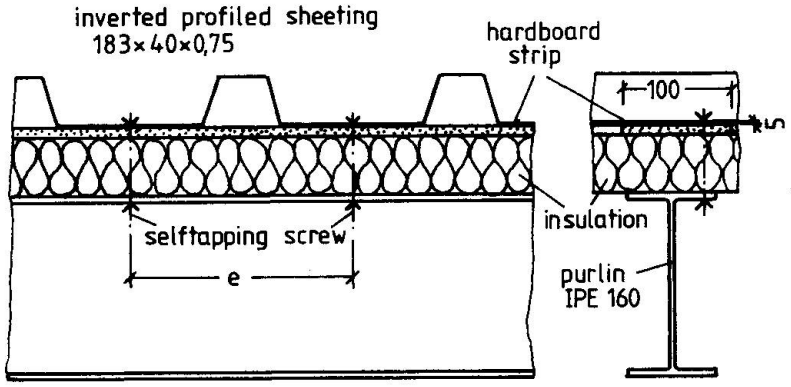

Fig. 2 Roof-construction with thermal insulation

3. TEST CONFIGURATION

The tests were conducted on realistically constructed roof-sections. For this purpose, two purlins were installed at a distance c/c of a=3.0 metres with the roofing-skin affixed. A torsional moment was introduced into the purlins and the resulting distortion δ being measured. Fig. 3 shows the principle of the test-configuration. The rotation of the purlin was being facilitated by the use of self-aligning ball-bearings and the horizontal dis-location in direction of the roofing-skin span by inserting ball-bearing-racks beneath the rotational bearings. By virtue of this configuration, bearing friction could be reduced to a negligible amount. The complete test-piece, including the bearings, was then installed in a test-rig which also provided the anchorage for the hydraulic cylinders, required to simulate the live-loading.

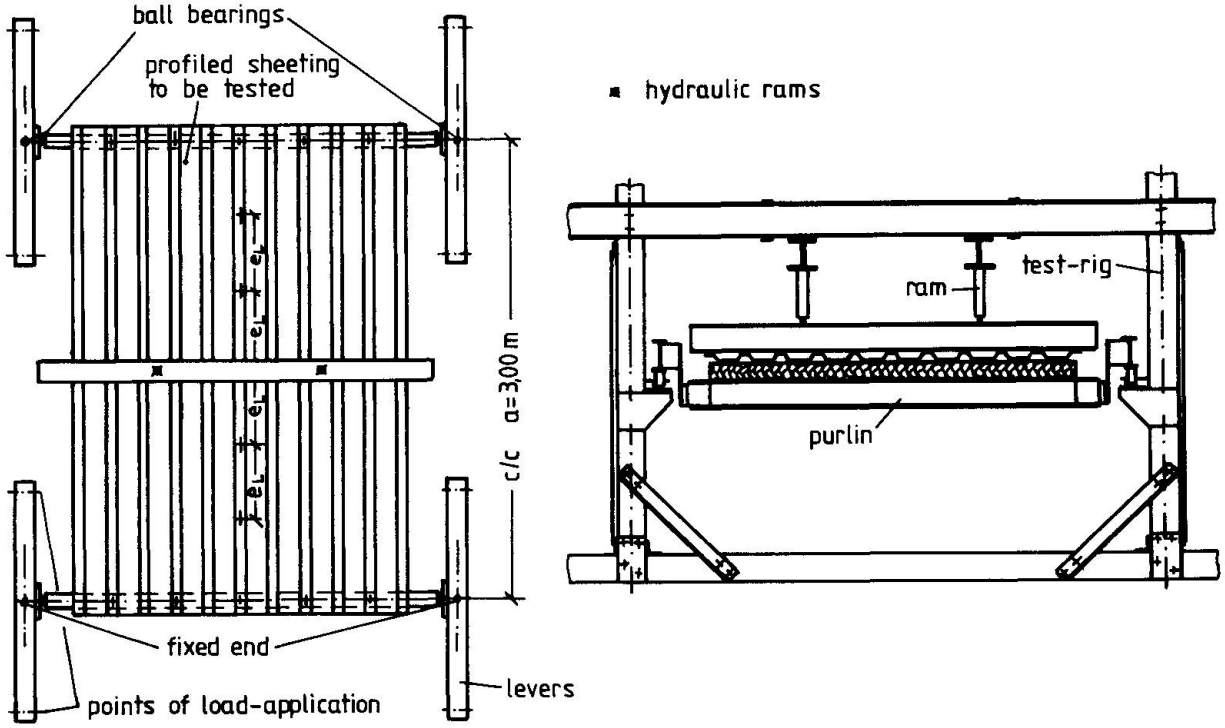

Fig. 3 Test Configuration

4. CONDUCTING OF TEST

4.1 Load application

The imposed load generated by 2 hydraulic cylinders was applied to the roof by way of a steel beam, as uniform distributed load acting at mid-span of the profiled sheeting. The resultant reaction of the profiled sheeting at the purlins amounted to approx. 1 kN/m. At a span of 3 m, this equivalent to a uniform distributed load of 0.66 kN/m^2 being applied to the profiled roof-sheet.

4.2 Torsional Moment

The purlins are connected to levers on both sides. The torque necessary to cause distortion of the purlins was achieved by suspension of weights at the cantilevers. The loading of the cantilevers took place only at the fixed-end (see fig. 3), as load-introduction at both purlins would only result in a different moment-distribution in direction of the roof-sheet span. Assuming the connection between profiled roof-sheet and purlin to be rigid, this proportion of the deflection in the roof-skin can easily be established via the flexural stiffness of the sheets.

The torque was bi-directionally applied, alternating and of increasing magnitude, so that the graphical analysis resulted in "hysteresis curves", which made it possible to establish any residual plastic deformation after cessation of load-application.

4.3 Measuring of Deformations

The torsional deformation of the purlin was measured at both ends as well as at mid-span. Additionally, for checking-purposes, the rotation of the torsion inducing cantilevers as well as the deflection of the profiled sheeting at mid-span were recorded. All deformations encountered during the test were measured by application of mechanical dials.

5. TEST RESULTS

5.1 Evaluation of the Moment-Rotation-Diagrams

For each test, a moment-rotation-diagram was prepared, in which the mean-values of distortion ϑ [rad] were logged at the abscissa, and at the ordinate the value of the torque m_t [kNm/m] applied per width unit of the roof-skin. The torsional restraint coefficient c_ϑ can be read directly from the incline of the curve.

The diagram shows that the increase in distortion is non-linear to the moment applied. For practical application, it is not recommended to use a torsional bearing which is dependent on the load applied. Therefore, in simplification, c_ϑ is being determined as radial-torsional resistance ϑ=0.100 [rad]. In the event of distortion during a test amounting to less than ϑ=0.100 , the curve is being extrapolated with the incline between the last two measured values.

Fig. 4 reflects the evaluation of a test with thermal insulation.
The fixing was located in the bottom-chord in alternate troughs.
The points leading to the determination of the results $c_{\vartheta 1}$ for positive and $c_{\vartheta 2}$ for negative distortion are marked thus ① in the diagram.

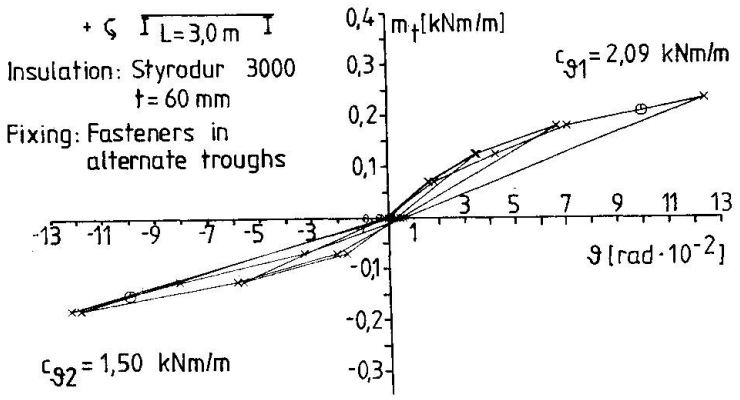

Fig. 4 Example of the graphical evaluation

5.2 Mathematical Model for the Determination of the Rigidity of the Connections

The elastic distortion of the purlin, resulting from torsional loading, consists of a bending-deflection of the profiled sheeting in direction of it's span (theoretical value when assuming a rigid connection), the cross-sectional deformation of the purlin itself, and a local deformation-component in the connection (connection-stiffness). As described in [6], this can be assumed as a system of multiple, interacting torsional springs.

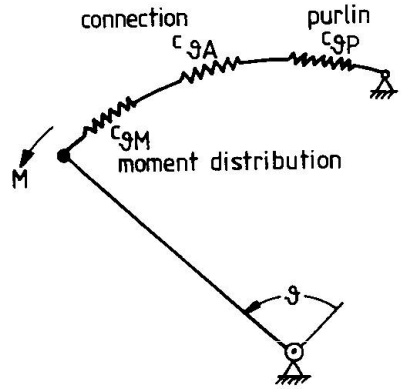

Fig. 5 Spring-Model

The connection-stiffness $c_{\vartheta A}$ can be calculated from the cumulative deformation, as follows:

$$\frac{1}{c_{\vartheta A}} = \frac{1}{c_{\vartheta Vers}} - \frac{1}{c_{\vartheta M}} - \frac{1}{c_{\vartheta P}} \qquad (1)$$

$c_{\vartheta Vers}$ ≙ the value $c_{\vartheta 1}$ and $c_{\vartheta 2}$ respectively (see diagram) as measured in the test

$c_{\vartheta A}$ ≙ rigidity of connection, dependent on no. of screws, sheet-thickness, ø of washers, thermal insulation etc.

$c_{\vartheta M}$ ≙ theoretical value on assuming rigid connection:

$= K \frac{EI}{a}$ K=f(M) see [3], [6]

Due to the introduction of torque into the purlins during these tests, $c_{\vartheta P}$ assumes infinite value.

Since the tests were conducted on a roof-section (width of sheet = 1.83 m), the number of fixing-studs per metre of sheet-width was not always representative of that in an infinitely wide bay. To facilitate a better comparison of the results, the values of the torsional bearing were re-calculated to be representative for an infinitely wide profiled sheeting with even distribution of the fixing-studs. It was here presumed that the torsional bearing-values are significantly dependent on the tightening force excerted on the studs (deformation of the sheet due to application of the tightening-force), and this again is proportional to their distance from the compression-edge of the purlin.

5.3 Statistical Evaluation

The number of tests conduced with individual fastening-types was insufficient to facilitate a representative statistical evaluation. However, in order to enable the test-results with the various types of fastening systems to be combined and to obtain a working-basis for the assessment of the stress-related influences, the torsional bearing values $c_{\vartheta A}$ for fixing in the bottom-chord at alternate troughs and with thermal insulation thickness t=60 mm installed between sheet and purlin, were considered. The standard deviation in 6 torsional restraint coefficient values amounted to: $s=0.1\ \bar{m}$ ($\bar{m}$ = mean-value).

This value is being applied in approximation for the evaluation of all tests, as the causes for the standard deviation can basically be found in the inaccuracies in the sheeting being fitted to the purlins.

Table 1 shows the resultant mean-values $c_{\vartheta A,m}=\bar{m}$, as well as the fractile values $c_{\vartheta A}=\bar{m}-2 \times s=0.8 \times \bar{m}$ of the individual fixing-designs. As the tests are being continued, it is feasible that the finally proposed values might be slightly different from those shown in table 1.

Table 1 torsional restraint coefficients with applied external loading, for profiled sheeting 40 x 183 x 0.75 in inverted installation
- lower limiting values $c_{\vartheta A}$
- mean values $c_{\vartheta A,m}$

type of connection	$c_{\vartheta A}$ [kNm/m]	$c_{\vartheta A,m}$ [kNm/m]
without thermal insulation bottom chord, $e=2b_r$; ø 19 washer	1.3	1.6
without thermal insulation bottom chord, $e=2b_r$; ø 29 washer	1.5	1.9
without thermal insulation bottom chord, $e=b_r$; ø 19 washer	2.1	2.6
without thermal insulation bottom chord, $e=b_r$; ø 29 washer	2.7	3.4
without thermal insulation top chord, $e=2b_r$;	3.4	4.3
without thermal insulation top chord, $e=b_r$	7.1	8.9
with Styrodur 3000 g, t=60 mm bottom chord, $e=2b_r$; ø 19 washer	1.7	2.1
with Styrodur 3000 g, t=60 mm bottom chord, $e=b_r$; ø 19 washer	2.6	3.3
with Styrodur 3000 g, t=60 mm top chord, $e=2b_r$	1.9	2.3
with Styrodur 3000 g, t=60 mm top chord, $e=b_r$	3.0	3.8

6. APPLICATION OF THE TESTRESULTS

Table 1 constitutes a summary only of the connection-stiffnesses which result from the local connection of roofing-skin to the purlin. For proof of stability, however, the in para. 5.2 listed influences need to be considered:

$$\frac{1}{c_\vartheta} = \frac{1}{c_{\vartheta A}} + \frac{1}{c_{\vartheta M}} + \frac{1}{c_{\vartheta P}} \qquad (2)$$

Example:

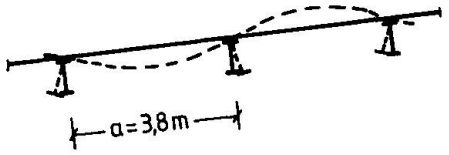

---line of deflection

Roof Centre-Section
profiled sheeting 40 x 183 x 0.75 mm
I_{eff} = 21.62 cm⁴/m
inverted installation
Fixing in each bottom-chord
ø 19 mm washers
thermal insulation Styrodur 3000, t=60 mm
Purlins IPE 140, Web t=4.7 mm

$$c_{\vartheta M} = \frac{4 \cdot EI_{eff}}{a} = \frac{4 \cdot 21000 \cdot 0.216}{380} = 47.7 \text{ kNm/m}$$

$$c_{\vartheta P} = \frac{E \cdot s^3}{4 \cdot h} = \frac{21000 \cdot 0.47^3}{4 \cdot 13.3} = 41.0 \text{ kNm/m}$$

$$c_{\vartheta A} = 2.6 \text{ kNm/m}$$

$$\frac{1}{c_\vartheta} = \frac{1}{47.7} + \frac{1}{41.0} + \frac{1}{2.6} \qquad c_\vartheta = 2.3 \text{ kNm/m}$$

It is recognizable that the influence of the deformation of the profiled sheeting itself and the cross-sectional deformation of the purlins is negligible. This cross-sectional deformation of the purlins can, however, be significant in thin-walled sections.

For the further proof of the stability of the purlin when subjected to imposed loading the torsional restraint coefficient of c_ϑ=2.3 kN/m should be taken into account.

If the here established values are to be applied to profiled sheets of different dimensions, the following needs to be taken into consideration:

The location and pitch of the fixing-studs must be similar to those in the test. The significant parameters in this context are the pitch e, diameter of washers and the location of the fixing in trough or ridge of the sheeting. Sheet thickness t must be at least the same as of the sheet used in these tests and possibly used thermal insulation must be of equivalent rigidity. Further tests, including roof-construction of cold-formed purlins, are presently in progress at the Technical University Berlin.

7. ACKNOWLEDGEMENTS

The aforementioned results represent interim-results of a research-project commissioned by the Studiengesellschaft für Anwendungstechnik von Eisen und Stahl e.V., Düsseldorf, with financial support from AIF funds, for which we express our gratitude. We are indebted to the Working Group within the Studiengesellschaft for their support and assistance and to Arbeed Saarstahl Co, Grünzweig und Hartmann PLC and EJOT Structural Fasteners Ltd for the supply of materials.

Literature:

[1] Fischer,M.: Zum Kipp-Problem von kontinuierlich seitlich gestützen I-Trägern. (The buckling-problems in continuously transverse supported I-beams). Der Stahlbau 45(1976), S.120-124.

[2] Petersen,L.: Statik und Stabilität der Baukonstruktionen. (Stressing and Stability of Building Structures). Friedr. Vieweg & Sohn, 1980.

[3] Roik,Carl,Lindner: Biegetorsionsprobleme gerader dünnwandiger Stäbe. (Problems of Bending and Torsion in straight, thinwalled Components). Verlag Wilhelm Ernst & Sohn, Berlin, München, Düsseldorf, 1972.

[4] Errera,J.S., Apparao,T.V.S.R.: Design of I-Shaped Beams with Diaphragm Bracing. ASCE, Vol.102, NoSt 4, April 1976, pp.769-781

[5] Wünsch,A.: Der Einfluß von Unterwind-Belastung auf Z-Pfetten bei einer Dacheindeckung aus Wellasbestzementplatten. (The Influence of up-lift Wind Loads on Z-Purlins at Roof Sheeting by corrugated Asbestos-Cement). Dissertation, Berlin 1974.

[6] Lindner,J., Kurth,W.: Ermittlung von Drehbettungsbeiwerten bei Unterwind. (Torsional Restraint Coefficients by up-lift Wind Loads). Versuchsbericht VR 2021 des Instituts für Baukonstruktionen und Festigkeit der TU Berlin, Berlin 1979. Bauingenieur 55(1980), S.365-369.

[7] Forschungsvorhaben P 134: Drehbettungswerte für Dacheindeckungen mit untergelegter Wärmedämmung. (Torsional Restraint Coefficients for Roofing with Thermal Insulation between Purlin and Roof-Skin). Studiengesellschaft für Anwendungstechnik von Eisen und Stahl e.V. Düsseldorf.

Roof Panel to Purlin Connection: Rotational Restraint Factor

Assemblage panne-panneau de toiture: facteur de résistance à la rotation

Dachblech-Pfetten-Verbindung: Drehwiderstandsfaktor

Roger A. LaBOUBE
Senior Structural Engineer
Amer. Iron and Steel Inst.
Washington, DC, USA

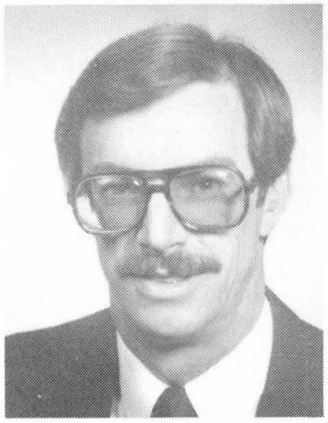

Roger LaBoube, born 1948, received his Ph.D. in Civil Engineering at the University of Missouri-Rolla, Rolla, MO. For five years he was involved in research and development at Butler Mfg. Co. where Dr. LaBoube's studies have focused on the behavior of coldformed steel members.

SUMMARY

The load carrying capacity of a metal building roof system subjected to wind uplift is significantly influenced by the rotational restraint or stiffness provided to the purlin by the connection of the roof panel to the purlin. This rotational restraint factor is commonly refered to as the «F» factor. A test program was executed to experimentally determine the «F» value for the variation in parameters that may have an influence on the rotational restraint. This paper summarizes the findings of numerous «F» tests and presents an empirical equation to estimate the «F» factor.

RÉSUMÉ

La capacité portante d'une toiture métallique d'un bâtiment soumise à la succion du vent est considérablement influencée par la résistance à la rotation fournie aux pannes par leurs assemblages aux panneaux de toiture. Le facteur de résistance à la rotation est communément appelé facteur «F». Un programme expérimental a été exécuté pour déterminer les valeurs de «F» en fonction des paramètres qui pourraient influencer la résistance à la rotation. Le présent article résume les résultats de plusieurs essais, et présente une équation empirique pour estimer le facteur «F».

ZUSAMMENFASSUNG

Die zulässige Traglast von blechverkleideten Stahldächern unter negativen Windlasten (Sog) wird wesentlich vom Drehwiderstandsfaktor oder der Drehsteifigkeit der Dachblech-Pfetten-Verbindung beeinflusst. Dieser Drehwiderstandsfaktor ist allgemein als F-Faktor bekannt. Das beschriebene Versuchsprogramm führte zu einer Bestimmung der F-Faktoren als Funktion von verschiedenen Einflussgrössen. Der Beitrag beschreibt die Resultate zahlreicher Versuche und stellt ein empirisches Verfahren zur Abschätzung des F-Faktors vor.

INTRODUCTION

The load carrying capacity of a metal building roof system, subjected to wind uplift, is significantly influenced by the rotational restraint or stiffness provided to the purlin by the connection of the roof panel to the purlin. This rotational restraint factor is commonly referred to as the "F" factor.

In the United States, the "F" value is experimentally determined using a test procedure developed by Haussler and Pabers [1]. This report summarizes the findings of numerous "F" tests and presents an empirical equation to estimate the "F" factor.

Test Fixture

A test fixture, Figure 1, was fabricated that complied with the guidelines prescribed in Reference 1. A complete description of this setup is given in Reference 2.

Parametric Study

The rotational stiffness inherent in a roof system is a function of the geometry of the individual components and the method of attachment of the components. Therefore, the significant parameters in a metal building roof system appeared to be: (1) Purlin depth and thickness, (2) Roof sheet depth and thickness, (3) Insulation thickness, (4) Fastener type and (5) Fastener location.

A series of tests were conducted to investigate the change in the "F" factor with variations in the above parameters. The "F" factor is defined by the slope of the load-deflection curve.

Purlin Depth and Thickness

Assuming rotational restraint provided by the roof sheet and its attachment to the purlin, the web and loaded flange (Figure 1) act as a cantilevered member. Therefore, the purlin depth and thickness were identified as important parameters influencing the "F" factor.

Figure 2 presents a typical load-deflection for a 203 mm deep Z-section. The figure clearly shows that the material thickness has a very significant affect on the stiffness of the roof system. However, the member depth imparts a lesser influence on the rotational characteristics. See Figure 3.

Roof Sheet Depth and Thickness

A representative roof sheet used by the metal building industry, in the United States, is 914 mm wide with major corrugations of 25 mm to 38 mm in depth. For this range of depths, the "F" factor is not affected - see Figure 4.

Unlike the roof sheet depth, the sheet thickness does have some impact on the numerical value for the "F" factor. Figure 5 graphically represents the affect of varying sheet thickness from .50 mm (26 ga.) to .65 mm (24 ga.). This range in sheet thickness represents the typical metal building industry standard.

Insulation Thickness

The presence of insulation, between the purlin flange and roof sheet, and its affect on the rotational stiffness was investigated. Specimens were tested which had 38 mm, 76 mm and 152 mm blanket insulation. The load-deflection characteristics of these specimens are compared to a specimen having no insulation (see Figure 6). As indicated by the plotted data, the insulation thickness had only a slight affect on the stiffness. This may be due to the fact that all of the blanket thicknesses studied are compressed to approximately an equal thickness between the purlin and roof sheet.

Fastener Type and Location

Metal building roof systems typically employ either self-tapping or self-drilling sheet metal screws. Figure 7 graphically shows the behavior of comparable self-tapping and self-drilling screws.

The enhanced performance of the self-tapping screw may be attributed to either a pre-punched hole versus a drilled hole, or better control over the location of the fastener in the purlin flange.

As indicated by Figure 8, the location of the screw in the flange of a Z-section is very critical. The specimens in question consisted of 203 mm deep Z-sections attached to a 26 ga. roof sheet by using a No. 14 self-tapping screw.

Empirical Equation

Results of the parametric study indicated that the more significant variables affecting the rotational stiffness are the purlin thickness, sheet thickness and fastener type and location. Therefore, tests were conducted to evaluate the "F" factor for typical Butler Manufacturing Company roof systems.

This test program was executed using Z-sections having a thickness of either 1.55 mm or 3.05 mm. The roof panels were either .65 mm or .50 mm steel or .66 mm aluminum sheets. Screw fasteners were of the self-drilling and self-tapping type. A self-clinching rivet was also employed. All fasteners were located at the center of the flange.

Figures 9 and 10 graphically depict the load-deflection characteristics for the various test specimens. Based upon a regression analysis, the "F" factor represented by Equation 1 is 2.39 pounds per inch of member length per inch of horizontal deflection (10.63 N/mm/mm), and the corresponding factor for Equation 2 is 3.60 lb/in/in (16.01 N/mm/mm).

A linear variation, with thickness, was assumed and Equation 3 was developed for the stiffness, or "F" factor, for all values of purlin thickness between 1.55 mm and 3.05 mm,

$$\text{"F"} = 20.41\ (t - .061) + 2.3 \qquad (3)$$

Equation 3 yields a value of "F" in units of lb/in/in where the purlin thickness t, is in units of inches.

Conclusion

Based upon the test results discussed herein, the numerical value of the rotational stiffness or "F" factor was shown to be primarily dependent upon the purlin thickness, roof sheet thickness and fastener type and location within the flange width. An equation was presented for computing the "F" factor for a typical metal building roof system.

References

1. Haussler, R. W., and Pabers, R. F., Connection Strength in Thin Metal Roof Structures, Proceedings, Second International Specialty Conference on Cold-Formed Steel Structures, University of MO-Rolla, October 1973.

2. Observer's Report, Determination of Rotational Restraint Factor "F" for Panel to Purlin Rigidity, MRI Project No. 7105-G, Midwest Research Institute February 1981.

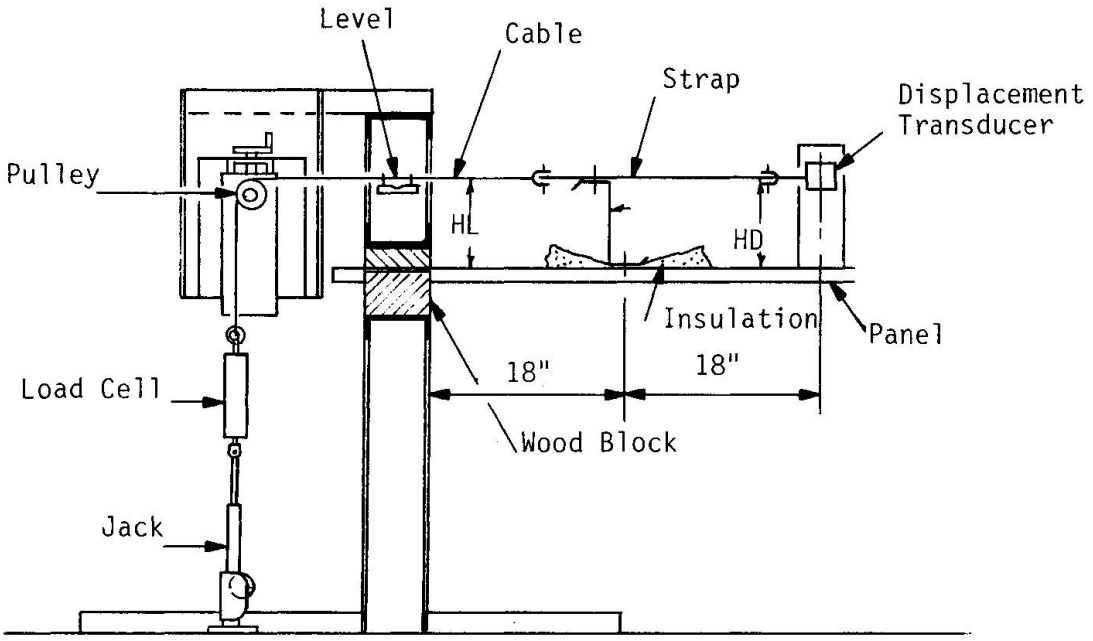

Fig. 1 - Test Apparatus

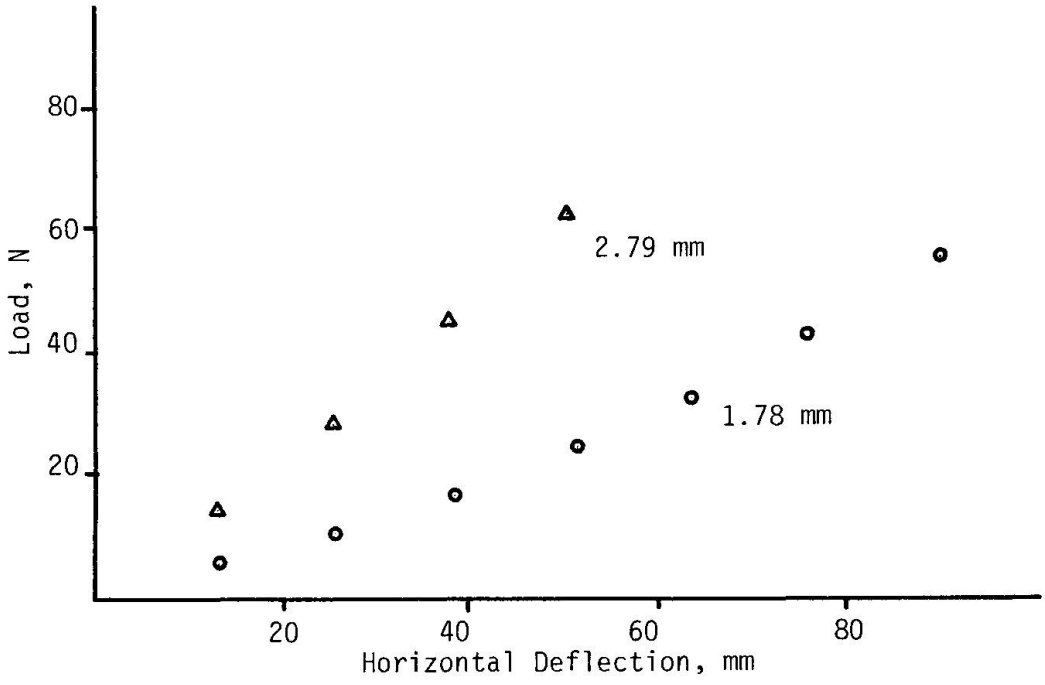

Fig. 2 - Affect of Purlin Thickness

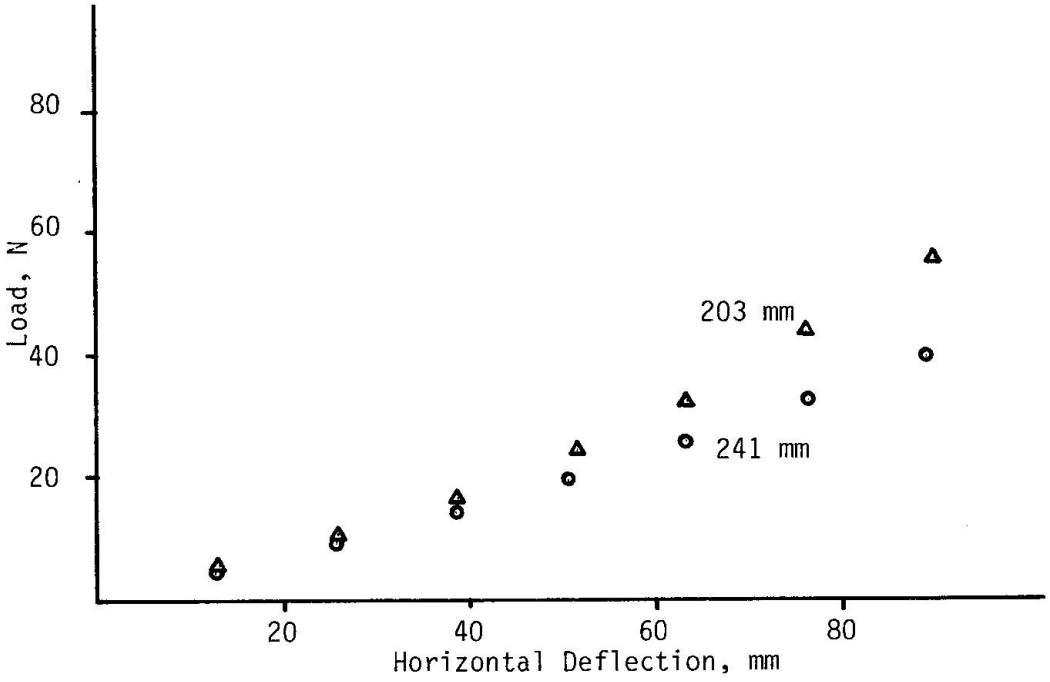

Fig. 3 - Affect of Purlin Depth

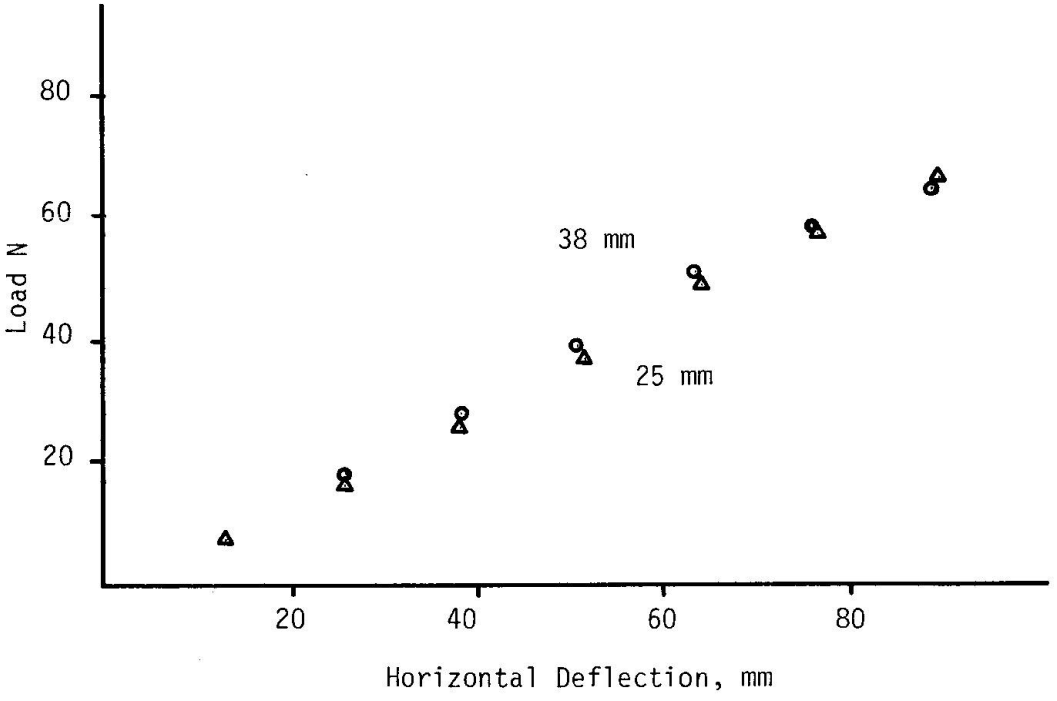

Fig. 4 - Affect of Panel Depth

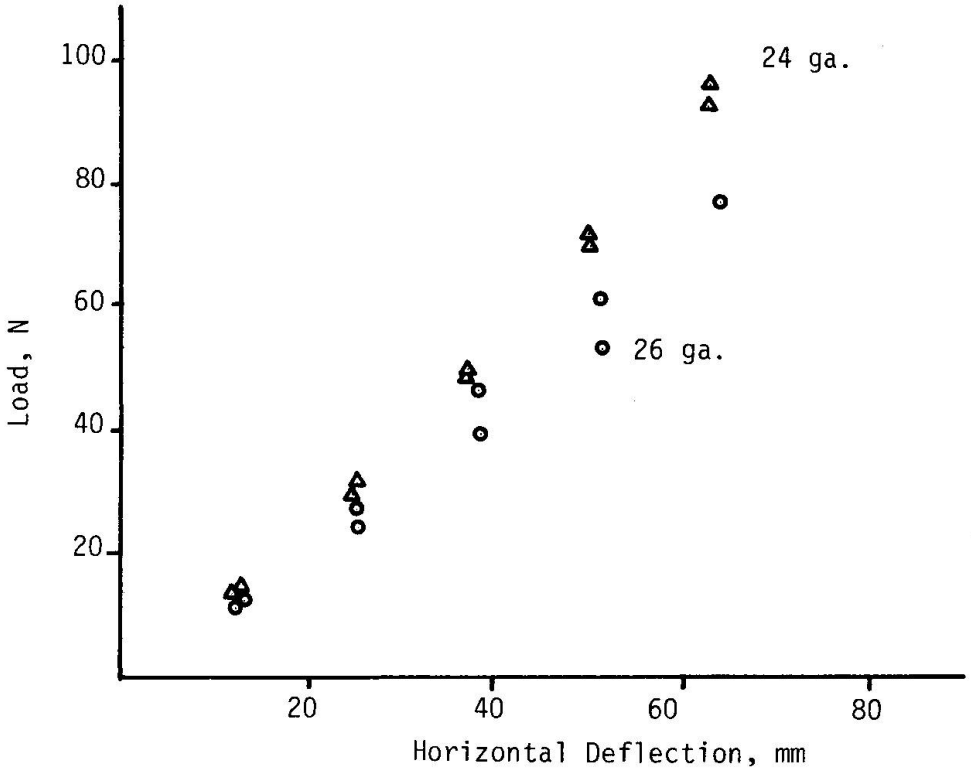

Fig. 5 - Panel Thickness Affect

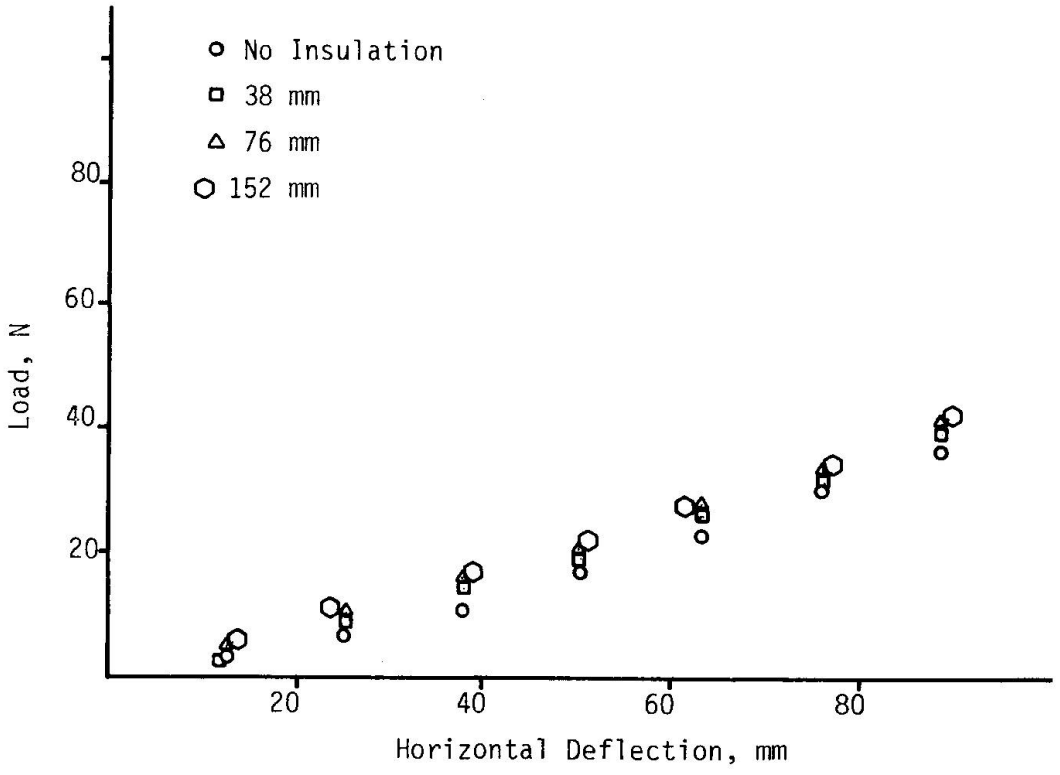

Fig. 6 - Affect of Insulation Thickness

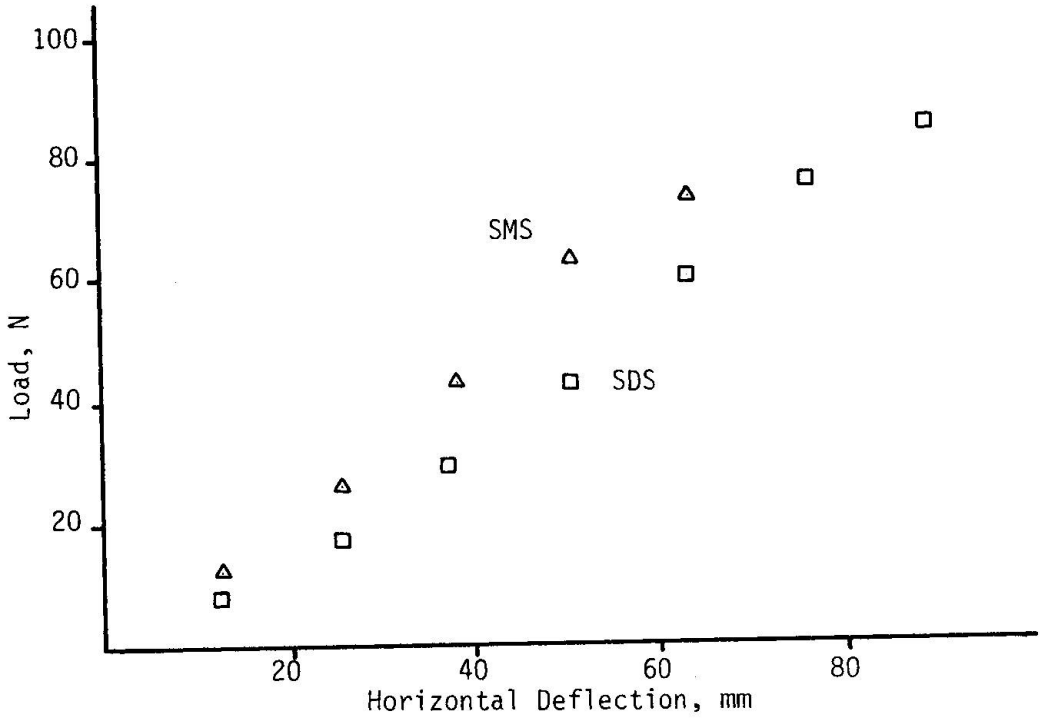

Fig. 7 - Affect of Fastener Type

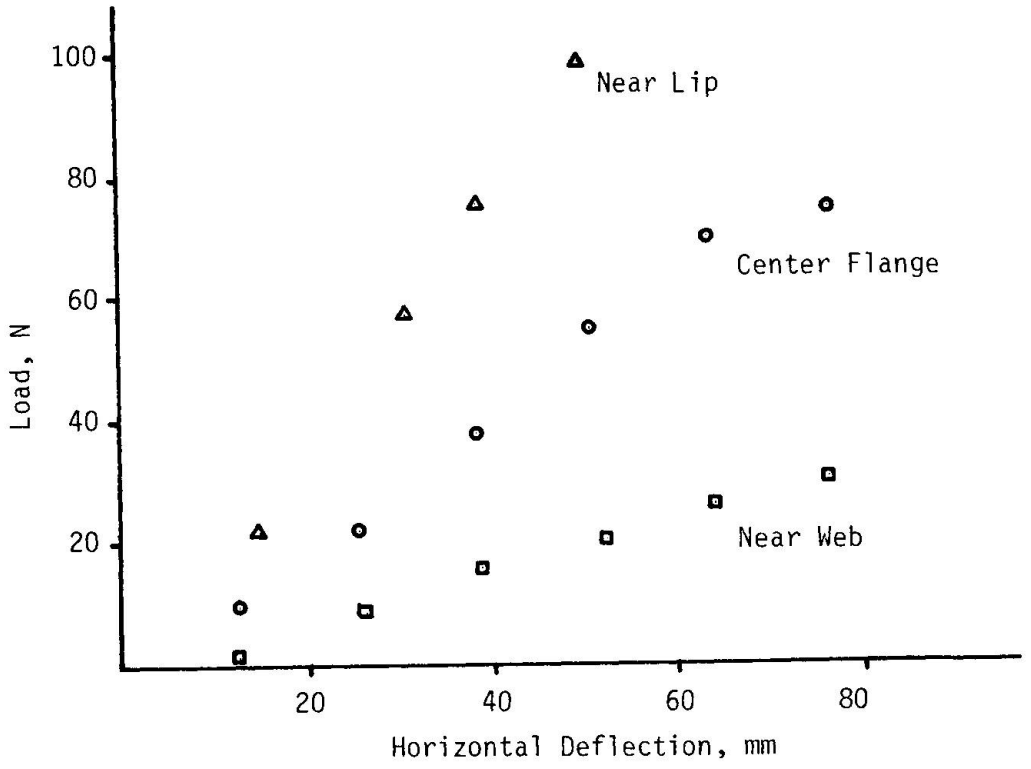

Fig. 8 - Affect of Fastener Location

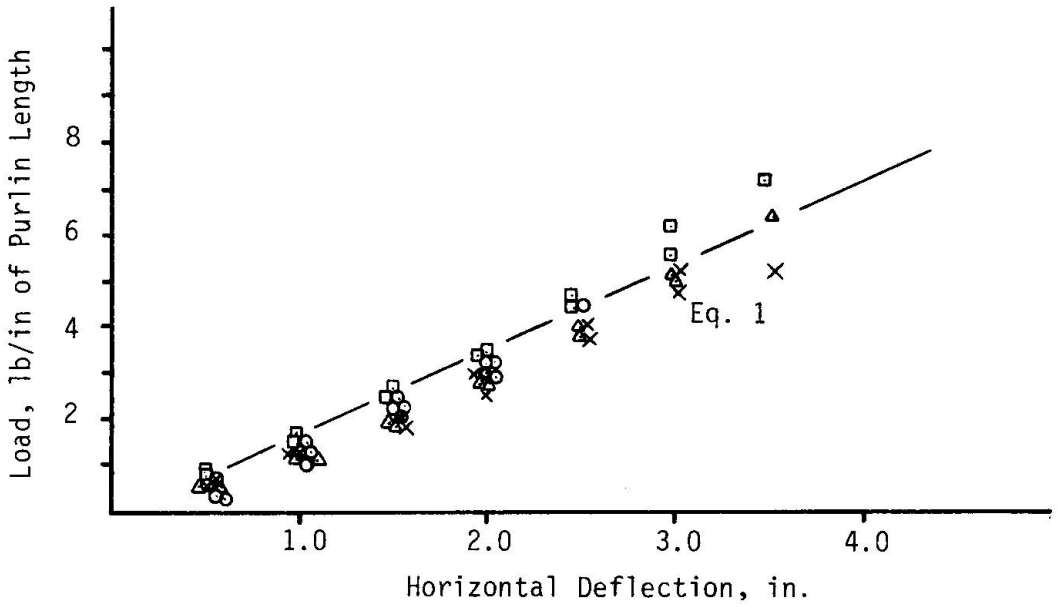

Fig. 9 - "F" for Typical Roof Systems Having .061" Purlin

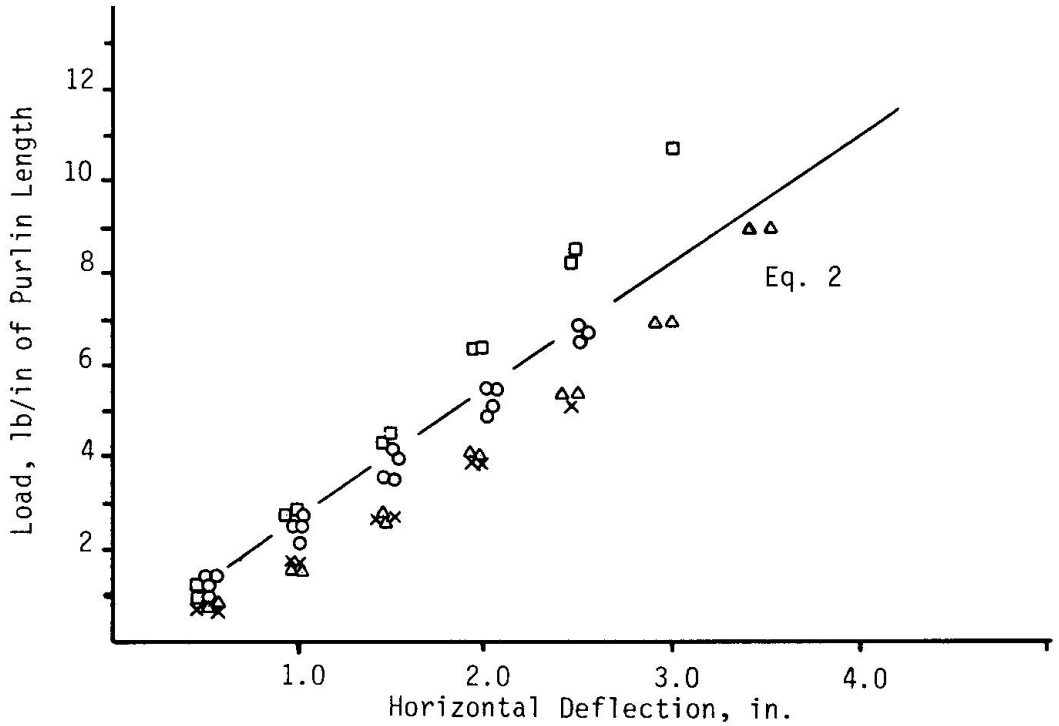

Fig. 10 - "F" for Typical Roof Systems Having .120" Purlin

Study of Thin-Walled Metal Building Roof Systems Using Scale Models

Etude des toitures métalliques à parois minces par l'utilisation de modèles réduits

Modellversuche an dünnwandigen Metalldachsystemen

Thomas M. MURRAY
Professor
Univ. of Oklahoma
Norman, OK, USA

Thomas M. Murray received his engineering degrees from Iowa State University, Lehigh University and the University of Kansas. He is currently Professor-in-Charge of the Fears Structural Engineering Laboratory, University of Oklahoma.

Venkatesh SESHAPPA
Former Research Assist.
Univ. of Oklahoma
Norman, OK, USA

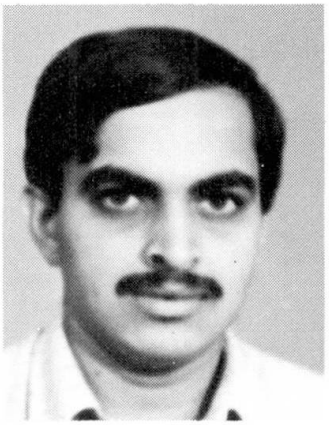

Venkatesh Seshappa received his Master of Science degree in Structural Engineering from the University of Oklahoma in 1985. He is currently a consulting structural engineer in Oklahoma City, OK.

SUMMARY

This paper presents the results of an extensive investigation on the use of quarter scale models to study the behavior of thru-fastener, metal building roof systems supported by Z-purlins and subjected to gravity loading. The objective of the study was to develop and verify methods for scale modeling of such systems. Experimental results are compared to analytical predictions and identical full-scale tests. Conclusions are made concerning the applicability of scale models for thin-walled metal structures research.

RÉSUMÉ

Cet article présente les résultats d'une enquête approfondie concernant l'utilisation des modèles à l'échelle un:quatre, pour étudier le comportement des toitures métalliques supportées par des pannes en tôle mince en forme de Z et soumises à des charges de gravité. Le but de cette étude était de développer des méthodes de modèlisation pour ce genre de structures, et de les vérifier. Les résultats expérimentaux sont comparés à ceux d'essais en vraie grandeur et à des prévisions analytiques. Les conclusions données concernant l'applicabilité du modèle réduit à l'étude expérimentale des structures en tôle métallique à parois minces.

ZUSAMMENFASSUNG

Die Ergebnisse einer umfassenden Untersuchung über die Anwendung von Modellen im Massstab 1:4 zum Studium des Verhaltens von Metalldachsystemen mit Z-Pfetten und unter Schwerkrafteinfluss werden vorgestellt. Das Ziel der Untersuchung war, Methoden für das massstabsgerechte Modellieren solcher Systeme zu entwickeln und zu prüfen. Experimentelle Ergebnisse werden mit analytischen Vorhersagen und den Resultaten identischer Tests an Tragwerken im Massstab 1:1 verglichen. Folgerungen über die Anwendbarkeit von massstäblichen Modellen für Untersuchungen von dünnwandigen Metalltragwerken werden gezogen.

1. INTRODUCTION

An extensive investigation on the use of quarter scale models to study the behavior of thru-fastener, metal building roof systems supported by Z-purlins and subjected to gravity loading is summarized here. A complete description of the research is found in Ref. [1]. The principal objective of the study was to develop and verify methods for scale modeling of such roof systems. Special fabrication, assembly and testing techniques were used to construct and test the model systems, which ranged in size from single span, two purlin line to three continuous span, six purlin line systems. Effects of different deck-to-purlin fastening systems and deck diaphragm stiffness were also studied.

Results from forty-three model tests are summarized and compared to some identical prototype tests and to analytical predictions. Comparisons include failure mode, failure load, vertical deflections and magnitude of restraint forces. Results from tests where edge stiffener orientation was varied are also presented herein.

2. MODELING AND METHODOLOGY

2.1 Z-Purlins

The Z-purlins were fabricated using 24 gage (0.6 mm) steel sheet material having a nominal yield stress of 345 MPa. The sheet was first sheared to the required width (developed length of the purlin cross-section) and then bent into a Z-shape without edge stiffeners using a press brake. The essential steps are shown in Figure 1. The edge stiffener was bent to shape by hammering against a mandrel machined from a steel block. The edge stiffener formed by this method was found to be accurate in length and in orientation and free of local distortions. Purlin depths ranged from 152 mm to 305 mm. The span length for all tests was 1.52 m. Standard ASTM tensile test coupons were cut from virgin sheet material and tested. The average measured yield stress was 357 MPa.

2.2 Roof Deck and Fasteners

Four types of panels were used in the test program. A corrugated fiber glass panel was used in one test. The system failed due to tearing of the panel at fastener locations and this panel type was discarded. Either commercially available corrugated aluminum panels or corrugated steel panels were used in all other tests. A steel "sine wave" sheet having 13 mm deep corrugations was used in most tests.

Two types of fasteners were used to attach panels to the purlin flanges: self-drilling fasteners or machine screws and nuts. All panels were fastened to the purlin flange in every corrugation valley. For multiple purlin tests, the panel-to-panel connection (sidelap fastening) was made using machine screws spaced at 150 mm on center.

Initially, shear (diaphragm) stiffness of the deck and the type of fasteners used were thought to effect the behavior of the system. The panels and the fasteners could not be accurately scaled because of the availability of material and other limitations. Hence, it was decided to conduct tests with combinations of several commercially available panels and fasteners to study the effect of these components on the behavior of the system.

Two tests of two purlin line, single span systems, one with corrugated steel panels and the other with corrugated aluminum panels, were conducted. The failure mode for both tests was local buckling of the compression edge

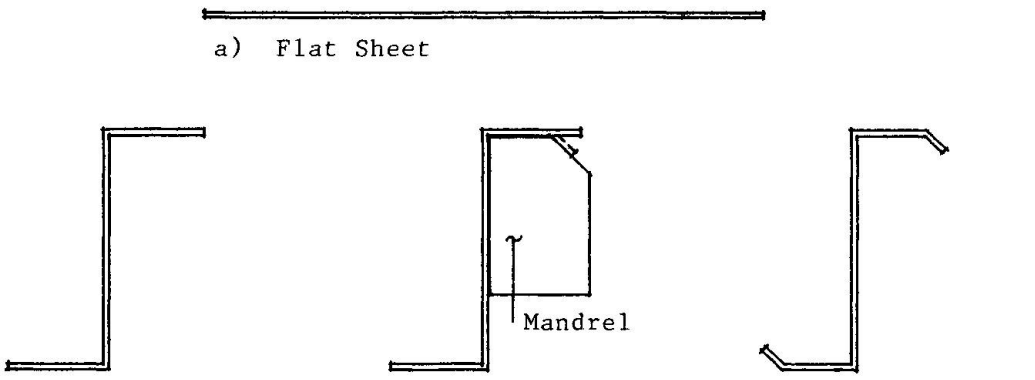

a) Flat Sheet

b) Press Broken Flanges

c) Bending of Edge Stiffener Against Mandrel

d) Finished Purlin

Fig. 1 Z-Purlin Fabrication Procedure

stiffener/flange/web near midspan. The failure load for the former test was 1.12 kN/m and the latter test, 1.04 kN/m. Forces in dynamometers placed at the supports and used to stabilize the system were 18.3% of applied working load for the steel panel test and 18.7% for the aluminum panel test. The corresponding percentages at failure were 19.5% and 19.2%. Since the diaphragm stiffnesses of the two systems were considerably different, it was decided to use steel panels in all further testing for economic reasons.

Analyses to determine restraint forces in systems with widely varying panel shear stiffnesses were conducted by Elhouar [2]. He found that panel stiffness has little effect on roof system behavior if the shear stiffness is greater than 1.82 kN/m. (A typical metal building thru fastener roof system exhibits a shear stiffness in excess of 1.22 kN/m). A shear stiffness test using the selected steel panel was conducted and was found to be 3.04 kN/m.

The effect on the behavior of the system due to the fastener type used to attach the selected steel panel to the purlin was also studied. Two identical, single span, two purlin line tests were conducted; one using machine bolts and the other using self-drilling fasteners.

Again, the failure modes for the two tests were identical. The failure loads were 1.12 kN/m and 1.16kN/m and restraint forces were 18.3% and 17.9% of the applied working load for the machine bolted and self-drilling fastenered systems, respectively. Since the test results showed that the effect of fastener type was not significant, machine bolts and nuts were used for most test setups because of ease of fabrication.

2.3 Test Setup and Testing Procedures

The test setups consisted of simulated building rafters and the purlin/deck assemblies. Support conditions along a purlin line consisted of rollers except at one location where a simulated pinned support was used. The pinned support consisted of a roller between two plates with a groove in each plate. One plate was attached to the bottom flange of the purlin; the second plate was attached to the rafter. The roller support was similar except the plates were flat allowing free movement of the roller.

Restraint braces were supplied at the rafter lines, at midspan or at span one-third points in the test setups. These braces were fabricated from small diameter, steel hydraulic brake line normally used in automobiles. Universal joints were used at each end to eliminate rotational restraint at the

connection. Selected braces were strain gaged and calibrated for use as dynamometers to measure restraint forces.

Instrumentation consisted of the dynamometers and linear displacement transducers to measure vertical deflections and horizontal displacements of the top and bottom purlin flanges. For the two purlin line tests, gravity loading was applied using clay brick masonry units. A small suction box was constructed to test multiple purlin line assemblies.

3. EXPERIMENTAL RESULTS

3.1 Program Objectives and Test Matrix

Tests were conducted to:

(1) Verify that scale models can be used to accurately study the behavior of full scale roof systems.

(2) To calibrate a proposed computer model to predict restraint forces.

(3) To study the effect of edge stiffener angle on purlin strength.

To accomplish the above, a total of 43 model tests and twelve full scale tests were conducted. All tests were conducted with the purlin flanges facing in the same direction. Restraint braces were provided at the rafter lines, at the midspans or at the one-third span locations. In the following discussion, the restraint braces at the rafter locations will be referred to as torsional braces.

3.2 Comparison with Full Scale Test Results

The failure mode for all the full scale and model tests was local edge stiffener/flange/web buckling near midspan in all single span and some multi-span tests or near the exterior end of the lapped portion in continuous three span tests. The shape of the locally buckled purlins was identical in all tests. In both the model and prototype tests, measured vertical deflections were linear with respect to loading, but exceeded predictions, using standard strength of material or stiffness analysis techniques, by approximately 15% until near failure when the deflections rapidly increased.

Experimental failure loads for 34 single span tests were compared to predicted failure loads based on cross-section strength calculated using local buckling criteria in the current AISI specification [3]. The average predicted-to-failure load ratio was 1.069 with a standard deviation of 0.087. A similar study for 85 full scale tests found this ratio to be 1.141 with a standard deviation of 0.199 [4].

3.3 Comparison with Predicted Restraint Forces

In a companion study [2,4], a direct stiffness, computer based model was developed to predict restraint forces in single or multiple span, multiple purlin line, Z-purlin supported, gravity loaded roof systems. Full scale tests were initially used to calibrate the model. Sixteen quarter scale tests were then conducted to further verify the adequacy of the analytical model. The test matrix consisted of two and six purlin line, single and three continuous span configurations. Each of the previously described restraint bracing configurations were used with each of the purlin line/span configurations.

Figure 2 shows typical applied load versus restraint force results. In these plots the solid line represents the predicted relationship and the dashed line, the experimentally measured relationship. The results shown in Figure 2(a) are from a two purlin line, single span test with restrait braces at the purlin ends (torsional braces). Similar results are shown in Figure 2(b) for a

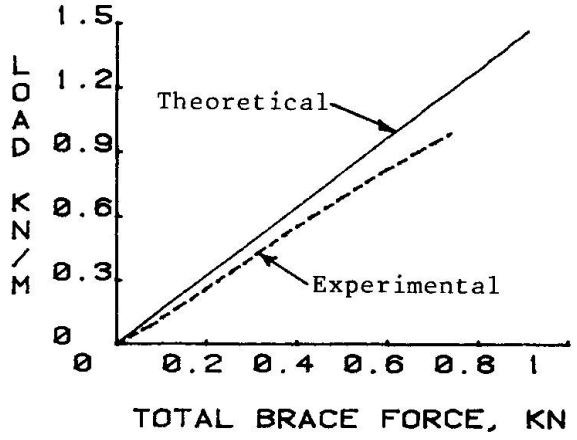

a) Two Purlin Line, Simple Span, Torsional Restraints

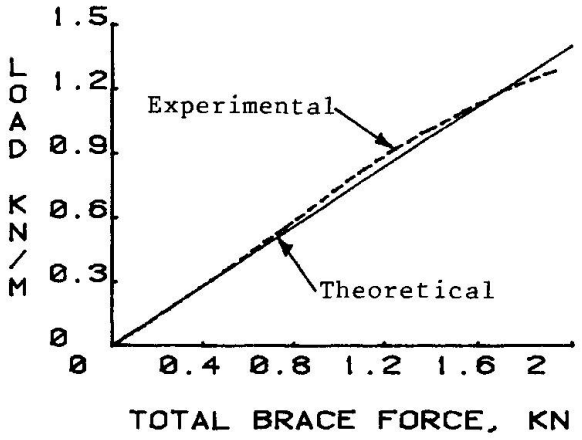

b) Six Purlin Line, Simple Span, Torsional Restraints

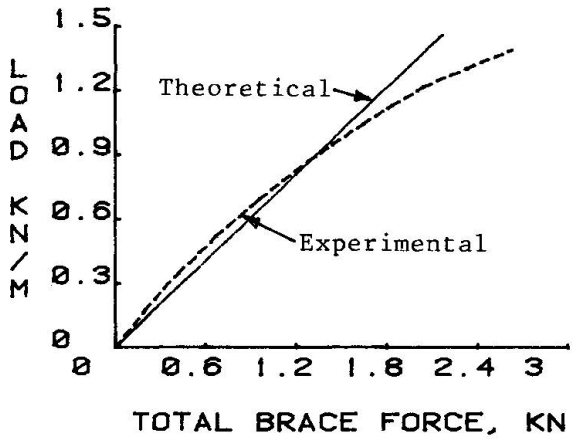

c) Two Purlin Line, Three Spans, Midspan Restraints

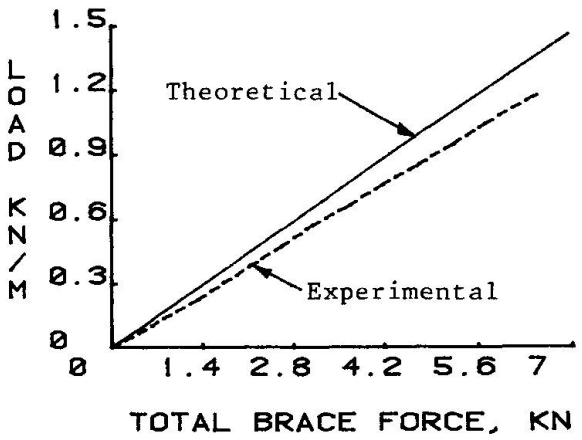

d) Six Purlin Line, Three Spans, Third Point Restraints

Fig.2 Applied Load Versus Brace Force Relationships

six purlin line, single span, torsional brace test. Figure 2(c) shows results for a two purlin line, three continuous spans test with restraints at each midspan. Finally, results are shown in Figure 2(d) for a six purlin line, three continuous spans configuration with third point restraint braces.

3.4 Effect of Edge Stiffener Angle

A series of tests was conducted to study the effect of edge stiffener orientation on the ultimate flexural strength of Z-purlins. Seven, two purlin line, single span tests were conducted using identical purlins except for edge stiffener orientation. The angle of orientation from the horizontal of the edge stiffeners was varied in 15° increments from 30° to 90°.

The ratios of the experimental ultimate loads W_u to the predicted ultimate loads W_p are shown in Table 1. The ratio increased from 78.1% for the 30° lip angle test to 97.5% for the 75° lip angle test. For the three 90° lip angle test, the results were 92.2%, 86.9% and 90.2%.

Lip Angle	W_u/W_p %	% Brace Force at Working Load		% Brace Force at Failure	
		Predicted	Measured	Predicted	Measured
30°	78.1	22.60	20.9	22.60	21.2
45°	90.3	21.70	18.3	21.70	19.5
60°	95.1	22.00	18.1	22.00	18.4
75°	97.5	21.30	17.6	21.30	17.2
90°	92.2	20.10	20.1	20.10	21.1
90°	86.9	20.27	28.6	20.27	31.0
90°	90.2	21.72	18.3	21.72	19.5

W_p = Predicted Ultimate Load

W_u = Failure Load

Table 1 Summary of Results for Lip Angle Test Series

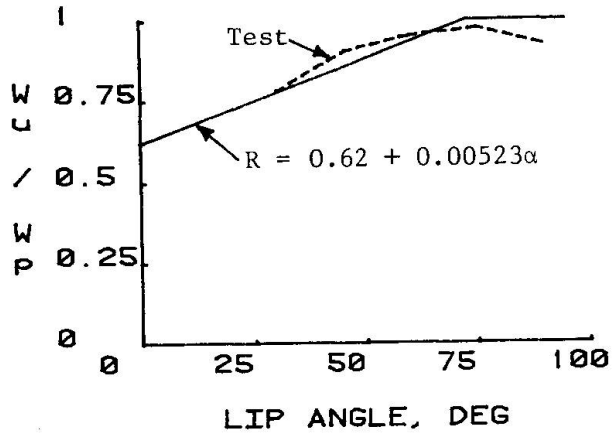

Fig. 3 Strength Ratio versus Lip Angle

A plot of W_u/W_p versus lip angle is found in Figure 3. The solid line is a prediction equation developed from prototype tests [5]

$$R = 0.62 + 0.00523\alpha \qquad (1)$$

where R = reduction due to edge stiffener inclination and α = orientation angle measured from the horizontal, in degrees.

Restraint forces were both measured and predicted for the tests. Except for the tests using the 90° edge stiffener inclination, the measured restraint force was slightly less than predicted as seen from Table 1. For one of the 90° tests, the measured forces were considerably greater than predicted.

4. CONCLUSIONS

The results of the study reported here show that cold-formed structural members can be effectively studied using quarter scale models. For the thru fastener, metal building type roof systems studied, it was found that the roof deck and fastener systems can be modeled using commercially available materials

and do not have to be accurately scaled. Full scale and model test results, including failure mode and failure load, were found to compare very well when the typical scatter of data found in thin-walled structural research is considered.

Evaluation of costs, effort, loading mechanisms, test setups and other variables shows that model based research of cold-formed structures is a desirable alternative to full scale testing.

5. ACKNOWLEDGEMENTS

The research reported in this paper was sponsored by the Metal Building Manufacturers Association and the American Iron and Steel Institute.

REFERENCES

1. SESHAPPA, V. and MURRAY, T.M., Experimental Studies of Z-Purlin Supported Roof Systems Using Quarter Scale Models. Research Report FSEL/MBMA 85-02 submitted to the Metal Building Manufacturers Association and the American Iron and Steel Institute, May 1985, 81 pages.

2. ELHOUAR, S. and MURRAY, T.M., Prediction of Lateral Restraint Forces for Z-Purlin Supported Roof Systems. Research Report FSEL/MBMA 85-03 submitted to the Metal Building Manufacturers Association and the American Iron and Steel Institute, May 1985, 107 pages.

3. Specification for the Design of Cold-Formed Steel Structural Members. American Iron and Steel Institute, September 1980.

4. MURRAY, T.M. and ELHOUAR, S., Stability Requirements of Z-Purlin Supported Conventional Metal Building Roof Systems. 1985 Annual Technical Session Proceedings, Structural Stability Research Council, 1985.

5. JOHNSON, DONALD, "Private Communication," May 1984.

Leere Seite
Blank page
Page vide

Stability of Column-Girt-Diaphragm Systems in Industrial Buildings

Stabilité des systèmes poteaux-entremises-diaphragme dans les bâtiments industriels

Stabilität des Systems Stütze-Riegel-Wandscheibe in Industriegebäuden

Esenam AKOUSSAH
Graduate student
Laval University
Québec, PQ, Canada

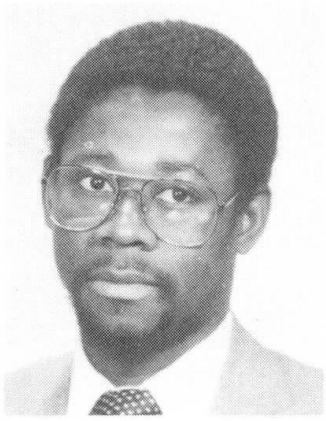

Esenam Akoussah received his Civil Engineering and Master's degrees at the Ecole Polytechnique of Montreal. He is presently a Ph.D. candidate at Laval University in Québec City, since the autumn of 1982.

Denis BEAULIEU
Professor
Laval University
Québec, PQ, Canada

Gouri DHATT
Professor
Laval University
Québec, PQ, Canada

André PICARD
Professor
Laval University
Québec, PQ, Canada

SUMMARY

Two finite element models to study column-girt-diaphragm systems are presented. The first one is a general model for all components; the second is a simplified model using beam elements for the column and equivalent elastic elements for the other components at girt level. The simplified model is mostly oriented towards practical design. The numerical results show that column resistance not only depends on the physical properties of the assemblage elements but is significantly influenced by the arrangement of these elements.

RÉSUMÉ

L'article présente deux modèles par éléments finis pour l'analyse des systèmes poteaux-entremises-diaphragme. Le premier est un modèle général où toutes les composantes sont modélisées tandis que le second, qui a été développé principalement pour les calculs pratiques, ne modélise que le poteau alors que les autres pièces du système sont remplacées par des ressorts équivalents au niveau des entremises. Les résultats numériques montrent que la capacité portante du poteau dépend non seulement des propriétés physiques des éléments du système, mais aussi de leur arrangement.

ZUSAMMENFASSUNG

Zwei Systemmodelle werden mit Hilfe der Finiten-Element-Methode formuliert. Das erste ist ein allgemeines Modell, das alle Systemteile einzeln erfasst. Das zweite ist ein vereinfachtes Modell, das ein Balkenelement für die Stütze und äquivalente elastische Elemente für die übrigen Teile benutzt. Das vereinfachte Modell ist für die Anwendung in der Ingenieurpraxis bestimmt. Die numerischen Resultate zeigen, dass die Stützenfestigkeit nicht nur von den Materialeigenschaften der Systemteile, sondern auch wesentlich von der Art ihrer Anordnung beeinflusst wird.

1. INTRODUCTION

Corrugated steel sheets generally attached to girts are frequently used as cladding in industrial buildings. The girts are either connected to the column web or external flange based on physical or economical considerations. For light columns, girts are generally attached to the web at the center of gravity of the column section (Fig. 1-a). For deep columns, girts are either attached to the web near the external flange, or simply lie outside the external flange and are attached to it (Fig. 1-b,c). The internal flange of deep columns is generally braced by means of diagonal elements attached to girts in order to reduce, if not eliminate, the possibility of column torsional buckling. In such column-girt-diaphragm (C.G.D.) systems, the lateral support provided by the diaphragm at girt level may substantially increase the column buckling resistance. In practical design, the girt-diaphragm system is either assumed fully rigid or is completely neglected when evaluating the column resistance. Due to the complex interaction existing between the different components of C.G.D. systems, it is necessary to use numerical models such as finite element models to correctly assess the stabilizing action of the girts and the diaphragms.

Some early designers have taken account of the influence of girt-diaphragm systems through column restraints [6,7,8,12]. These were represented by discrete or continuous systems whose equivalent rigidity was defined by some calibration criteria. Apparao, Errera and Fisher [2,3] carried out research on the stabilizing action of girt-diaphragm systems and developed design formulas for simple loading and boundary conditions.

The purpose of this paper is to present a tri-dimensional finite element model that simulates the behaviour of the global physical system in ordre to evaluate the load carrying capacity of the columns. Based on the numerical results obtained from this model, we developed a simplified model for practical design. A detailed numerical experimentation was undertaken to assess the efficiency and reliability of the simplified model.

2. FINITE ELEMENT MODEL OF C.G.D. SYSTEMS (FEM)

2.1 Linear buckling model: basic assumptions

The buckling model is obtained by equating the linearized expression of the second variation of the total potential energy to zero. It is also interpreted as the perturbed expression of the virtual work. The corresponding variational expression W may be written as follows:

$$\Delta W = \int_V (\delta e_{ij}\, \Delta\sigma_{ij} + \lambda_{cr}\, \sigma_{ij}\, \Delta\, \delta\eta_{ij})\, dV = 0 \qquad (1)$$

where $e_{ij} = \frac{1}{2}(u_{i,j} + u_{j,i})$: linear part of Green-Lagrange strain

$\eta_{ij} = \frac{1}{2} u_{k,i} \cdot u_{k,j}$: nonlinear quadratic part

with $u_{i,j}$ representing the j^{th} spatial derivative of displacement component u_i

λ_{cr} = critical load factor for the stress state σ_{ij}

$\Delta\sigma_{ij}$ = perturbed stress due to the perturbation Δe_{ij}

$\Delta(\delta\eta_{ij})$ = perturbed expression of the first variation of nonlinear terms of Green-Lagrange strain (linear in $\Delta u_{i,j}$)

The finite element discretization of Eq. (1) leads to the following usual eigenvalue problem:

$$[K]\{\Delta u_n\} = \lambda_{cr}[K_g]\{\Delta u_n\} \quad (2)$$

where $[K]$ is the rigidity matrix at the state $[\sigma_{ij}]$ and $[K_g]$ is the geometrical matrix; λ_{cr} and Δu_n represent the set of eigenvalues and eigenvectors, respectively.

The solution of Eq. (2), using for example the subspace iteration scheme, leads to the set of lowest values of the critical load factors λ_{cr} [4]. Equation (1) may be adapted to structures with plastic deformations requiring a proper calculation of σ_{ij} and estimation of λ_{cr} close to unity. In this study, we assume that the structural behaviour is elastic up to buckling thus allowing the definition of buckling stress $\lambda_{cr}\sigma_{ij}$ in terms of a certain initial state of stresses σ_{ij}.

The model considers the contribution of all the components of the C.G.D. system (column, girts, diaphragm, connections and diagonal braces) when evaluating the rigidity matrix [K] of the system. The state of stresses σ_{ij} is assumed to be equal to zero for all elements except the column since we are mainly interessed in getting buckling load estimates for column stress states. It should be noted that the desired buckling model must be properly included in the perturbed configurations $\Delta(\delta\eta_{ij})$.

2.2 Column and girt modeling

Column and girt components are represented as tri-dimensional beam elements (Fig. 2) including axial, bending and torsional deformations. The displacement components u, v, w (u_1, u_2 and u_3) of a material point (x, y, z) are defined as follows, making use of the approximations of Vlassov [13] and Timoshenko [12] for thin-walled beams which are generalizations of Bernoulli-Navier hypotheses (thin beams) and St-Venant hypotheses for pure torsion:

$$\begin{aligned} u(x,y,z) &= u_o(z) - (y-y_o)\,\phi(z) \\ v(x,y,z) &= v_o(z) + (x-x_o)\,\phi(z) \\ w(x,y,z) &= w_c(z) - x\,u_o'(z) - y\,v_o'(z) + \omega(s)\,\phi'(z) \end{aligned} \quad (3)$$

where u_o, v_o are transverse displacements at the shear axis, w_c the axial displacement along the neutral axis and ϕ the torsional rotation. The quantities u_o', v_o' and ϕ' are derivatives with respect to z. The warping function is defined as:

$\omega = -\int_o^s r_o(s)\,ds$, where s is the sectional coordinate.

The linear strain components simply reduce to $\varepsilon_z = w_c' - xu_o'' - yv_o'' + \omega(s)\phi''$ and $\gamma_{zs} = 2n_h\phi'$ [10]. By using the displacement relations (3) and choosing the corresponding $\Delta(\delta n_{ij})$ for a known σ_{ij}, we obtain the column and girt contributions to the [K] and $[K_g]$ matrices. If σ_{ij} is zero in the girt, the corresponding geometrical matrix $[K_g]$ is equal to zero.

2.3 Corrugated steel sheet modeling

We simulated the behaviour of corrugated steel sheets by a flat shell triangular element (DKT type) (Fig. 3) in order to consider equivalent orthotropic membrane and bending behaviour. More details are given in references [5,11]. Since the buckling load corresponds to a state of stresses in the column, the sheet steel cladding only contributes to the rigidity matrix [K] with corresponding $[K_g] = 0$.

2.4 Connection and brace modeling

In order to insure geometrical compatibility among the various eccentric components, special connection elements were used (Fig. 4) to introduce these constraints in a routine manner. The stiffness properties (K_x, K_y, K_z, $K_{\theta x}$,

$K_{\theta y}$, $K_{\theta z}$) of the connection elements (Fig. 4-a) may be adjusted to take account of flexible connections between girts and columns and between the diaphragm and the supporting elements. The diagonal braces are represented by the same type of elements and can be attached to any point on the column section (Fig. 4-b) even though the column is simulated by a linear finite element. More details are given in reference 1 on the development of connection and brace elements.

3. SIMPLIFIED MODEL (SM)

It is interesting to develop a simplified model for practical applications on micro-computers. The results of the general finite element model (FEM) may be used to define the accuracy of the simplified model (SM). In the first version of this model only the column is represented by a set of beam elements [9]. The other components of the system (diaphragm, girts, connections, braces) are modeled by equivalent elastic elements at girt level. The properties of these elements include the flexural rigidity of the girt about its strong axis, the girt-to-column connection rigidity and the shear rigidity of the diaphragm. The influence of braces was taken into account by increasing the flexural rigidity of girt elements. The diaphragm is assumed to act in simple shear by providing a rigidity evaluated from its effective shear modulus.

4. NUMERICAL EXAMPLES

4.1 Experimental test results and influence of girt-diaphragm eccentricity

Three tests were conducted at Cornell University to determine the buckling load (P_{cr}) of columns in C.G.D. systems. Details of these tests can be found in Ref. 2 . The test results are compared in Table 1 to the analytical results obtained from the general finite element model (FEM) and the simplified model (SM). The analytical results are less than 1% different from test results GT-2 and GT-3. However, there is a significant difference with the GT-1 test for which a perfectly pinned girt-to-column connection was considered. This difference may be attributed to the fact that it is difficult to realize a perfectly pinned connection in laboratory. The buckling load is highly sensitive to the rotational rigidity of the girt-to-column connection, as seen from test GT-3.

Test no.	$K_{\theta y}$ [1] (kNm/rad)	e (mm) (Fig.1)	Experimental results (kN)	FEM (error) (kN)	SM (error) (kN)	Buckling mode
GT-1	0	152	78.7	64.3 (18%)	64.3 (18%)	flexural-torsional (fig. 5)
GT-2	10^{10}	254	165.9	164.3 (1%)	164.3 (1%)	flexural
GT-3	1.469	152	113.4	112.0 (1%)	112.5 (1%)	flexural-torsional

[1] $K_{\theta y}$ is the rotational rigidity of the girt-to-column connection with respect to the column longitudinal axis.

Table 1 Comparison of experimental and theoretical results

The influence on column buckling load of girt and diaphragm eccentricities with respect to the column shear center (e_1 and e_2, respectively, as shown in Fig.1), was studied with the general model for the above three cases. The results are

given in Table 2. The eccentricity of the girts with respect to the column shear center reduces the column buckling resistance in a significant manner for flexible girt-to-column connections. However, the buckling load for fully restrained connections is independent of the eccentricity of the girts for the cases studied.

e_2 (mm) (Fig.1)	e_1 (mm) (Fig.1)	GT-1 (P_{cr}/P_E)[2] FEM (kN)	GT-2 (P_{cr}/P_E) FEM (kN)	GT-3 (P_{cr}/P_E) FEM (kN)
e[1]	0	164.3 (1.0) (flexural)	164.3 (1.0) (flexural)	164.3 (1.0) (flexural)
62	$(e-e_2)$	106.9 (0.65) (flexural-torsional)	164.3 (1.0) (flexural)	164.3 (1.0) (flexural)
32.4	$(e-e_2)$	82.2 (0.50) (flexural-torsional)	164.3 (1.0) (flexural)	146.3 (1.0) (flexural-torsional)
15	$(e-e_2)$	71.6 (0.44) (flexural-torsional	164.3 (1.0) (flexural)	126.2 (0.77) (flexural-torsional)
0	e	64.3 (0.39) (flexural-torsional)	164.3 (1.0) (flexural)	112.0 (0.68) (flexural-torsional)

[1] e = 152 mm for the GT-1 and GT-3 tests and 254 mm for the GT-2 test.

[2] P_E = 164.3 kN is the critical load assuming flexural buckling between girts.

Table 2 Influence of eccentricities

4.2 Influence of diagonal braces

The sub-system shown in Fig. 6 was used to study the influence of diagonal braces. Two different diaphragm rigidities were considered together with perfectly pinned and highly rigid girt-to-column connections. The critical column flexural load, considering the unsupported length between girts, was 5514 kN. The results given in Table 3 show a good agreement between the two models. It is interesting to note that for relatively high values of the diaphragm effective shear modulus (G_{eff}), the diagonal braces provide an efficient torsional restraint even if the girts are pin-connected to the column. In the case of more flexible diaphragms, the critical flexural load was never reached.

5. CONCLUSION

Two finite element models have been presented to analyse column-girt-diaphragm systems. The first model (FEM) is applicable to a wide variety of C.G.D. systems, including those with openings, and is used in the present case for assessing the accuracy of the simplified model. The second is oriented towards design and can easily be supported by micro-computers. The results indicate that the two models are practically equivalent in the elastic domain for the problems considered. This implies, considering the assumptions retained in each model,

that the axial rigidity of the girts is negligible and that the axial and flexural stiffnesses of the cladding have no significant effect on the column buckling resistance.

The results also show that the critical buckling load of columns braced by girt-diaphragm systems is not only a function of the diaphragm shear resistance but also of parameters such as the girt-to-column connection rigidity, diaphragm and girt eccentricities, diagonal braces, and the flexural rigidity of the girts. Further developments are under way to include plastification, among others, in the finite element model.

Example	G_{eff} (MPa)	$K_{\theta y}$ (kN.m/rad)	Diagonal area $A(mm^2)$	FEM (P_{cr}/P_E) (kN)	SM (P_{cr}/P_E) (kN)	Buckling mode
CGD1	1000	0	0 (no brace)	2061 (0.37)	2071 (0.37)	flexural-torsional
CGD2	2300	0	0 (no brace)	2252 (0.41)	2264 (0.41)	flexural-torsional
CGD3	1000	0	216	4903 (0.89)	-	flexural-torsional
CGD4	2300	0	216	5514 (1.0)	-	flexural
CGD5	1000	10^{10}	216	4905 (0.89)	4876[1] (0.88)	flexural-torsional
CGD6	2300	10^{10}	216	5514 (1.0)	5514[1] (1.0)	flexural

[1] Diagonals are replaced by overlapped girts (Fig. 6-c).

Table 3 Influence of diagonal braces

6. REFERENCES

1. AKOUSSAH, E., BEAULIEU, D. et DHATT, G., "Etude par éléments finis de la stabilité des poteaux dans les bâtiments industriels", Rapport technique, dépt. de Génie civil, Université Laval, to be published.
2. APPARAO, T.V.S.R., "Problems in structural diaphragm bracing", Ph.D. Thesis, Report no 331, Cornell University, Ithaca, N.Y., 1968.
3. APPARAO, T.V.S.R., ERRERA, S.J. and FISHER, G.P., "Columns braced by girts and diaphragms", ASCE Journal of Structural Division (ST5), 1969.
4. DHATT, G. and TOUZOT, G., "The finite element method displayed", (Translated by Cantin, G.), John Wiley & Sons, London, 1984.
5. FAFARD, M. et BEAULIEU, D., "Etude par éléments finis de la stabilité de profilés formés par assemblage d'éléments plats dans l'espace", Rapport GCT-84-06, Dépt. Génie civil, Université Laval, déc. 1984.
6. FLINT, A.R., "The influence of restraints on the stability of beams", The Structural Engineer, 29, Sept. 1951.
7. HORNE, M.R. and AJMANI, J.L., "Stability of columns supported laterally by side-rails", Int. Journal Mech. Sci., 11, 1969.
8. KITIPORNCHAI, S. and RICHTER, N.J. "Elastic lateral buckling of I-beams with discrete intermediate restraints", The Inst. of Engineers, Australia CE20(2), 1978.

9. MASSICOTTE, B., BEAULIEU, D. et PICARD, A., "Effet des systèmes entremises-diaphragmes sur la stabilité des poteaux", Revue canadienne de Génie civil, 12 (3), sept. 1985.

10. NISHINO, F., KASEMSET, C. and LEE, S.L., "Variational formulation of stability problems for thin-walled members", Ingénieur-Archiv., 1973.

11. TALBOT, M. et DHATT, G., "Comparaison de deux éléments de coque fondés sur la formulation lagrangienne actualisée", Rapport technique, dépt. de Génie civil, Université Laval, to be published.

12. TIMOSHENKO, S.P. and GERE, J.M., "Theory of elastic stability", 2nd Ed., McGraw-Hill Book Co., Inc., 1961.

13. VLASSOV, V.Z., "Thin-walled elastic beams", (Translated from Russian), Israel Program for Scientific Translation, Jerusalem, 1961.

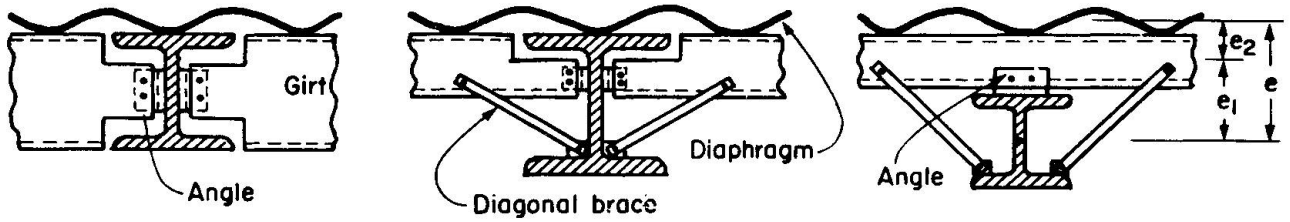

a) Light column *b) Deep column with girts between the flanges* *c) Girts outside the external flange*

Fig. 1 — Girt-to-column connections.

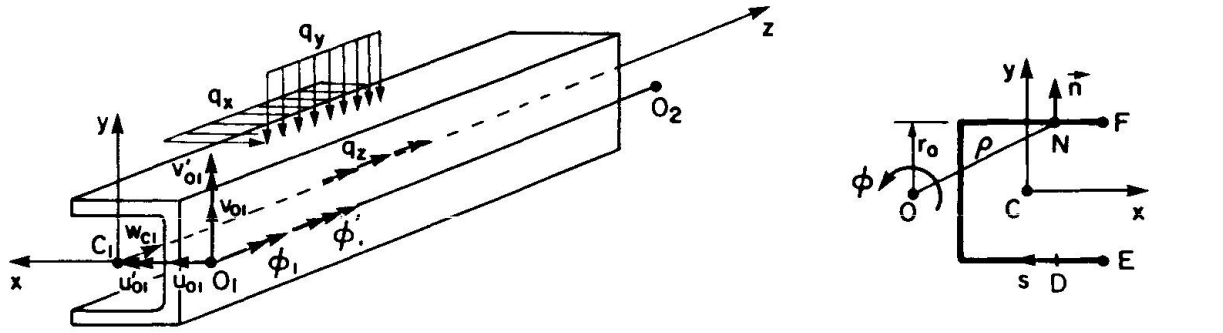

a) Degrees of freedom of the beam element *b) Thin-walled open cross section*

Fig. 2 — Tri-dimensional beam element (7 DOF per node).

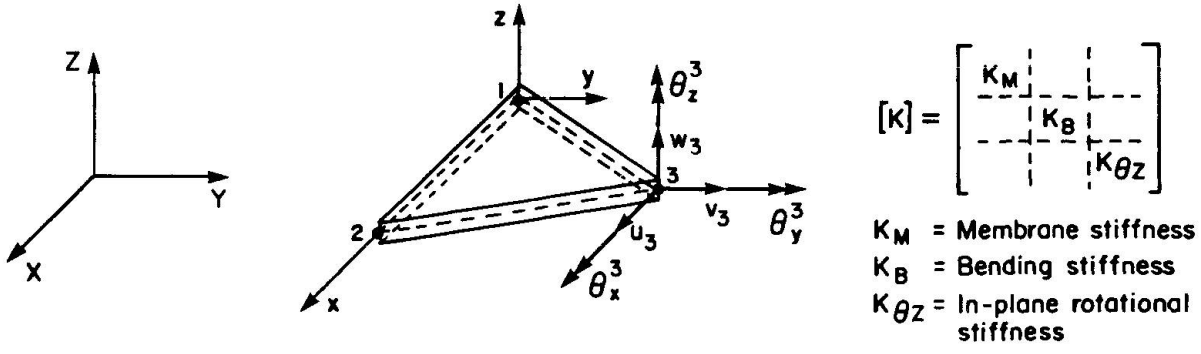

Fig. 3 — Orthotropic shell element (6 DOF per node).

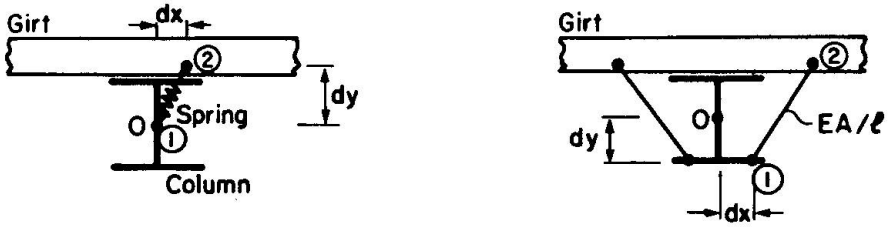

a) Girt-to-column spring b) Diagonal braces

Fig. 4 — Connection elements.

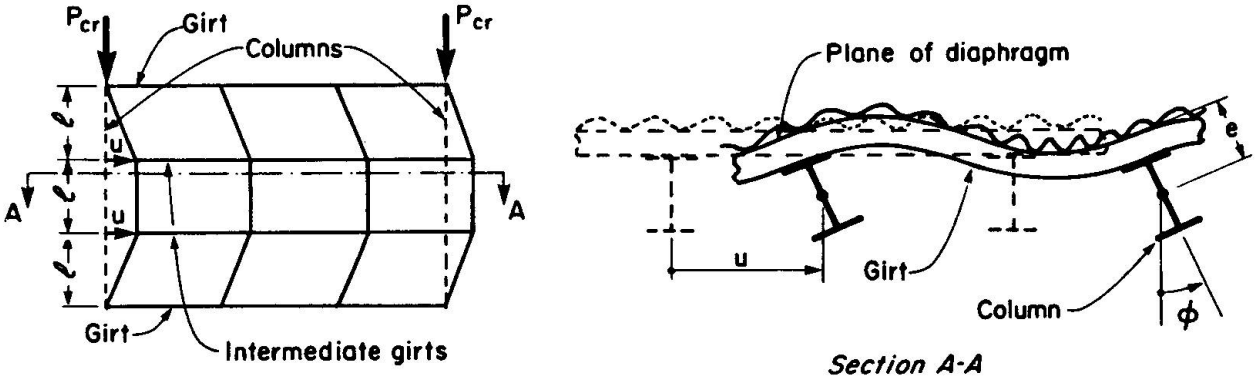

Fig. 5 — Flexural-torsional buckling mode.

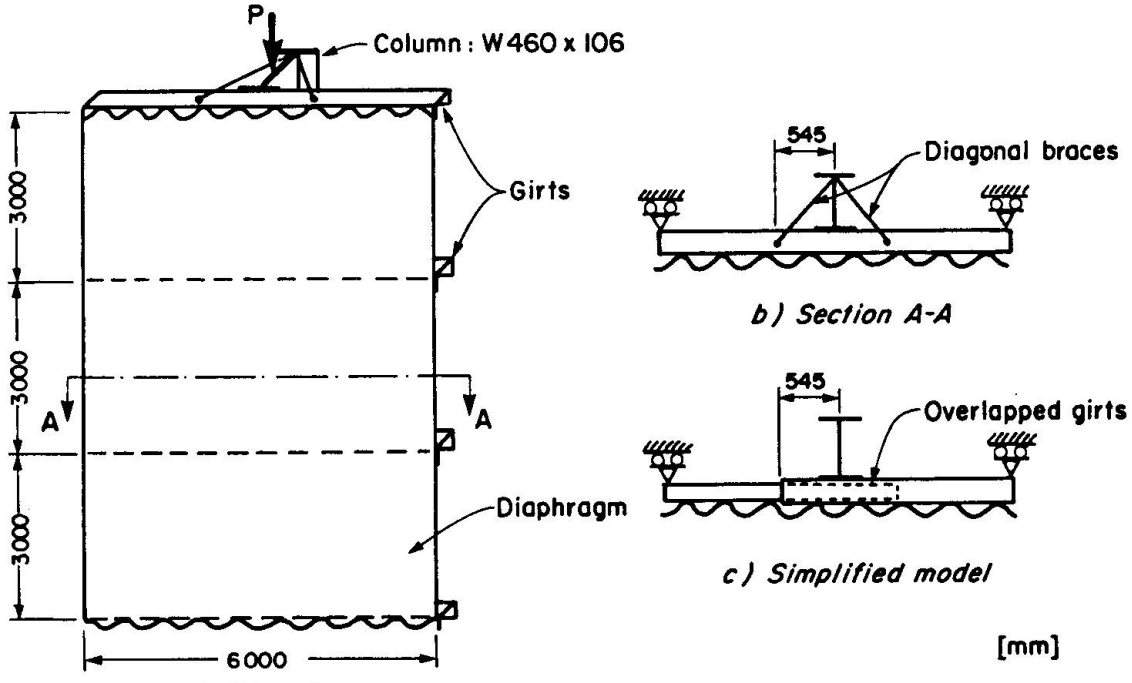

a) Elevation b) Section A-A c) Simplified model

Fig. 6 — C.G.D. sub-system with diagonal braces (pin-ended column)

Basis of New Polish Recommendations for Stressed Skin Design

Base des nouvelles recommandations polonaises du calcul des structures

Grundlagen der neuen polnischen Richtlinien für Tragwerke

Jan BRÓDKA
Prof. Dr.
MOSTOSTAL
Warsaw, Poland

Rafal GARNCAREK
Prof.
MOSTOSTAL
Warsaw, Poland

Andrzej GRUDKA
Civil Engineer
MOSTOSTAL
Warsaw, Poland

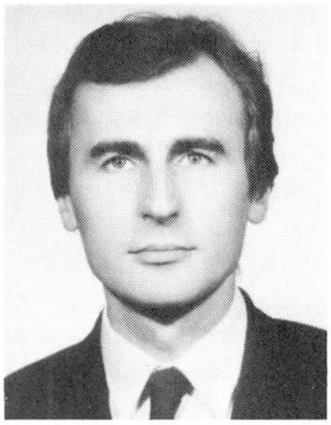

SUMMARY

The new polish design recommendations for stressed skin design are based on ECCS recommendations, as well as on the results of extensive theoretical and experimental investigations carried out in Poland. This document includes a simplified procedure of checking the stability of struts and beam-columns, braced by corrugated sheet and braced by girts with corrugated diaphragm. In structures which do not fulfil all recommended requirements many members and fasteners, in particular secondary members, have been found to be overloaded.

RÉSUMÉ

Les nouvelles règles polonaises concernant les structures qui agissent en collaboration avec les tôles d'acier nervurées sont basées sur les recommandations CECM et aussi sur les résultats des vastes études théoriques et expérimentales faites en Pologne. Les règles contiennent une méthode simplifiée d'estimation de la stabilité des poteaux comprimés et des poutres comprimées et fléchies renforcés par la tôle d'acier nervurée et par les traverses avec tôle d'acier nervurée. Dans les constructions qui avaient été calculées sans respecter toutes ces règles, on a constaté une surcharge dans beaucoup de barres et d'assemblages, surtout dans les éléments qu'on traite d'habitude comme secondaires.

ZUSAMMENFASSUNG

Neue polnische Richtlinien für den Entwurf von Stahlkonstruktionen, die mit den Umhüllungselementen aus Trapez-Profilblech zusammenwirken, sind auf den EKS-Richtlinien und auch auf umfangreichen theoretischen und experimentellen polnischen Versuchsergebnissen aufgebaut. Die neuen Richtlinien geben vereinfachte Abschätzungsmethoden für die Stabilität von gedrückten Stäben sowie von druck- und/oder biegebeanspruchten Stäben an, die mit Hilfe von Profilblech oder von Riegeln und Profilblech gestützt sind. In Konstruktionen, die dem Entwurf nach nicht alle Anforderungen der Richtlinien erfüllen, wurde die Überlastung von vielen Stäben sowie Verbindungsmitteln festgestellt, insbesondere in solchen die üblicherweise als untergeordnet betrachtet werden.

1. GENERAL REMARKS

The actual Polish Temporary Recommendations were issued in 1979. They are based on the 1975 issue of ECCS Recommendations. In the main they concern only structures that consist of planar bar members and diaphragms of corrugated sheets with framing. There are no formulae given to check stability of members in bending and beam–column braced by corrugated sheet diaphragms. They have also no instructions on analysis of building as a spatial system of steel skeleton with plates of corrugated panels.
Since 1978 year a study on application of finite element method to design of stressed skin structures as well as (since 1980) theoretical and experimental research on lateral stability of elements in bending and beam-column braced by corrugated sheet diaphragms has been carried out at Metal Structures Research and Design Centre „Mostostal" in Poland.

2. STABILITY PROBLEMS

It is known that diaphragm increases considerably bearing capacity of members in flexural–torsional buckling. Ignoring the influence of this phenomenon during design increases unnecesarily steel expense for building skeleton. For full utilisation of bracing member by a diaphragm in design there is necessary to get a lot of experimental data and calculation methods that are adequate to structures with different parameters of bracing along member length. To get these data procedures were worked out for computers. There were done research of struts in beam–column and beams in bending connected directly with corrugated sheets and struts braced by wall girts to which corrugated sheets were fastened. It has been confirmed that the bending capacity of connections of a corrugated sheet with a bar (or girt with column), determining the bar bracing against distorsion, influences greatly the stability. Investigations of Hilti fired pins and self–driving pins with rubber pads in corrugated sheet with bar connections have been carried out. The rotational rigidity k_ϕ of a bar - to corrugated sheet attachement of Hilti pin is represented in Fig. 1.

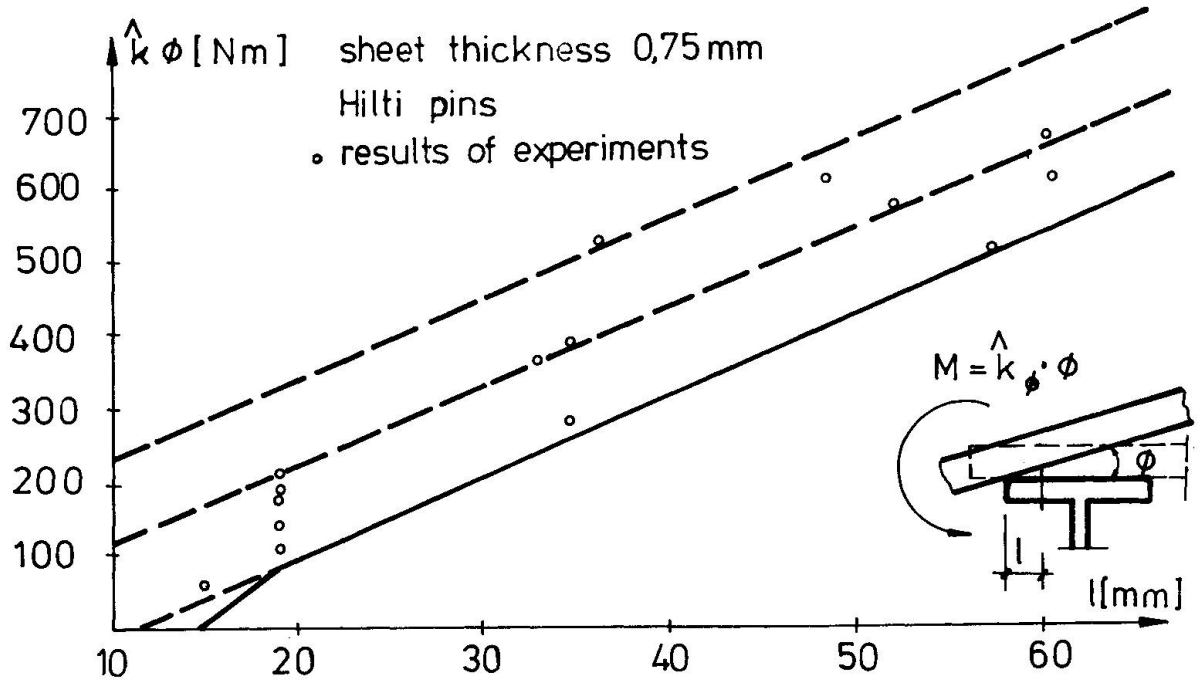

Fig.1. The rotational rigidity of a flange to corrugated sheet attachement.

Experiments on column with girt connections and those on frame girt with purlin connections, in typical projects of steel girder come to the end just now.
During the experimental research analysis the following method of bearing capacity determination has been applied.
For the geometry of skeleton and data of bracing parameters, buckling load and respective bar buckling length have been calculated. Further calculations were carried out according to the standard for the calculation of steel constructions.
For the calculation of bars braced by diaphragm having a varying rigidity along the bar axis or varying load and non typical end conditions the procedures in BASIC language on minicomputer Wang have been worked out:
– for calculation of bars directly connected with corrugated sheet,
– for calculation of bars connected with girts (purlins) to which corrugated sheets are attached.
Experiments and theoretical analysis have given an occasion to elaborate a simplified method of stability calculation.

3. SIMPIFIED CHECKING PROCEDURE FOR I–SHAPED BEAM–COLUMN BRACED BY GIRTS (PURLINS) AND DIAPHRAGM

3.1. Notations

A – area of I–section;
I_x – moment of inertia about x–axis;
$\hat{K}_x$ – shear rigidity of a diaphragm of corrugated sheets for one beam–column;
$\hat{K}_\phi$ – rotational restraint constant of a corrugated sheet diaphram directly attached to a flange for one beam–column;
K_ϕ – rotational restraint constant of a girt (purlin) for one beam–column
$L = l \cdot n$ – length of a beam–column;
$M = P \cdot e$ – bending moment about x–axis;
M_1, M_2, M_3 – moments about O–axis;
P – compression force;
$\overline{P}$ – lateral force;
Q – reaction force;
a_1, h_1, r – geometric dimensions (Fig. 3);
i – polar radius of gyration;
n – number of girts (purlins) minus one;
u – lateral displacement (Fig. 3);
u_1 – displacement in direction of x–axis;
σ – compression stress;
ϕ – rotation about O–axis (Fig. 3).

3.2. Introduction

The exact checking of stability of a beam–column braced by girts (purlins) and corrugated sheets (Fig. 2) is possible only by means of a computer procedure [1]. A simpler method given in [2] can be used merely for columns, when a number of girts is less then six. The objective of this paper is to report equally simple but a more versatile method, presented first time in [3].

3.3. Simplifications

– Stiffness of a beam–column is neglected; it is fictitiosly cut in x, y plane at connections with girts (purlins);
– A beam–column is hinged at the ends;

– e, P, $\hat{K}_x$, K_ϕ = constant.

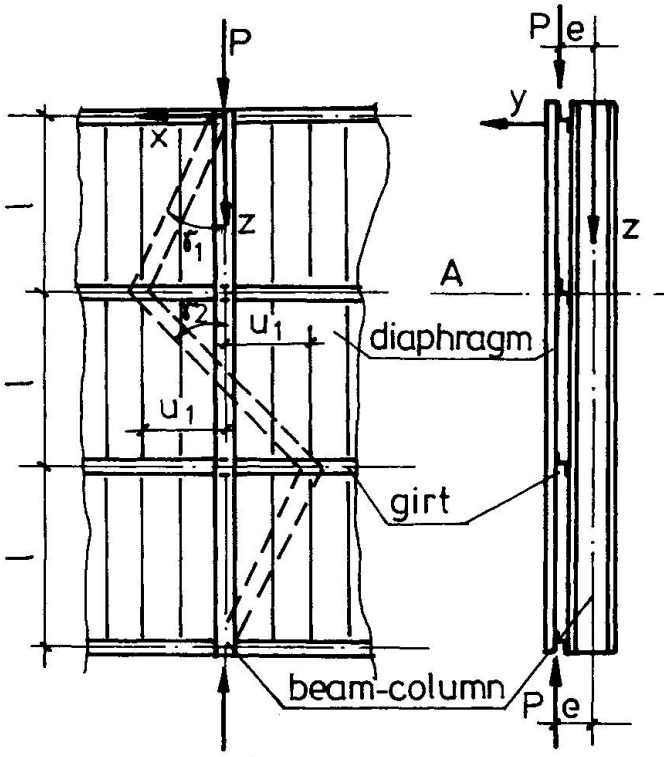

Fig. 2, A beam–column and its bracing

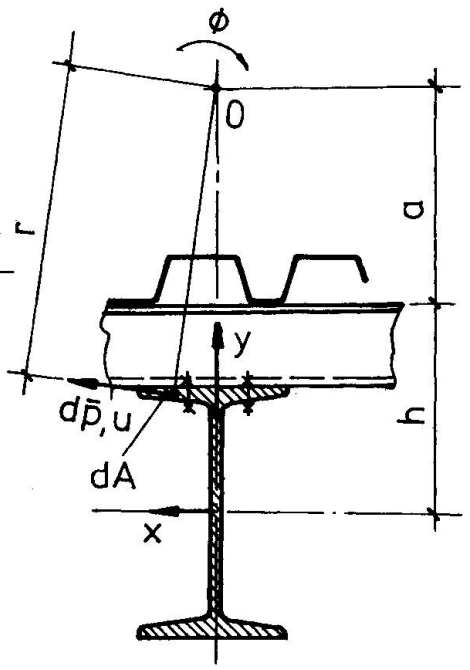

Fig. 3 A–A section

3.4. Conditions of stability

From Fig. 2 and Fig. 3 $d\bar{P}$ force can be stated as

$$d\bar{P} = \sigma \cdot dA \cdot \mathcal{L} \cdot u/l, \qquad /1/$$

in which $u = \phi r$, $\sigma = P/A + M \cdot y/J_x$, $\mathcal{L} = 3$ for $n = 3$.
A moment about O–axis is given by

$$\bar{M}_1 = \int_A d\bar{P} \cdot r \qquad /2/$$

The result of putting /1/ into /2/ is

$$\bar{M}_1 = \phi \, \mathcal{L} \, P \, [i^2 + (a_1 + h_1)^2 - 2e(a_1 + h_1)]. \qquad /3/$$

A girt reaction is given by $\bar{M}_2 = - K\phi \, \emptyset$.
From Fig. 2 a diaphragm reaction can be stated as

$$\bar{M}_3 = Q \cdot a_1 = -(\gamma_1 + \gamma_2)\hat{K}_x \cdot a_1 = -\mathcal{L} \phi \cdot a_1 \hat{K}_x / l.$$

The condition of stability is given by

$$\bar{M}_1 + \bar{M}_2 + \bar{M}_3 \leqslant 0 \qquad /4/$$

If the condition /4/ is fulfilled then a beam–column is supported immovable in x, ϕ directions at connections with girts (purlins). It can buckle only in y direction or between the connections – for the buckling length equal to l. $\mathcal{L}$ – factor calculated from static analysis is given in Table 1.

n	2	3	4	5	6	7	9	11	∞
£	2	3	3.41	3.63	3.73	3.8	3.88	3.92	4

Table 1

From the condition of a minimum of the total potential energy $\partial K_\phi / \partial a_1 = 0$. Solving this for a_1 and putting it into /4/ gives

$$K_\phi \geq £ \cdot P [i^2 + h_1^2 - 2eh_1 + P(h_1 - e)^2 /(\hat{K}_x - P)] / l. \qquad /5/$$

The second condition of stability is

$$\hat{K}_x > P. \qquad /6/$$

For $\beta = [2eh_1 - (h_1^2 + i^2)]/(e^2 - i^2) > 0$ there is only one condition of stability given by

$$P \leq \beta \cdot \hat{K}_x \qquad /7/$$

3.5. Effect of stiffness of a beam–column

Stiffness of beam–column increases buckling resistence of girts (purlins) and a diaphragm. A buckling load can be presented as

$$P_{cr} = P_{1cr} + P_{2cr}, \qquad /8/$$

in which P_{1cr} buckling load for a beam–column braced by corrugated sheets attached directly to a beam–column flange, calculated for a buckling length L and constants $\hat{K}_\phi = 0,\hat{K}_x \cdot P_{2cr}$ is an increase of a buckling load in consequence of girts (purlins) stiffness. Putting $(\bar{M}_1 + \bar{M}_2 + \bar{M}_3)$ equal to zero and $(P - \hat{K}_x)$ equal to $(P_{1cr} + P_{2cr} - \hat{K}_x)$ yields

$$P_{2cr} = (-B + \sqrt{B - 4AC})/2A, \qquad /9/$$

in which $A = e^2 - i^2$,

$$B = [i^2 + h_1 (h_1 - 2e)] (\hat{K}_x - P_{1cr}) + K_\phi \cdot l/£$$

$$C = - l \cdot K_\phi (\hat{K}_x - P_{1cr})/£$$

3.6. The checking procedure

The procedure for „The New Polish Recommendation for Stressed Skin Design of Steel Structures" was developed from /5/ and /9/ expressions by putting into them safety factors and taking into account elasto–plastic characteristics of a beam–column material. A numerical confrontation of the reported method and the method from [2] for a compressed column braced by a diaphragm and four girts yielded very approximate results.

4. CONCLUSION

Ample studies deal with the static analysis of building, as a bars and plates system. In such a system the construction of windows and gates was neglected. The flexibility of connecting pieces was added to the flexibility of corrugated sheet and the flexibility of diaphragm was determined according to the ECCS Recommendations. Main columns and gable walls columns, frame girts and summer girts, girder flanges and lattice columns flanges are assumed as elements having six degrees of freedom, other skeleton members as bracing, cross–braces, window girts etc. are assumed as elements having three degres of freedom. The model of corrugated sheet was made by means of orthotropic elements with nodes having two degrees of freedom

(see ref.4) in the sheet plane. The co–action of corrugated sheet with steel skeleton level down considerably the building horizontal deflexion and the forces acting in the main skeleton columns (upon over a dozen per cent), when their directions are parallel to the composants direction of corrugation waves. However the lattice stifeners of roof and walls are considerably overloaded. Also number of which, on account of standard wind load in many areas of the building, should be greater than the number resulting only from the vertical loads action.

Co–action of corrugated sheets with steel skeleton gives many advantages (reduction of horizontal deflection, distribution of internal forces in main bars, stability of main bars, overcritical behaviour of secondary bars) but can also provide negative results. If the results do not come out evidently this is because the hurricane load assumed in design occurs very seldom and pass across the open area. However this can happen otherwise. When the main connections are destroyed and the corrugated sheet does not co–act with skeleton.

One can safely profit from the co–action of corrugated sheet with building skeleton only in the four hinge system of planar members, where the sheet contributes to the geometrical invariability of building but does not interfere with the distribution of planar members internal forces.

REFERENCES

1. APPARAO T.V.S.R., ERRERA S.J. and FISHER G.P., Columns Braced by Girts and a Diaphragm, Journal of the Structural Division. ST5, May. 1969.
2. ERRERA S.J. and APPARAO T. V. S. R., Design of I–Shaped Columns with Diaphragm Bracing.. Journal of Structural Division, ST9, September 1976.
3. GARNCAREK R.J., Simplified Method of Checking of Stability for Beams and Columns Braced by Girts and a Diaphragm (in Polish). Inżynieria i Budownictwo, No 9, 1985.
4. BRÓDKA J., GARNCAREK R., GRUDKA A. and PIOTROWSKA–GRUDKA B., Analysis of Structures Interacting with Corrugated Sheets as a Frame and Plate System. Third International Conference on Space Structures. Elsevier Applied Science Publishers. London 1984, p.326 –331.

Behaviour of Thin-Walled Corrugated Sheets and Restrained Beams

Comportement des tôles ondulées à paroi mince et des poutres

Verhalten von wellenförmigen Dünnwandblechen und ausgesteiften Trägern

Jindřich MELCHER
Prof. Dr. Ing.
Technical University
Brno, Czechoslovakia

Jindřich Melcher, born 1939, received his civil engineering degree at the Technical University of Brno, Czechoslovakia. He is involved mainly in the stability of steel structures and limit states design problems. He is Professor in the Department of Steel Structures and Bridges and Dean of the Civil Engineering Faculty.

SUMMARY

The paper provides information on the experimental research programme directed to the problem of local buckling of metal thin-walled corrugated wave-formed sheets under bending moment and to the problem of local and general buckling of beams restrained by sheeting and sag rods. The procedure referred to as the vacuum test (Cornell) method was utilized for the experiments.

RÉSUMÉ

Cet article concerne un programme de recherche expérimentale orienté vers les problèmes de voilement local de tôles profilées en acier à paroi mince sous l'effet d'un moment de flexion; et de voilement local et global de poutres stabilisées par la tôle et des tirants. La procédure expérimentale utilisée est la méthode d'essais sous vide développée à l'Université Cornell.

ZUSAMMENFASSUNG

Der Beitrag berichtet über ein Versuchsprogramm, das auf das Problem der lokalen Stabilität von wellenförmigen Metallblechen unter Biegemomenten und auf das Problem der lokalen Stabilität und der Gesamtstabilität von Trägern abzielt, die durch profilierte Bleche und Zugstangen gehalten sind. Für die Versuche wurde die von Cornell entwickelte Vakuumprüfungsmethode angewandt.

1. LOCAL BUCKLING OF CORRUGATED SHEETS UNDER BENDING

In the problem of local buckling of thin-walled metal sheets subjected to bending moment much attention has been given to the trapezoidal (ribbed) profiles. One of our research projects was concerned with corrugated (wave-formed) panels because of a little amount of the information about both the theoretical and experimental results in this field.

1.1 An Experimental Investigation

The experimental research programme was conducted on single-span and two-span steel panels with the nominal cross section geometry and actual characteristics for one wave (i.e. for the width of 95 mm) shown in Fig. 1.

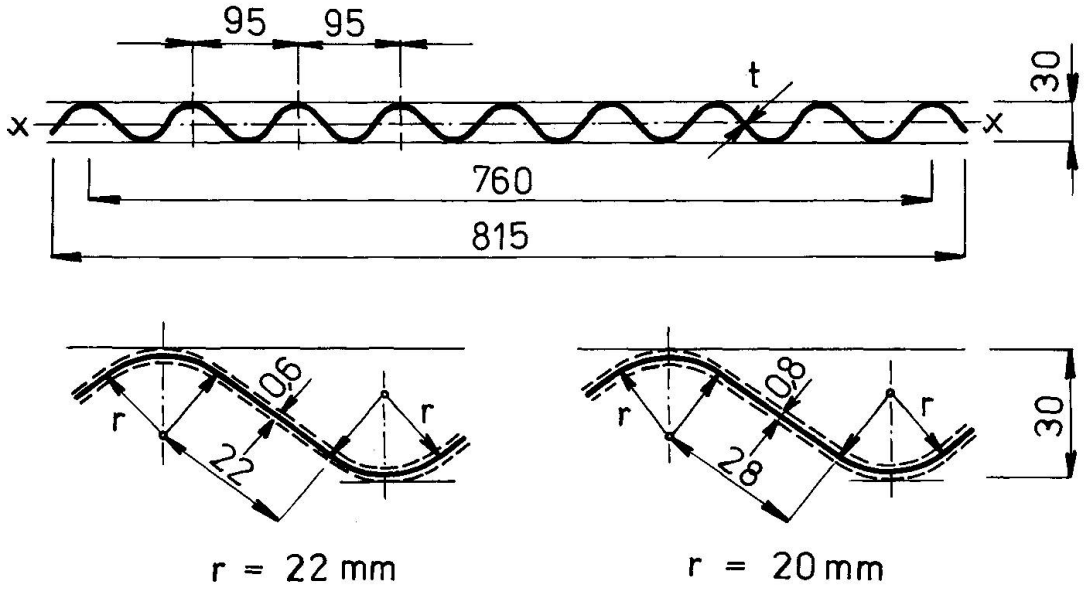

t [mm]	A [mm^2]	I_x [mm^4]	W_x [mm^3]
0,6	57,68	5903	415,7
0,8	80,89	8822	607,2

Fig. 1 Cross section and characteristics of the specimens

The steel panels are zinc coated. The actual thickness of the steel sheet was t = 0,52 mm (nominal t = 0,6 mm) and t = 0,72 mm (nominal t = 0,8 mm) respectively.
Totaly 12 specimens were tested, namely 6 simple supported panels with a span of L_1 = 1440 mm and 6 continuous panels of two equal spans of L_2 = 1480 mm. The overall width of wave sheets was 815 mm. The breadth of the transverse support elements was b = 40 mm.

The actual material characteristics were measured in 6 tensile test specimens for sheets of nominal thickness t = 0,6 mm and in 3 specimens for t = 0,8 mm. The mean values of the yield stress and the ultimate tensile strength were R_y = 237 MPa (minimal R_y = 225 MPa; maximal R_y = = 259 MPa) and R_u = 284 MPa (minimal R_u = 272 MPa; maximal R_u = = 304 MPa) for the nominal sheet thickness of t = 0,6 mm and R_y = 264 MPa (minimal R_y = 248 MPa; maximal R_y = 281 MPa) and R_u = 314 MPa (minimal R_u = 298 MPa; maximal R_u = 327 MPa) for the nominal sheet thickness of t = 0,8 mm, respectively.

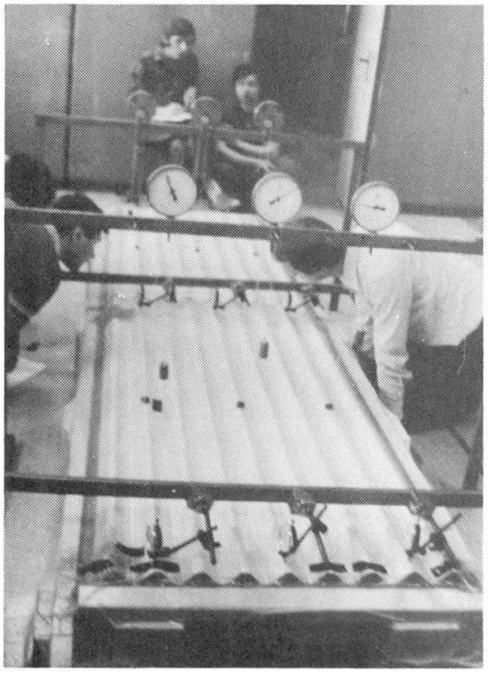

Fig. 2 Test Arrangement

To simulate the behaviour of thin-walled corrugated sheets under uniformly distributed load, an experimental procedure referred to as the vacuum test method was utilized (autor learned the application of this method in the field of steel stability research problems during the study stay by

SPECIMEN	t [mm]	TEST ARRANGEMENT	LOAD BY BUCKLING p_{max} [$kN \cdot m^{-2}$]	
			AT CENTRAL SUPPORT	IN THE SPAN
D 1	0,6	TWO - SPAN PANEL 2 x 1480 mm (width 815 mm)	4,0	7,0
D 3	0,6		4,0	7,0
D 4	0,6		4,0	7,0
D 2	0,8		7,0	11,3
D 5	0,8		7,0	11,5
D 6	0,8		7,2	11,0

Table 1 Two-span Test Results

R.N. White and T. Peköz, Cornell Univ., Ithaca, N.Y.). The method involves producing a vacuum under the test specimen covered by clear plastic, and then measuring the difference in pressure

SPECIMEN	t [mm]	TEST ARRANGEMENT	p_{max} [$kN \cdot m^{-2}$] LOAD BY BUCKLING IN THE SPAN
X 1 (D 2)	0,8	SINGLE-SPAN PANEL 1 x 1440 mm (width 815 mm)	9,5 (10,2)
X 2 (D 5)	0,8		9,4 (9,6)
X 3 (D 6)	0,8		9,5 (9,6)
X 4 (D 1)	0,6		6,0 (6,2)
X 5 (D 3)	0,6		6,0 (5,1)
X 6 (D 4)	0,6		5,8 (5,9)

Table 2 Single-span Test Results

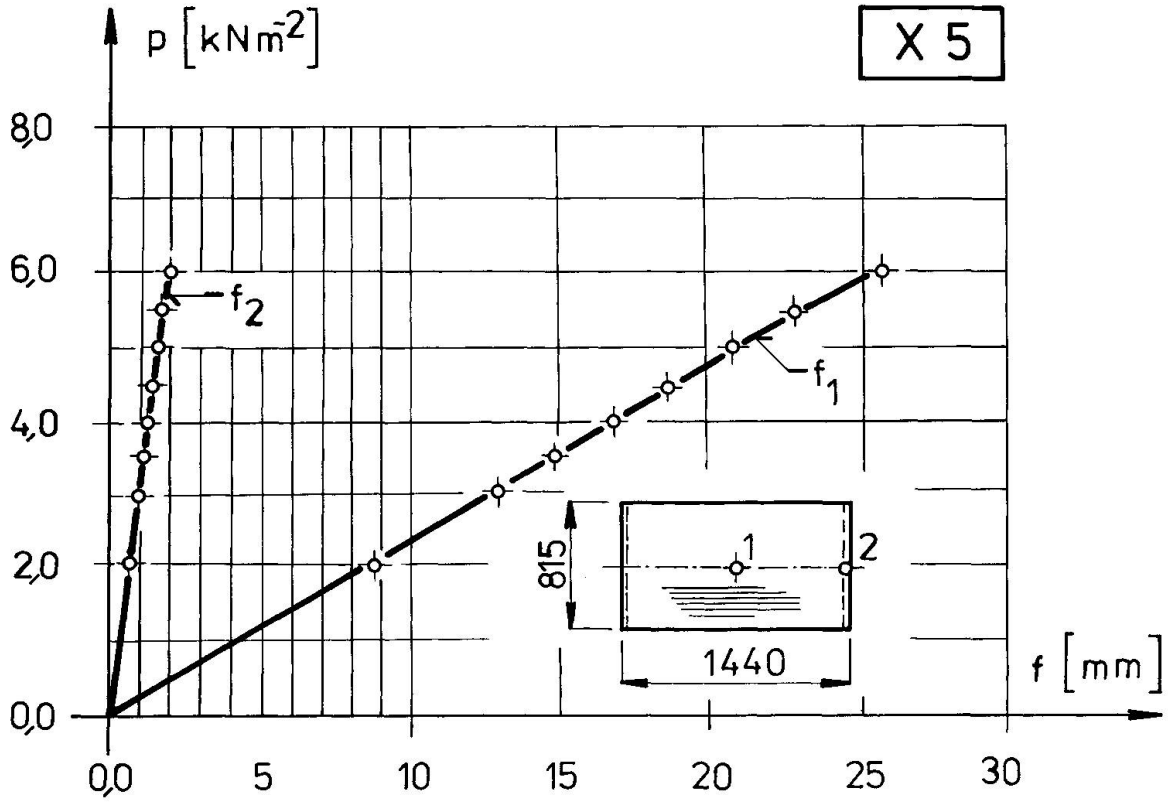

Fig. 3 Load - Deflection Relationship for Single-span Panel

between the outside atmospheric pressure and inside the test frame. The test setup and instrumentation are shown in Fig. 2. The support settlements and maximum span deflections were measured using a stroke dial gages.

The description of specimens and the experimental results are summarized in Table 1 and Table 2.

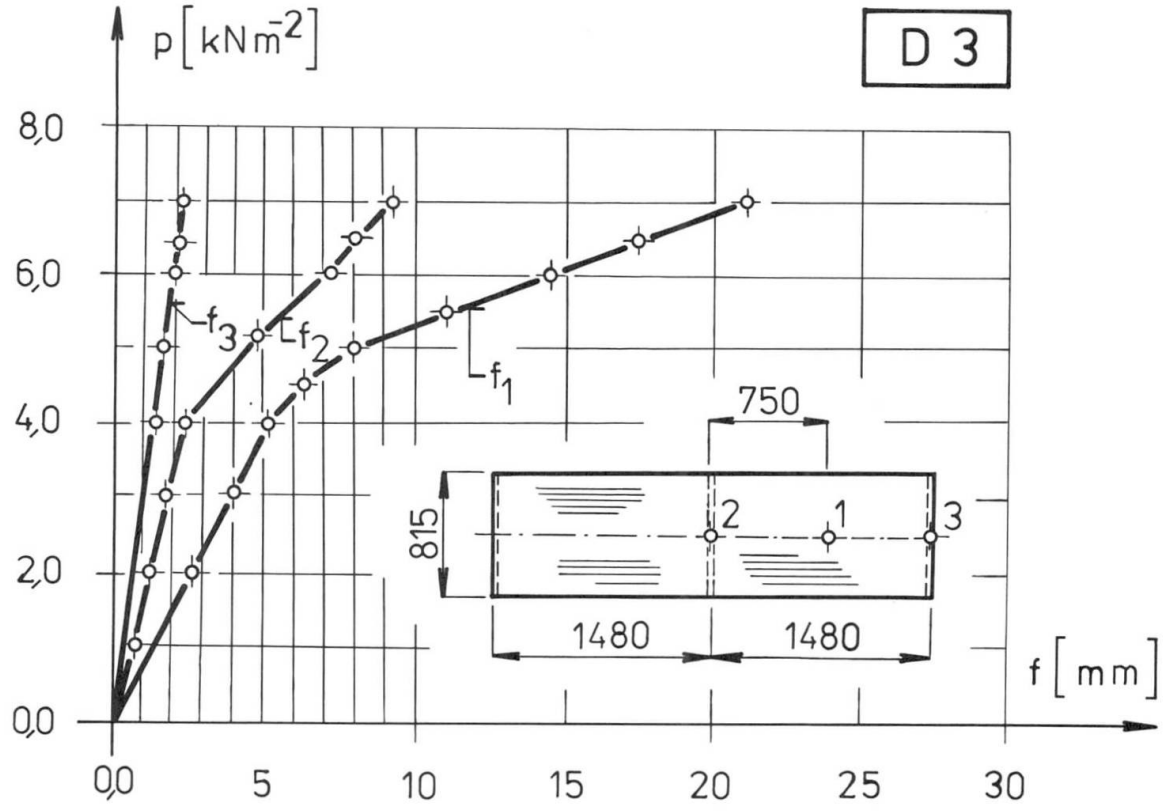

Fig. 4 Load - Deflection Relationship for Two-span Panel

Fig. 5 Span Buckling

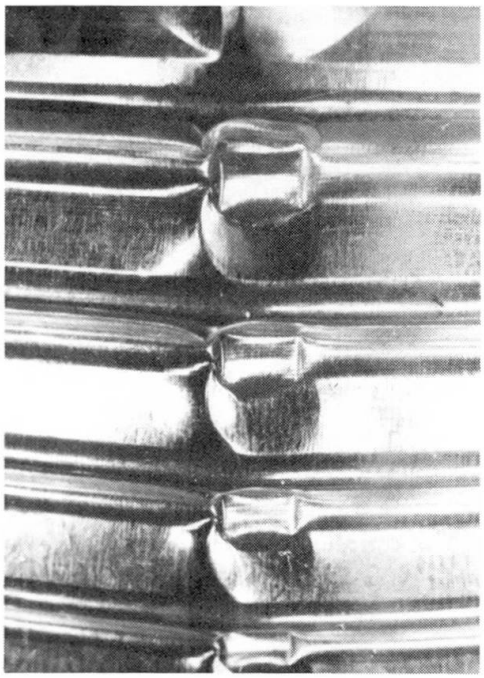

Fig. 6 Support Crippling

The typical example of applied uniform load "p" plotted against the maximum span and support deflections "f" is for the single-span specimen X5 in Fig. 3 and for the two-span specimen D3 in Fig. 4.

The influence of the plastic hinge arising, combined with web crippling at central support of two-span specimen can be clearly seen from Fig. 4. None of significant effect of the sheet support deformation upon the ultimate load carrying capacity of single span specimens was observed.
The behaviour of the corrugated sheets at ultimate load was characterized by outright and abrupt local buckling of the compression cross-section part in the span (see Fig. 5). After sheet waves deformation and bearing on the central support (see Fig. 6) the process of load increasing had been stabilized again until local buckling occured in the span.

1.2 Analysis of the Test Results

This part of the paper is aimed to the problem of local buckling strength in the span of the wave-formed sheets. The critical moment and corresponding buckling stress follows directly from the ultimate load of single-span specimens. In the case of two-span panels the critical moment in the span is influenced by actual value of negative moment at central support. This moment obviously depends on cross section deformation cau-

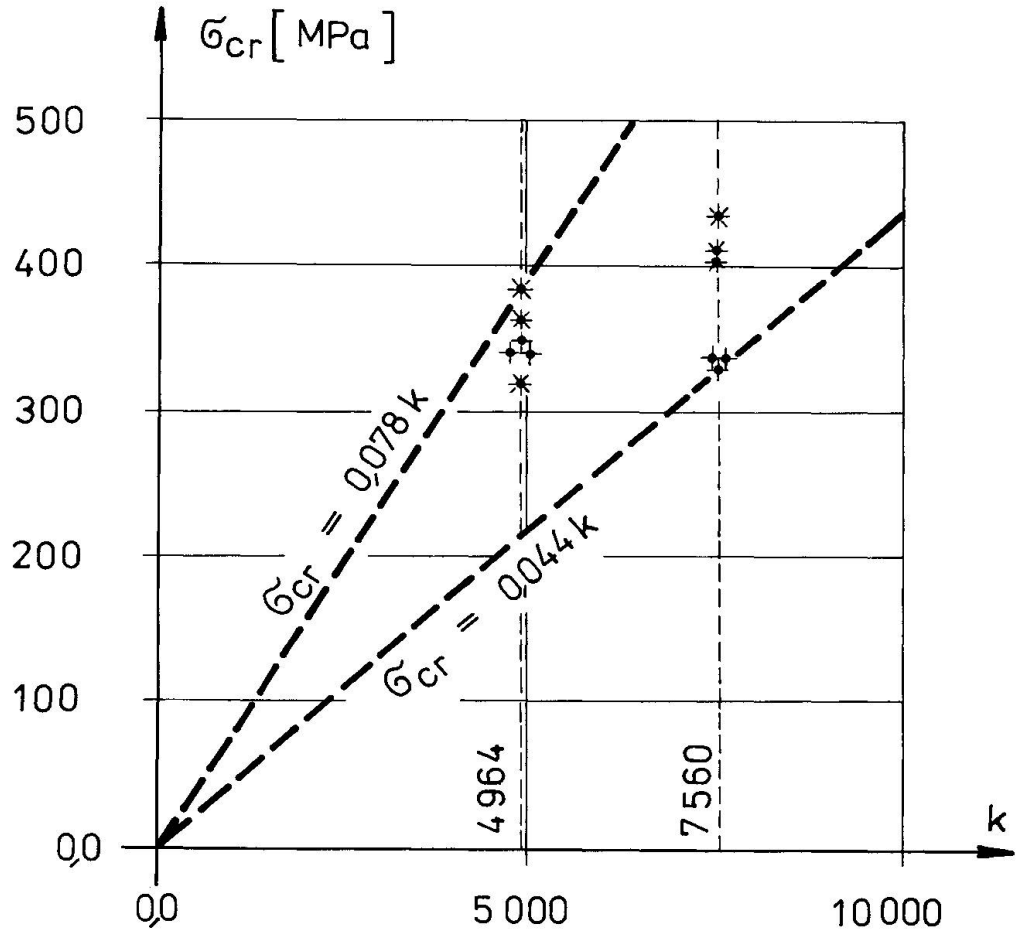

Fig. 7 Test Results Evaluation

sed by web crippling and can be easily determined using the measured values of maximum deflection in the span. Thus the ultimate buckling load for a conventional single span panel can be derived from the tests of two-span specimens. The corresponding specimen descriptions and conventional buckling loads are summa-

rized in parentheses, Table 2.
Based upon the theory of local buckling of unstiffened cylindrical shells [1] , [2] , [3] , the buckling stress of ondulated plates is given by the following general equation:

$$\sigma_{cr} = \alpha \frac{E\,t}{r} = \alpha \cdot k \quad . \qquad (1)$$

The buckling coefficient α for the range of parameters k considered in this study varies from $\alpha = 0{,}044$ to $\alpha = 0{,}078$ (see Fig. 7, where the star-symbols indicate the test results for the two-span specimens). The value of measured ultimate buckling load includes the influence of both the imperfections and material non-linearity. The experimental results are in a good agreement with [4] where $\alpha = 0{,}06$ for ondulated plates is proposed.

2. LOCAL AND GENERAL BUCKLING OF RESTRAINED BEAMS

The contemporary trend in the development of structural design procedures is characterized by a successive transition from the analysis of the "ideal member incorporated into the ideal structure" to the problem of "actual member incorporated into the actual structure". In the theory of beams braced by discrete and

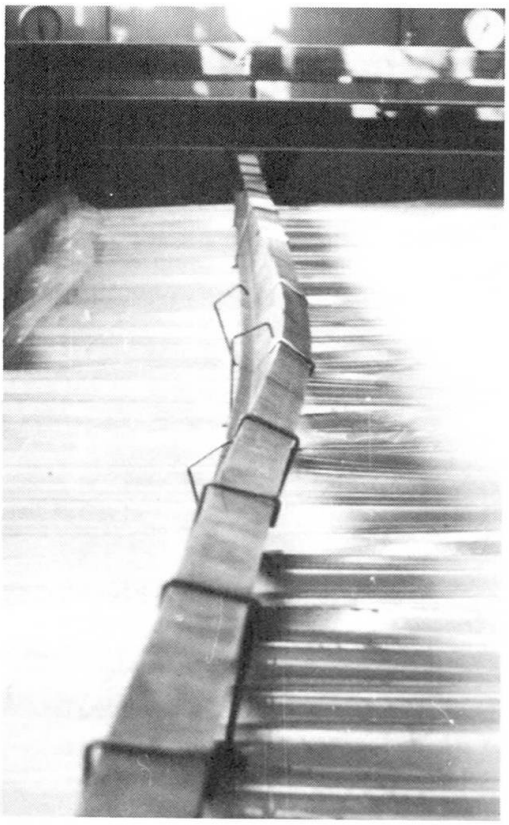

Fig. 9 Restrained Buckling

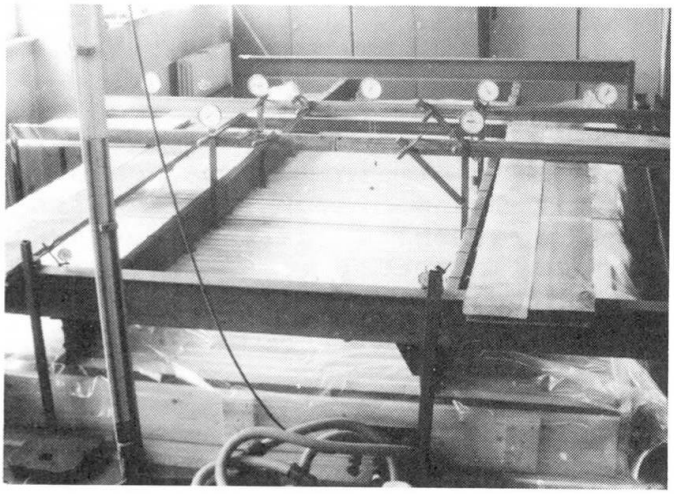

Fig. 8 Test Setup

continuous restraints (H. Nylander, T. Peköz, T. Höglund, N.S. Trahair, D.A. Nethercot, G.J. Hancock and others) a fair progress was made in the last period. But more attention to check the validity of the several assumptions and simplifications by experiments is needed. Interesting results of research in this field are for example in [5] , [6] . At Technical University of Brno the experimental programme directed to the behaviour of restrained beams is presently being conducted. The full-scale specimens arrangement is typical of those used in the metal building industry. The procedure referred to as vacuum test method is used, as well. The span of the beams tested is 6 m and the total loading breadth of the two parallel members is 3 m (Fig. 8).

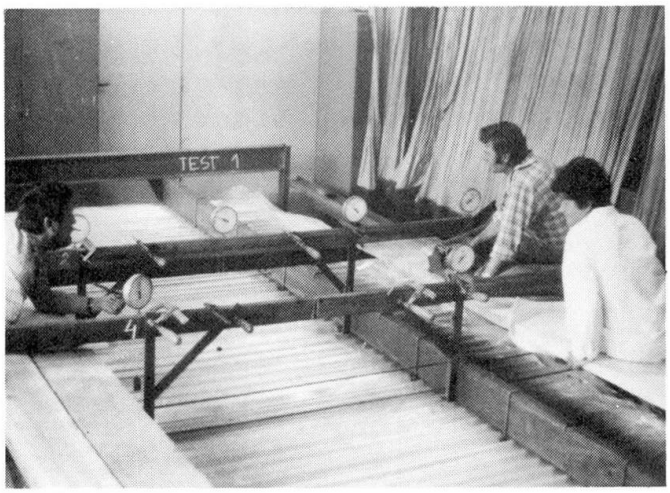

Fig. 10 Shot of Testing

Fig. 11 Local Buckling

The influence of sheeting and sag roads upon the behavior of restrained beams is studied under the conditions corresponding to the effect of wind uplift loading upon the secondary roof or wall structures.

Typical example of restrained general buckling of hot-rolled I - section is presented in Fig. 9. Also the general and local buckling tests of thin-walled cold-formed steel channel flexural members are being conducted (see examples in Fig. 10 and Fig. 11). From the test results follows that the ultimate buckling strength of restrained beams could be associated with conciderable lateral and distorsional deflections, their limitation should be respected deriving the design (specified) limit state. In thin-walled beams restrained by sag rods at third-point along the span the local buckling of compression flange can govern the ultimate strength in bending.

REFERENCES

1. FUNG Y.C., SECHLER E.E., Instability of Thin Elastic Shells. Proc. of the 1st Symposium on Naval Struct. Mechanics, Stanford Univ., August 11-14, 1958.
2. POGORELOV A.V., Cilindriczeskie oboloczki pri zakriticzeskikh deformaciyakh (Cylindrical Shells under postcritical deformations). Kharkov State Univ., 1963.
3. TIMASHEV S.A., Ustoyczivost podkreplennykh oboloczek (Stability of Stiffened Shells). Stroyizdat, Moscow, 1974.
4. STABILITY OF METAL STRUCTURES - A World View, Chapter 10 - Cold-formed Steel. Engineering Journal, AISC, Vol. 19, No. 2, 1982.
5. PEKÖZ T., Diaphragm-Braced Thin-Walled Channel and Z-section Beams; Beams and Beam Columns. Applied Science Pub., London - New York, 1983.
6. LA BOUBE R.A., Purlin Braces: Measured Forces. Proc. of the Third Colloquium on Stability of Steel Structures, Toronto, 1983.

Development and Ultimate Strength Test of New Steel Gable Roof Structure

Développement et essai de résistance ultime d'un nouveau type de fermes métalliques pour toit à deux pans

Entwicklung und Bruchfestigkeitsprüfung einer neuen Giebeldach-Stahlkonstruktion

Tetsuro ONO
Professor
Nagoya Inst. of Technol.
Nagoya, Japan

Masayuki ARAYA
Manager
Nippon Steel Co.
Tokyo, Japan

Mamoru IWATA
Manager
Nippon Steel Co.
Tokyo, Japan

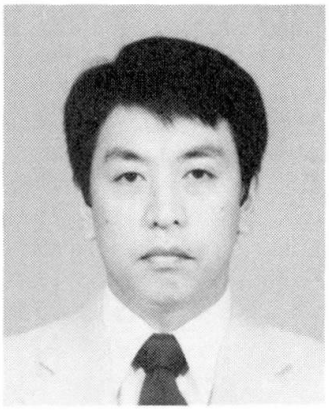

SUMMARY

This text is a report on a recently developed steel gable roof structure designed to simplify the framing process, shorten the construction time and, by reducing weight, cut down on cost. Especially with regard to the planning of the members and frameworks, expectations are high for improvements in yield strength and deformation capacity brought about by the use of these new main and secondary members. Large-scale tests are now under way to confirm the anticipated results.

RÉSUMÉ

Le présent texte concerne le développement de nouvelles fermes métalliques pour toit à deux pans, conçues pour simplifier le procédé de montage, réduire la durée de construction et diminuer le prix de revient en minimisant le poids. En particulier, la conception des éléments et de l'ossature devrait permettre une amélioration de la résistance ultime et de la capacité de déformation lors de l'utilisation de ces nouveaux éléments principaux et secondaires. Des essais à grande échelle sont en cours pour confirmer les résultats prévus.

ZUSAMMENFASSUNG

Die vorliegende Arbeit berichtet über eine neuentwickelte Giebeldach-Stahlkonstruktion, mit dem Ziel, die Entwurfsbearbeitung zu vereinfachen, die Bauzeit zu verkürzen und die Baukosten durch Gewichtsverringerung zu senken. Besonders in Bezug auf den Entwurf der Bauteile und des Rahmens sind die Erwartungen hoch, was die Verbesserung der Fliesslast und des Verformungsvermögens bei Ausnutzung der Nebenbauteile, wie z.B. Fertigbauteile, betrifft. Versuche im Massstab 1:1 sollen die erwarteten Resultate bestätigen.

1. Introduction

Many of the gable roof steel frames used for factory buildings, warehouses, etc. consist of gabled plane frames arranged side by side. In developing these frames, major emphasis is placed on simplification of the steel frame production process, reduction of work time, and cost cutting by reduction of the frame weight. Under such circumstances, the type of main frame used and the design and arrangement of secondary members to improve the ultimate strength and deformation capacity of the main frame members are important considerations. This paper outlines a newly developed system frame which employs thin-walled members, and presents the results of an ultimate strength test conducted on the structure and its members.

2. Outline of the New System Frame

The major points in the development of the new system frame were to improve the main frame member production process and to integrate cross beams in the ridge direction with the siding.

1) Formation of Main Frame Members by Special Process
With a gable roof frame fixed to column base pins, the corner knee member is generally subject to substantial bending moment due to vertical loads (dead load, live load, etc.) and horizontal loads (earthquakes, winds, etc.). In terms of stress, therefore, members of non-uniform section which have sufficient bending rigidity at the corner knees are effective. The problem is how to form such members efficiently. For the new system frame, rolled H steel was cut and bent into members of non-uniform sections as illustrated in Fig. 1. The cross-sectional shape of the members of these non-uniform sections was determined such that, in the column member, the joint between the uniform and non-uniform sections and the vertex of the corner knee member reach their yield moments at almost the same time.

2) Integration of Special-Shaped, Cold-Formed Member with Siding
In order to secure the ultimate strength and deformation capacity required of a frame and to use steel products economically, it is important to ensure that the individual members of the frame fully display their capacities. For the new system frame, a newly developed cold formed channel steel of special shape is used for the main frame cross beam in the ridge direction. In addition, a special metal is used to integrate this cross beam with the roofing members, external walls, and other siding members, so as to produce a sort of stress skin effect. By so doing, the rigidity, ultimate strength, and deformation capacity required of the frame are secured by the interaction of the main frame, secondary members, and siding members, In concrete terms, the frame is set up as shown in Fig. 2. In the new system frame, an unequal leg channel steel with intermediate stiffener is used as the cross beam, which is connected to the roofing members by Type A metals provided at 50 cm intervals. In addition, a Type B metal is provided at a position corresponding to the bracing point for buckling to transmit the bracing force on the channel steel to the roofing member in the form of a couple of forces, enabling the bending rigidity of the roofing member to hold back the out-of-plane deformation which accompanies twisting. In designing the cross beam, the interval between Type B metals was used as the buckling length. As a result, it has become possible to design a simple, rational frame which dose not require the sub-beams and stud members used with conventional frames. The new design has reduced the frame weight by 15 to 20%.

3. Strength Test of Cold Formed Cross Beam

3.1 Outline of Strength Test

This test is a bending strength test conducted on the cross beam to measure the effect of integrating the cross beam with the roofing member which serves as a bracing member for lateral buckling.

In the new system frame, the roofing members are connected via metals to a cold formed channel steel used as the beam in ridge direction which connects the main frames. When the upper frange of the channel steel to which the roofing members are connected is subjected to compression, the out-of-plane deformation of the flange is completely held back by ordinary (Type A) metals provided at intervals of 50 cm. However, when a wind load is applied from below, the lower flange of the channel steel is subjected to compression. In this case, the buckling bracing effect of the roofing members connected to the upper flange (tension flange) is uncertain. In the new system frame, in particular, the lateral buckling bracing force on the compression flange is transmitted in the form of a couple of forces to the roofing members connected to the tension flange via special-shaped (Type B) metals, so as to enable the strength and rigidity of the roofing members to hold back the out-of-plane deformation which accompanies twisting of the compression flange. It is, therefore, necessary to experimentally confirm that the special-shaped metal has sufficient strength and rigidity as the bracing point for lateral buckling and that the roofing members have sufficient capacity as bracing members.

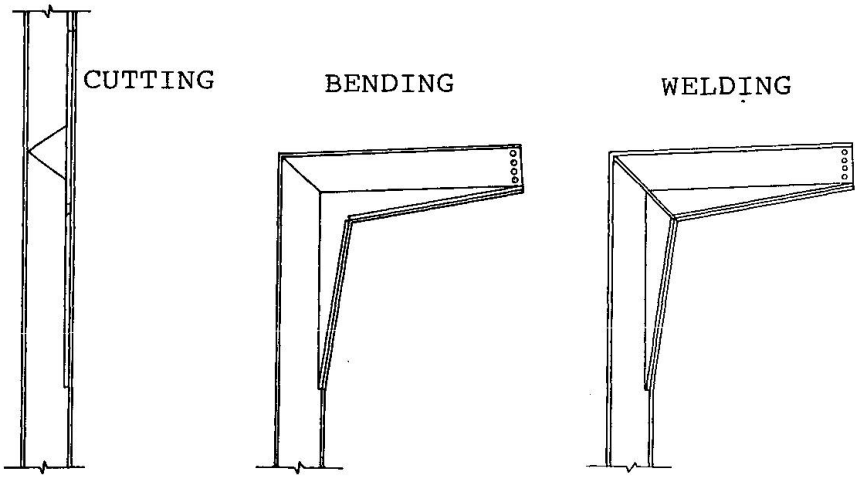

Fig.1 Formation of Main Frame Members

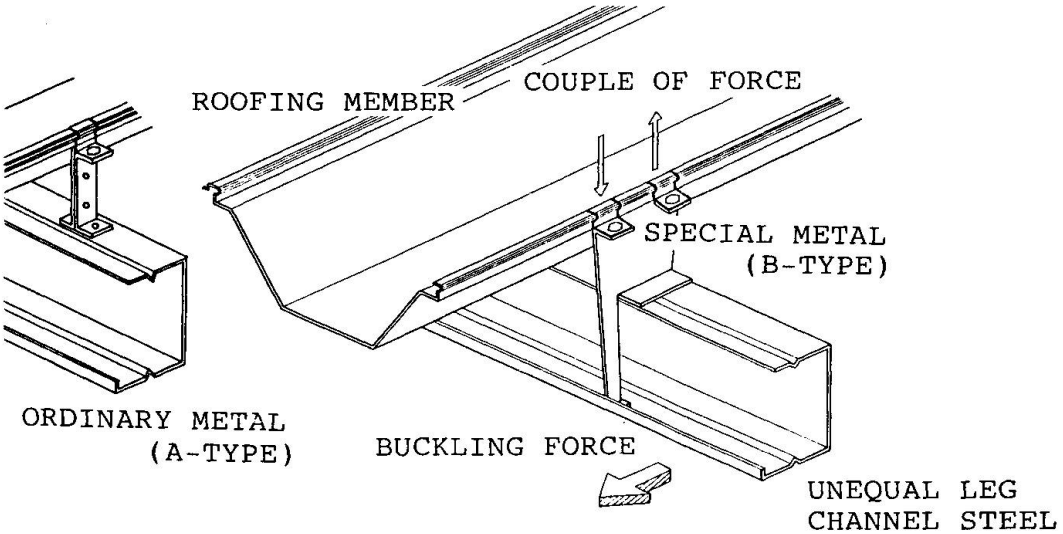

Fig.2 System of Channel Steel and Roofing

The parameters used for the testing were the direction in which a bending load is applied and the position of the special-shaped (Type B) metal to hold back lateral buckling deformation. A total of five different test pieces were used. C-1 is a cold formed channel steel without roofing members. C-2 is a cold formed channel steel provided with ordinary metals at intervals of 50 cm and connected with roofing members. C-3 has one special-shaped (Type B) metal at the center of a cold formed channel steel. C-4 has two Type B metals at points which divide the channel steel beam into three equal sections. C-5 is the same as C-3, except that the load is applied from the opposite direction. The test pieces are outlined in Table 1. The test was conducted in the manner illustrated in Fig. 3. The test pieces were subject to equal moment. Each test piece was pinned at both ends in the strong axis and was fixed in the weaks axis to hold back end warping.

3.2 Test Results

Fig.4 shows a load-deformation curve obtained as a result of the test. The load applied was yield moment M_y, and the deformation was made dimensionless by δ_y corresponding to M_y.

With C-1 having no roofing member, torsional deformation began to occur in the initial stage of application of load. Compared with other test pieces provided with roofing members, C-1 showed lower elastic rigidity, its ultimate strength being about $0.76M_y$. C-2, which was prepared by welding ordinary (Type A) metals to a channel steel at intervals of 50 cm and connecting roofing members thereto, showed higher initial rigidity than C-1, comparable to the rigidity around the principal axis. With C-2, torsional deformation became conspicuous when the load reached about $0.90M_y$. After the ultimate strength of $0.97M_y$ was reached, C-2 showed a sharp decline in strength.

C-3, provided with roofing members in the same manner as C-2 and also with one special-shaped (Type B) metal at the center of the beam, showed slightly higher rigidity than C-2. At the ultimate strength of $1.00M_y$, torsional deformation and local buckling occurred and the strength declined. Also, after the ultimate strength was reached, local deformation occurred with roofing members at their joints with the beam due to increased of deformation of the beam. C-4 provided with two special-shaped metals showed almost the same behavior as C-3. Its ultimate strength was $1.01M_y$ and the deterioration of strength after the ultimate strength was reached was less conspicuous, indicating that the Type B metals have appreciable buckling bracing effect. With both C-3 and C-4, torsional deformations showed axial symmetry against the bracing point.

4. Strength Test of Corner Knee Member of Main Frame

4.1 Outline of Test

The corner knee member of the main frame having a non-uniform section was subjected to a strength test. In a gable roof frame, a vertical load normally causes the point of maximum moment to occur at the corner knee member. In designing such a frame, safety is studied for each of the members, such as beams and columns, on the assumption that the out-of-plane deformation is completely held back at their joints. Actually, however, the out-of-plane deformation is not always held back completely at the corner knee member. Also, in actual design, the outer flanges of the beam and column members, as well as the corner knee members, are normally braced by a cross beam in the ridge direction, but the inner flanges are seldom provided with any lateral bracing members. However, bending stress due to vertical load, etc. becomes a compressive force applied to the inner flange and can cause out-of-plane buckling deformation of the vertex inside the corner knee member. This in turn can adversely affect the safety of the frame including type corner knee members. The new system frame, too, had to be studied from this viewpoint.

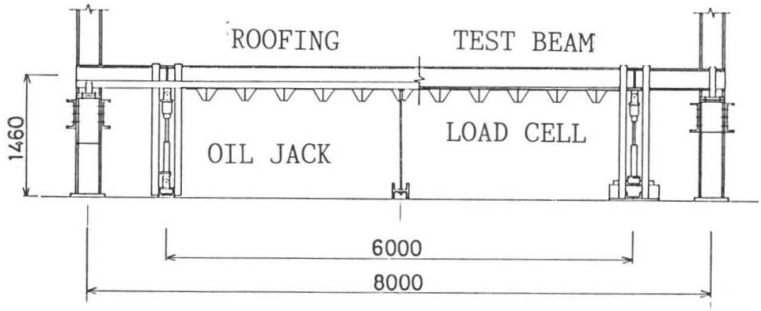

Fig.3 Test Set-up of Channel Steel

Test No.	Roofing	Metal	σ_y(t/cm²)
C-1	no	no	2.76
C-2	yes	A	〃
C-3	no	A, B_1	〃
C-4	no	A, B_2	〃
C-5	no	A, B_1	〃

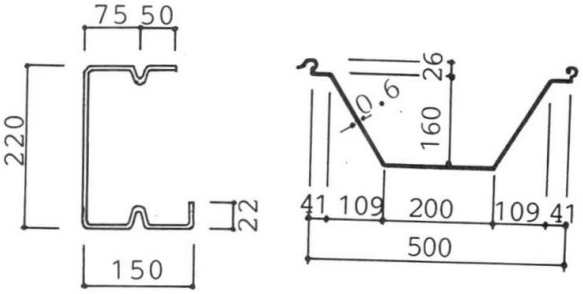

Table 1 Test Specimen of Channel Steel

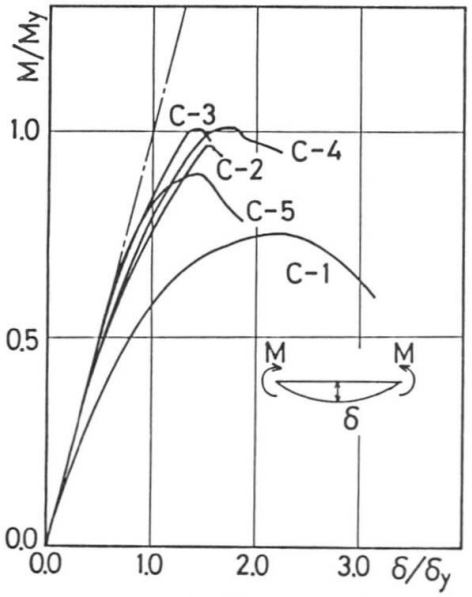

Fig.4 Load-Deflection Curves of Channel Steel

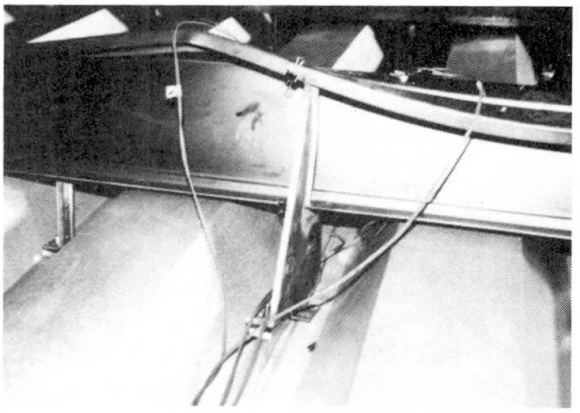

Fig.5 Local Buckling of Channel Steel

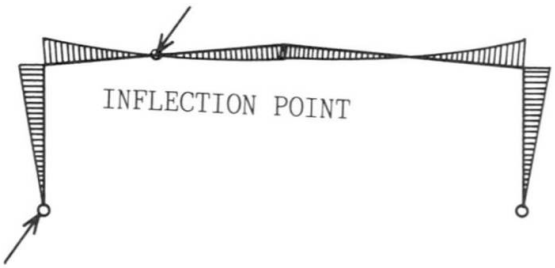

Fig.6 Moment Distribution of Frame

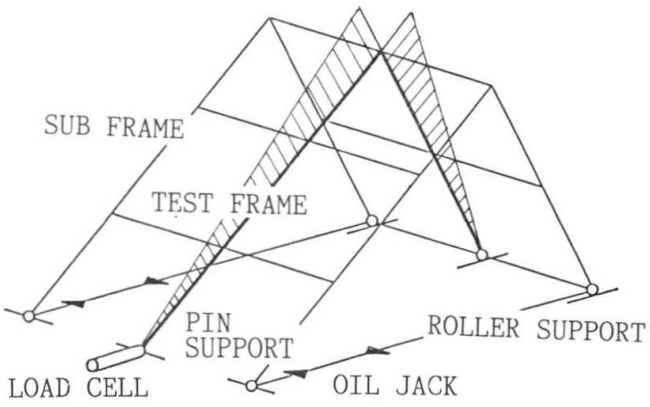

Fig.7 Loading System of Frame

In the new system frame, the point of inflection of moment on the beam member a vertical load is located at approximately 6 m from the corner knee and the moment zero point on the column member is located in the column base from the design assumptions of the frame. Hence, the subassembly frame with the beam and column moment zero points as pins (see Fig.6,7) was subjected to the test. Test pieces used were 1/2 scale models of the actual frame.

For each test piece, two cross beams were connected to the column and one cross beam was connected to the beam. The parameters used for the testing were the type of bracing of the corner knee member and the presence or absence of stiffener bracing at the non-uniform section. A total of four different test pieces were used. The test pieces are outlined in Table 2.

4.2 Testing Equipment

The testing equipment used was such that it could measure the ultimate strength and deformation capacity of the corner knee member of the gable roof frame in as near the actual condition as possible. Compressive force was applied by pulling with a hydraulic jack the section between the column base as the pin support and the point on the beam corresponding to the point of inflection moment as the pin roller support. By so doing, a stress condition similar to the moment distribution under vertical load could be obtained (see Fig.7). At either and each test piece, a support frame was provided along the outer flange of the test piece to support the cross beam serving to brace the lateral buckling of the main frame. The support frames were placed on the same stand as the test piece was placed on so that they could be deformed in the same manner. Thus, the secondary members, such as the cross beam, are subject to the same in-plane deformation as the test piece. Load applied was detected by a load cell installed at the pin support of the test piece. As can be seen from the model diagram in Fig.7, this load cell detects only the force that is actually passed through the test piece. Fig.9 shows lateral buckling deformation of frame view of the testing.

4.3 Load-Deformation Relationship and Plastic Behavior

Fig.10 and 11 shows the load-deformation curves obtained as a result of the test. In the diagram, the one-dot chain line represents the result of a elastic analysis.

1) F-1
This test piece has no bracing plate at the starting point of the non-uniform section, and only the outer flange is braced at the vertex. The load-deformation relationship became nonlinear when a load of about 1.75 tons was applied. As external force was increased, the amount of deformation increased. The ultimate strength was 2.75 tons, and thereafter, the strength decressed sharply. At a load of about 2.7 tons, local buckling deformation occurred at around the starting point of the non-uniform section of the beam. As the load was increased further, the local buckling deformation and out-of-plane deformation at the point continued to increase.

2) F-2
This test piece is the same as F-1, except that both the outer and inner flanges are braced at the vertex of the corner knee member. It showed almost the same load-deformation relationship as F-1. The ultimate strength was 2.8 tons. No marked difference in ultimate strength could be observed among F-2 with both flanges braced, and F-1 with only the tension flange braced. This is due to the fact that the local buckling precedes another buckling and that the bracing member at the vertex appreciably held back the out-of-plane deformation of the compression flange owing to stiffner. Incidentally, the vertex bracing member attached to the tension flange of F-1 was subjected to greater bending stress than that of F-2.

Test No.	Section	σ_y(t/cm^2)	Stiffened Plate	Lateral Bracing at Corner Knee
F-1	BH-200×100×3.6×6	3.3	no	Tens. Flange
F-2	BH-300×100×3.6×6		no	Both Flanges
F-3			yes	Tens. Flange
F-4			yes	Both Flanges

Table 2 Dimensions of Frame Test

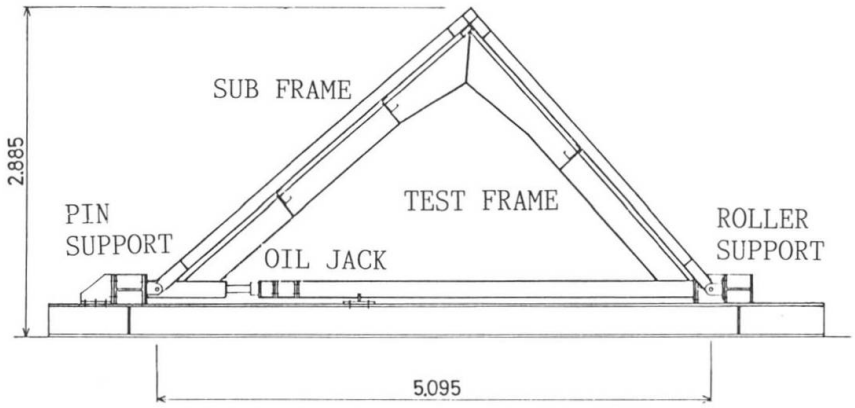

Fig.8 Test Set-up of Frame

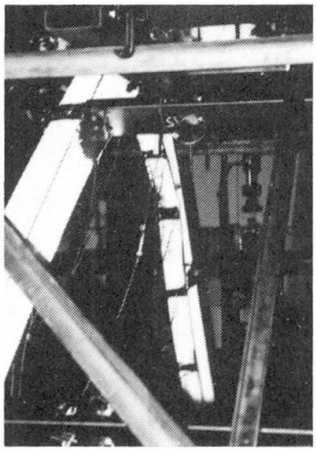

Fig.9 Lateral Buckling of Frame

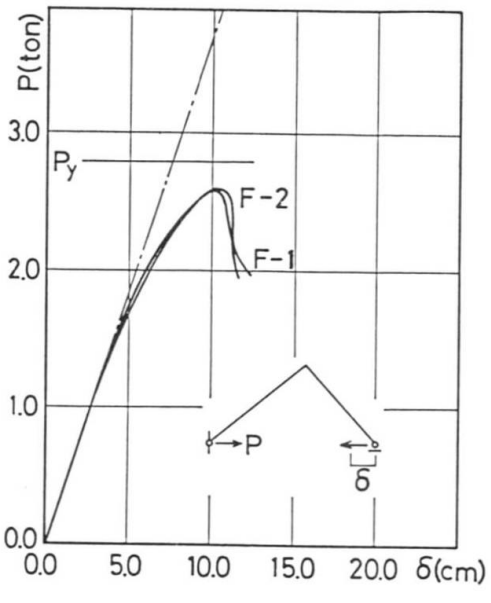

Fig.10 Load-Deflection Curves of Frame

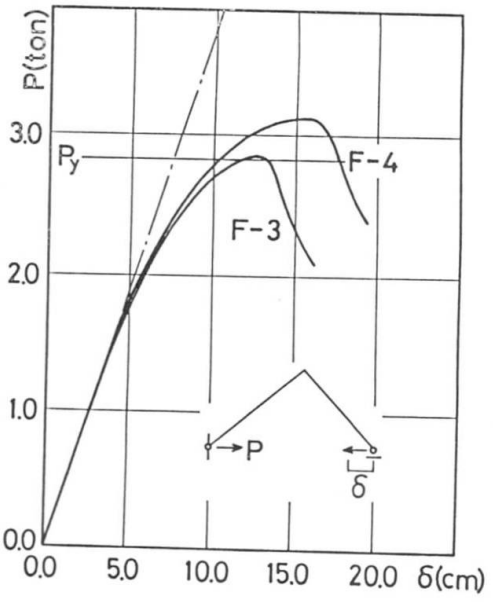

Fig.11 Load-Deflection Curves of Frame

3) F-3
This test piece is provided with a local buckling bracing plate at the starting point of the non-uniform section. Only the tension flange of the corner knee was braced. The load-deformation curve in the elastic region of F-3 was exactly the same as those of F-1 and F-2. The load-deformation relationship became nonlinear when a load of about 2.0 tons was applied. After the ultimate strength of 2.8 tons was reached, F-3 showed deterioration in strength. The lateral buckling deformation after the ultimate strength was reached was inversely symmetrical with that on the opposite side of the cross beam, indicating that the cross beam of unequal leg channel steel served as an effective buckling bracing member. With this test piece, the compression flange at the vartex of the corner knee had not been braced, hence a small amount of out-of-plane deformation occurred, making the inversely symmetrical deformation somewhat incomplete.

4) F-4
This test piece is the same as F-3, except that both the tension and compression flanges were braced at the vertex of the corner knee member. The rigidity deteriorated slightly when a load of about 2.0 tons was applied. However, the ultimate strength reached 3.25 tons. The type of breaking was out-of-plane lateral buckling of the compression flange. The buckling deformation was sufficiently held back by the cross beam and vertex bracing member, and F-4 showed a perfect S-shaped deformation. Compared with the other three test pieces, this test piece showed greater deformation capacity and a plasticity coefficient (μ) of about 1.5.

5. Study of Frame Design

Based on the above-mentioned test results, the new system frame was reviewed. In designing main frame member of non-uniform section, it was anticipated that the starting point of the non-uniform section and the corner knee member would yield at the same time. In the test, however, plasticization of the starting point of the non-uniform section progressed earlier, and hence the ultimate strength was determined by the lateral buckling deformation of the compression flange containing that point. This indicates that in order to obtain a more efficient non-uniform section, it will be necessary to let the starting point of the non-uniform section of the column member come closer to the column base. As for the bracing of the corner knee member, since the main frame is a full web provided with a stiffener, only the tension flange need be braced from the viewpoint of strength, provided that the cross beam has sufficient rigidity. However, in order to ensure good deformation behavior in the plastic region and to maintain sufficient safety of the frame, it would be better to brace the compression flange, as well as the tension flange. The effect of combining the cold formed channel steel used as the cross beam with the roofing member can be secured by use of special-shaped metals. With a 6 m span beam, it would be sufficient to provide one special metal at the center. The use of this cross beam in the new system frame has made it possible to eliminate stud members and sub-beams from the design.

6. Conclusion

This paper has outlined the newly developed system frame, confirmed the validity of the frame design by tests, and presented problems involved.

The test results have proved that the new system frame as a whole is valid. Compared with conventional system frames, the present system has made it possible to reduce the frame weight by 15 to 20% and to shorten significantly the time required for building the frame.

Full Scale Tests and Analysis of Two Light Gauge Steel Pyramid Roofs

Essais et analyse de toitures pyramidales tronquées en acier formé à froid

Bauteilversuche und Berechnungen von zwei Pyramidendächern in Leichtbauweise

J. Michael DAVIES
Prof. of Struct. Eng.
University of Salford
Salford, UK

Professor Davies obtained degrees of Ph.D. and D.Sc. from the University of Manchester for his research into structural steel design. He worked for five years for a firm of consulting engineers before returning to academia. He now specialises in cold-formed steel construction and acts as consultant to several companies.

M. Taher M. NEMIR
Lecturer
Univ. of Alexandria
Alexandria, Egypt

Mohamed Taher Nemir, born 1952, obtained his B.Sc. degree at the University of Alexandria, Egypt, where he subsequently worked as a teaching assistant for six years. He was awarded his M.Sc. degree at the same University and his Ph.D. at the University of Salford in 1986.

Kenneth TAYLOR
Director
Oldryod Bros. Ltd.
Runcorn, UK

Obtained Civil Engineering Degree at Sheffield Polytechnic. Spent five years with consultants specialising in steelwork design. Two years on development of computer programs. Currently Director of a Structural Steelwork Fabricator with responsibility for design and computer development.

SUMMARY

This paper reports on tests on a single hipped roof structure and a two-unit prefabricated development. At the time of testing, it was not found possible to provide an analysis for the asymmetrical load case which relies for its stability on stressed skin (diaphragm) action. In this paper, a suitable analysis is developed and a comparison between the experimental and theoretical deflections is made. Consideration is also given to the prediction of the forces in the fasteners connecting the sheeting to the framing members.

RÉSUMÉ

Cet article rapporte les essais effectués sur des structures pyramidales tronquées uniques ainsi que sur celles composées de deux unités préfabriquées. Au moment où les essais ont été effectués, il était impossible de fournir une analyse pour un cas de chargement asymétrique qui mette à contribution pour sa stabilité l'effet de diaphragme. Dans cet article une analyse spécifique est développée et une comparaison entre flèches expérimentales et théoriques est effectuée. On fait également des considérations quant à la prévision des efforts dans les fixations liant la couverture à l'ossature.

ZUSAMMENFASSUNG

Es wird über Versuche an einem einfachen und einem doppelten Pyramidendach berichtet, für die eine Vorfertigung entwickelt wurde. Zur Zeit der Versuche war eine rechnerische Behandlung des unsymmetrischen Lastfalls, bei dem die Tragfähigkeit auf der Scheibenwirkung beruht, noch nicht möglich. In diesem Beitrag wird eine geeignete Berechnungsmethode entwickelt. Vergleiche zwischen rechnerisch und experimentell ermittelten Durchbiegungen werden vorgenommen. Ausserdem werden die Kräfte in den Befestigungen zwischen den Blechen und den Tragelementen betrachtet.

1. INTRODUCTION

1.1 The MACE Structure

The 'MACE' Structure was originally conceived by the Metropolitan Architects Consortium for Education as a low cost unit designed to meet the needs of nursery education. The novel feature of the structure is a roof with the shape of a truncated pyramid as shown in Fig. 1. Light framing members form the edges of four trapezoidal folded plates and these comprise the complete roof structure which relies for its stability on diaphragm action in the profiled steel cladding. At the time these units were designed, it was not possible to offer a satisfactory analysis of the behaviour of the structure under asymmetric loading and it was deemed necessary to subject a typical unit to acceptance tests to BS 449 [1]. Fig. 1 shows the dimensions of the tested structure and Fig. 2 shows the structure under test.

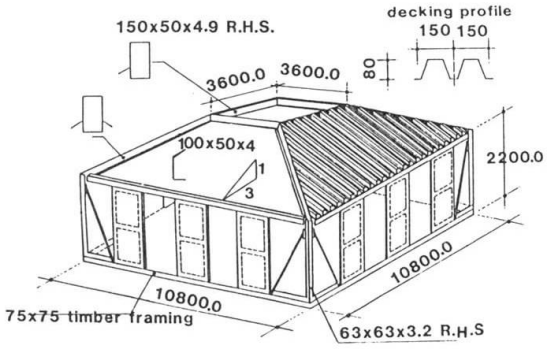

Fig. 1 MACE Type 30 unit as tested.

The roof sheeting had a trapezoidal profile with a depth of 80mm and a net steel thickness of 0.67mm. It was fastened to the supporting members with 6.1mm diameter self-drilling, self-tapping screws through the troughs of alternate corrugations. The seam fasteners were self-drilling, self-tapping screws of 4.1mm diameter at 250mm centres. More complete details of the structure and tests are given in [2] and [3].

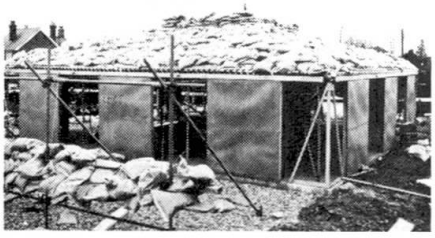

Fig. 2 MACE unit under test

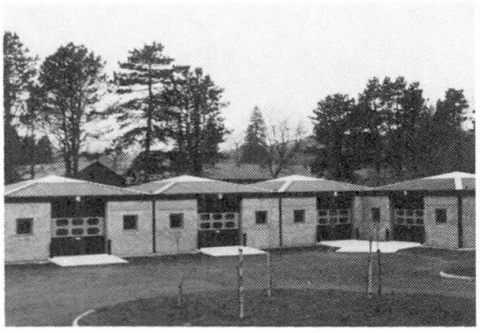

Fig. 3 Pyradomes in use

1.2 The Pyradome

The 'Pyradome' is a development of the MACE concept in which the individual trapezoidal panels are prefabricated for rapid erection and in which there is a facility for eaves members to span 10 metres between corner columns. A number of structures have been built using assemblies of Pyradomes as shown in Fig. 3. During development, a two module assembly was tested at the University of Salford. Fig. 4 shows the general arrangement and Fig. 5 the structure under test.

The members of the Pyradome roof comprise an upper compression ring which supports a plastic roof light and a lower tension ring at eaves level, the two being separated by sloping hip members. Steel cladding, spanning between the eaves and upper ring members, serves both to carry asymmetrical load by diaphragm action and to contribute to folded plate behaviour when adjacent modules act together, thus permitting a clear internal span between corner columns. Edge members required either an intermediate column or a

strengthening member as shown in Fig. 4. However, subsequent development has resulted in the use of an eaves beam which can clear span 10 metres.

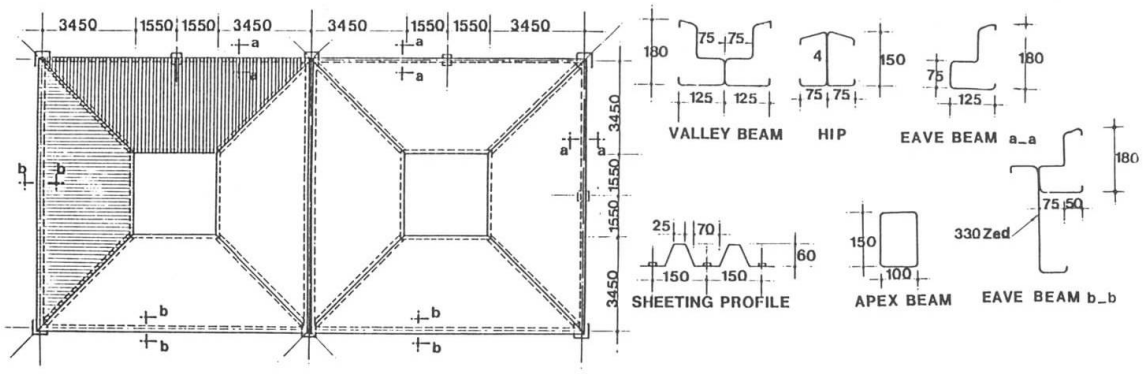

Fig. 4 Plan of tested Pyradome structure

The trapezoidally profiled steel cladding had a depth of 60mm with a nominal thickness of 0.7mm and, in contrast to the MACE panel, was fastened to the supporting members in every trough using 6.1mm diameter self-drilling, self-tapping screws. Seam fasteners were also self-drilling, self-tapping screws at 200mm centres.

The test load levels were based on the draft revision of BS 449 which was current at the time of testing (1980). Based on a working load of 1.0kN/m^2 and a dead load of 0.27kN/m^2, the loading sequence was as follows:

Test 1: Load in five increments up to working load on one Pyradome followed by similar loading on the other.

Test 2: Load up to acceptance load (1.39kN/m^2) on both Pyradomes in increments.

Test 3: Load the whole area of the roof up to half the working load.

Increase the load on half of the area (shown shaded in Fig. 13) to full working load. Apply uniform working load to the whole roof and increase in increments up to the prototype test load of 1.68kN/m^2.

Loading was applied using 25kg sand bags. At each load increment and after the test loads had been maintained for 15 minutes, the deflections at various points were recorded. Vertical deflections were measured by observing suspended scales through an optical level and lateral movements were measured by theodolite. After each test the load was reduced to the factored dead load and the residual deflections recorded.

Fig. 5 Pyradome under test

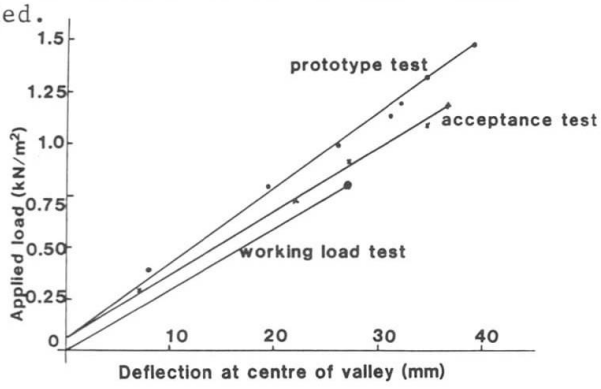

Fig. 6 Typical load-deflection curves for Pyradome.

1.3 Test results and previous analyses

From the practical point of view both the MACE and Pyradome tests were seen as non-destructive tests of prototype structures. The success of the test was assessed in terms of the percentage recovery of deflection and no calculations were required.

For the MACE structure, detailed test results and recovery values are given in [2]. Some simple calculations were carried out for the uniform load case, where stressed skin action has secondary importance, and preliminary consideration was given to the forces arising as a consequence of diaphragm action using finite element analysis of individual trapezoidal panels. However, no calculations were attempted for the assymmetrical load case.

For the Pyradome structure, no calculations had been undertaken prior to the present work. A typical set of load deflection curves is shown in Fig. 6. From these and other similar graphs, it can be concluded that the response is linear and for subsequent comparisons, it will be sufficient to consider patternsof deflection at a given load level. These will be given later after the theoretical analysis has been discussed.

2. MATHEMATICAL MODELLING

2.1 Models for individual panels

Two-dimensional analysis of the individual trapezoidal roof panels using finite elements had been carried out previously for the MACE structure [2]. The mathematical model used, which included detailed consideration of individual fasteners, is shown in Fig. 7. There are considerable practical difficulties in extending this model to the full three-dimensional roof structure.

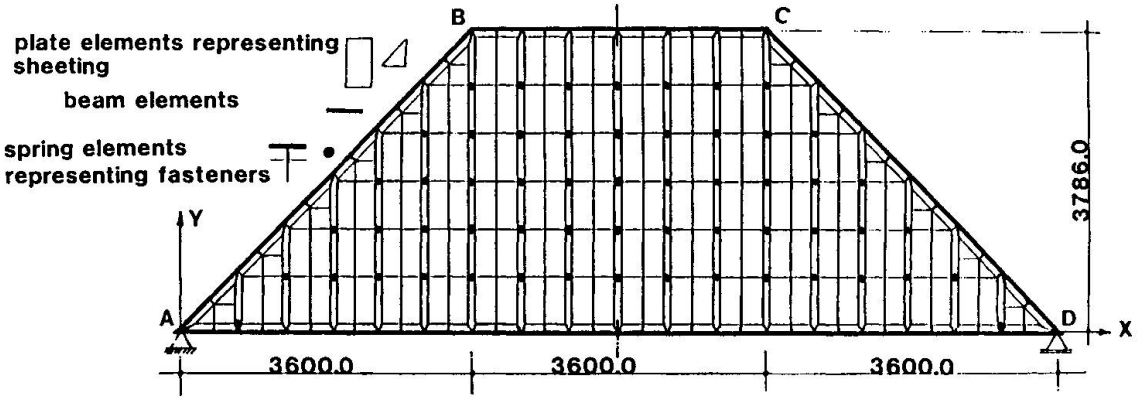

Fig. 7 Finite element model of MACE roof panel.

However, it has been shown [6] that the detailed behaviour of both regular and irregular diaphragms can be accurately simulated using a plane truss model. The original concept requires modification to deal with the trapezoidal shape and a suitable representation is shown in Fig. 8.

This model includes additional 'spring' members to simulate the flexibility of the sheet to edge member fasteners in a direction parallel to the edge members and can be used to analyse a complete hipped roof structure using a suitable computer program for the analysis of space structures. This is, however, a very cumbersome operation and, for practical purposes, it is necessary to seek further simplification.

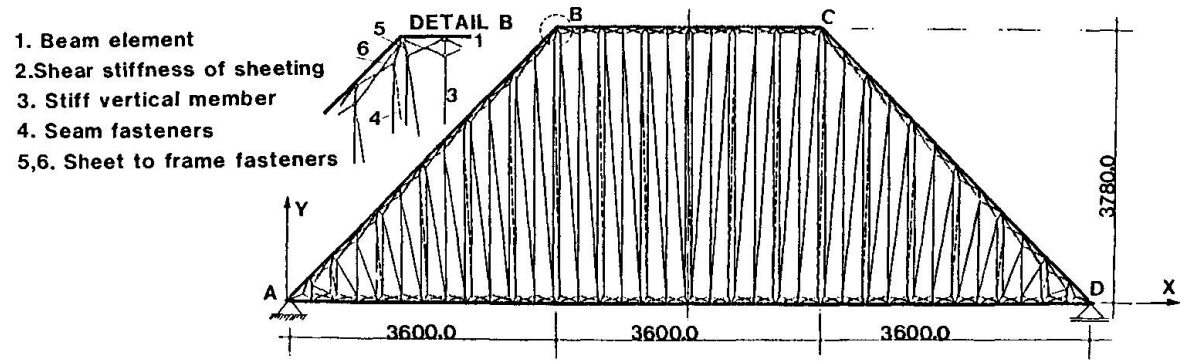

Fig. 8 Full truss simulation of MACE panel

The flexibility c of a complete diaphragm can be calculated as the sum of the flexibilities of the various components including such factors as distortion of the sheeting profile and movement in the various fasteners [7]. If a very simple truss model is used, such as is shown in Fig. 9, the total flexibility of all of the components can be simulated by an arrangement of diagonals and relatively stiff members in the y direction.

It is easy to show that the necessary cross sectional area A_d of the diagonals is given by

$$A_d = \frac{L_d}{Ec \cos^2 \theta}$$

where L_d is the length of the diagonal and θ its inclination to the y axis. Before this simplified model can be incorporated into a three-dimensional analyses, its accuracy requires detailed investigation. A comparison was therefore made between the performance of the three alternative models of the MACE panel with both pinned and rigid joints between the perimeter members for the following load cases:

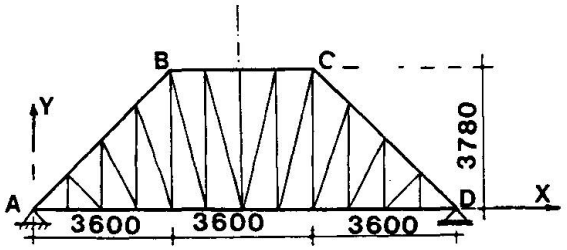

Fig. 9 Simple truss simulation

- uniformly distributed load on eaves member AD
- point loads in y direction at B and C
- point load in y direction at B only
- point load in x direction at B

Full details of this investigation are given in [5].

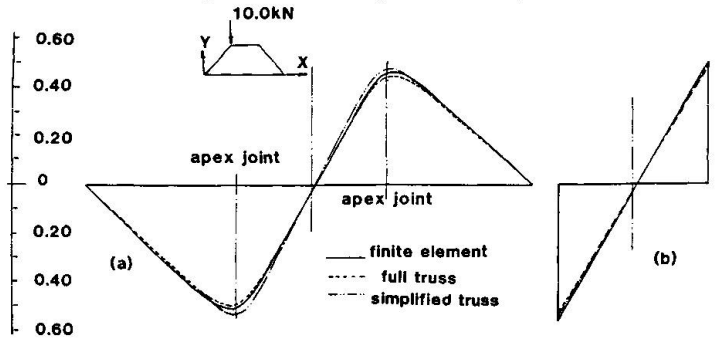

Fig. 10 In-plane deflections (mm) from alternative analyses of the MACE panel - (a) bottom flange, (b) top flange.

A typical comparison of deflections is shown in Fig. 10 and it is clear that the simple truss model gives an accurate estimate of the deflected shape. However, it is known from earlier work [2] that large forces in the sheet to edge member fasteners occur at the junction between the hip and the upper horizontal members. A typical distribution of fastener force in the critical region is shown in Fig. 11. This was obtained from an analysis of the MACE panel with pinned joints and with a distributed load of $2.6kN/m^2$ on the bottom flange. If the four fasteners at and adjacent to the joint have forces F, F^1, F_1, F_1^1, then the internal vertical force resultant

$$V = F_D \cos\theta - F_V$$

can be equated to the approximate resultant to the fastener forces

$$V_p = F + F_1 + (F^1 + F_1^1)\frac{a-p}{a}$$

It then follows that the maximum fastener force may be obtained from the internal forces in the simple truss model as $F_{max} = VF/V_p$

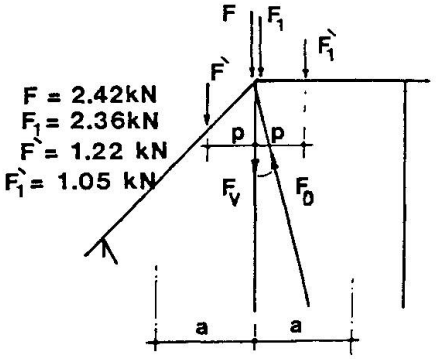

Fig. 11 Fastener forces in critical region of MACE panel

Detailed investigation of the MACE panel [5] shows that this approach gives consistent results for the four loading cases considered and that, for practical purposes, it is sufficient and safe to neglect F^1 and F_1^1 and take $F_1 = F$.

However, the MACE panel had sheet to edge member fasteners in alternate corrugation troughs at 300mm centres whereas, in the Pyradome, these fasteners were in every trough at 150mm centres. While the above approach may be expected to give safe answers for this case, it is likely to prove very conservative.

2.2 Models for the complete structures

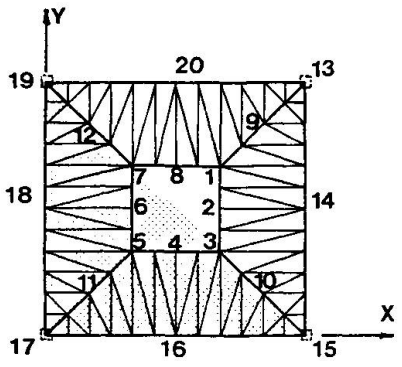

Fig. 12 Plan of model for analysis of MACE unit.

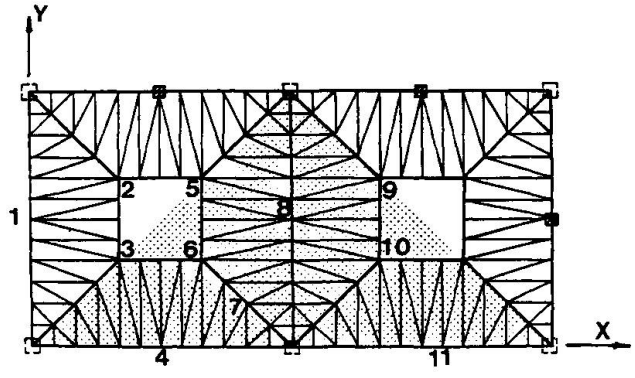

Fig. 13 Plan of model for analysis of Pyradome.

It follows that a suitable model for the analysis of the full MACE unit is shown in plan in Fig. 12. An assembly of two such units was used to analyse the Pyradome as shown in Fig. 13. In each case, the shaded area is the area loaded in the assymmetrical load condition and the numbers refer to those of the load measurement positions for which values are quoted later. It should be noted that the support conditions for the Pyradome are such that the two bays are not identical.

3. COMPARISON OF TEST RESULTS WITH THEORY

In each case, the theoretical analyses were performed twice, once with hinged joints between the framing members and once with rigid connections.

3.1 Comparison between theory and experiment for the MACE unit

Under a uniformly distributed load of 0.8kN/m^2 over the entire roof, the comparison between the experimental and theoretical deflections is given in Table 1. Here, the stressed skin action is of a secondary nature and the generally higher experimental deflections may be attributed to movement in the bolted joints between the framing members. However, the vertical movement at point 9 is restrained by stressed skin action and it is interesting to note that the experimental result falls between the two alternative analyses. The calculated maximum fastener forces are 0.3kN (hinged joints) and 0.09kN (rigid joints) and are not critical.

Location	Experiment	Theory	
		Hinged	Fixed
1z	12.6	9.26	9.06
2z	13.9	12.6	10.8
9z	7.5	10.5	5.75
13x	0.92	1.05	1.02
14x	4.17	3.5	3.35

Table 1 Deflections (mm) for the uniformly loaded MACE unit (x horizontal, z vertical)

Location	Experiment	Theory	
		Hinged	Fixed
1	-21.0	-85.1	-21.0
2,8	-12.5,-13.2	-39.0	-10.7
3,7	12.4, 8.77	6.86	6.79
4,6	34.5, 34.9	57.6	26.9
5	55.2	98.8	34.5
9	-11.2	-42.7	-15.2
10,12	7.15, 6.51	7.81	4.31
11	39.9	58.3	23.8

Table 2 Vertical deflections (mm) for the assymmetrically loaded MACE unit

Under assymmetric loading of 1.21kN/m^2 over half of the area of the roof, the comparison between the experimental and theoretical deflections is given in Table 2. The experimental deflections are mostly between the two theoretical limits. The calculated maximum fastener forces are 4.23kN (hinged joints) and 0.70kN (rigid joints). Whereas the latter are quite acceptable, the values obtained with hinged corner joints exceed the capacity of the connection and the difference between the two is too large for a reasonable estimate to be made. The diaphragm behaviour is clearly very sensitive to the assumptions made regarding joint rigidity.

3.2 Comparison between theory and experiment for the Pyradome

In Table 3, a comparison is given between the experimental and theoretical deflections for two load cases, namely:

Case A - uniform load of 0.80kN/m^2

Case B - uniform load of 0.80kN/m^2 over the shaded area in Fig. 13, the remainder of the roof carrying 0.40 kN/m^2.

Here, with sheet to edge member fasteners in every corrugation trough, the theoretical results for hinged and fixed joints are generally closer together. Bearing in mind the factors contributing to the deflection pattern, the comparison between the theoretical and test results is, with the exception of location 8, considered to be satisfactory.

Approximate investigation of the fastener forces using the procedure indicated in section 2.1 showed these to be generally within acceptable limits. However, individual fastener forces of the order of the ultimate load were predicted in the diaphragms adjacent to the central valley for both loading cases and it is likely that non-linear behaviour of these fasteners contributed to the large deflections at location 8. This problem has been resolved by subsequent development which includes the provision of eaves and valley

members which can span 10 metres without the assistance of diaphragm action.

Location	CASE 'A'			CASE 'B'		
	Experimental results	Theoretical results		Experimental results	Theoretical results	
		Hinged	Fixed		Hinged	Fixed
1	12.0	16.0	8.31	5.50	8.0	4.06
2	7.0	7.28	7.19	3.50	-0.94	2.0
3	7.0	7.96	7.47	4.50	6.24	5.44
4	12.0	16.0	5.17	12.0	16.0	5.19
5	9.0	9.22	7.77	5.0	9.18	6.55
6	9.0	8.16	7.52	9.0	10.9	9.45
7	8.50	9.63	5.35	8.50	11.0	6.81
8	19.5	11.7	9.86	18.0	10.6	8.8
9	9.50	10.0	8.24	5.50	8.70	6.76
10	9.0	8.0	8.02	8.0	11.8	9.85
11	12.0	16.0	5.40	16.5	16.0	5.31

Table 3. Vertical deflections (mm) for the Pyradome

CONCLUSIONS

- The simple truss simulation provides a practical and sufficiently accurate method of analysis for three-dimensional stressed skin assemblies.
- The analysis is sensitive to the assumptions made regarding the stiffness of the joints between the framing members, particularly for diaphragms where the sheeting is fastened to the framing members through alternate troughs and this condition should be avoided unless the forces arising as a result of diaphragm action are small.
- Fastener forces can be critical where the framing members meet. A suitable method of estimating these forces has been given.

REFERENCES

1. BS 449: Part 2: 1969 "Specification for the use of structural steel in building" Appendix A, loading tests.
2. J.M. DAVIES, R.M. LAWSON and J.G. YOUNG "Calculated and observed behaviour of the steel folded plate roof of a nursery school" Proc. Conf. on the Performance of Building Structures, Glasgow, Pentech Press, March 1976, pp 31-44.
3. A.R. LAMB "The design and testing of a stressed skin structure for a range of nursery school buildings" Acier-Stahl-Steel. Vol. 11, 1975.
4. W.H. DEAKIN "Loading tests on Pyradomes" University of Salford, Dept. of Civil Engineering, Report. Ref. No. 80/142, July 1980.
5. M.T.M. NEMIR "Finite element stability analysis of thin-walled steel structures" PhD Thesis, University of Salford, 1985.
6. J.M. DAVIES "Simplified diaphragm analysis" Proc. A.S.C.E.,J. Struct. Div., Vol. 103, No. ST11, November 1977, pp 2093-2109.
7. J.M. DAVIES and E.R. BRYAN "Manual of stressed skin diaphragm design" Granada, London, 1982.

Stainless Steel Membrane Roof

Membranes en acier inoxydable pour toitures

Nichtrostende Stahlmembrane für Bedachungen

Ben KATO
Prof. of Struct. Eng.
University of Tokyo
Tokyo, Japan

Takashi NAKAMICHI
Techn. Adm. Bureau
Nippon Steel Corporation
Tokyo, Japan

Eiichiro SAEKI
Struct. Engineer
Nippon Steel Corporation
Tokyo, Japan

Ben Kato, born 1929, received his degree of Dr. Eng. from the University of Tokyo. Through the continuing service as lecturer, associate professor at the University of Tokyo, Ben Kato, now occupies the chair of steel structures and welding engineering.

Takashi Nakamichi, born in 1938, received his Bachelor's degree from Kyushu Univ. Since 1962 he has been engaged in building design and construction and now is engaged in the development and engineering of architectural materials and structures.

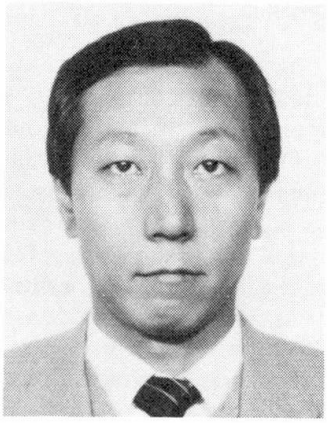

Eiichiro Saeki, born 1951, received his M. Eng. from Tokyo Institute of Technology and M.Sc. from Northwestern Univ., USA. Since 1976 he has been engaged in the design and construction of buildings, now involved in the research and development of special structures.

SUMMARY

The design procedure for stainless steel membrane roofs is described with reference to the recently completed double-membrane roof project. Especially the behaviour of the contraction joints is discussed taking into account the stress condition of the cold-forming process.

RÉSUMÉ

La procédure de dimensionnement d'une toiture utilisant des membranes d'acier inoxydable est décrite en se référant à un projet de couverture utilisant des doubles membranes d'acier inoxydable dont la construction fut réalisée tout récemment. On examine en particulier le comportement des assemblages de contraction en tenant compte de l'état de contrainte lors du processus de profilage à froid.

ZUSAMMENFASSUNG

Das Konstruktionsverfahren einer nichtrostenden Stahlmembran-Bedachung ist hierin beschrieben, wobei auf das Projekt eines Doppelmembrandaches Bezug genommen wird, das vor kurzem fertiggestellt wurde. Das Verhalten der Kontraktionsverbindungen wurde eingehend behandelt, wobei der Spannungszustand infolge Kaltverformung berücksichtigt wurde.

1.INTRODUCTION

In the period from the latter half of the 1960s to the early years of the 1970s, extensive studies were conducted on metallic membrane roofs in Canada. As a result of such studies, it was found that chrome-nickel stainless steel is most suitable as a material for permanent type membrane roofs. Moreover, the basic behavior of such membrane roofs under pressures and loads was elucidated. The suitability of stainless steel as a material for membrane roofs is due to its excellent characteristics, such as high strength to withstand large stresses with small thickness, corrosion resistance high enough to assure long-term durability, toughness high enough to resist pitting, tearing, etc., and excellent weldability to facilitate fabrication and assembly. For the practical application of stainless steel membrane to large-scale structure, however, the following three conditions must be satisfied:

-(1)It must be possible to assemble the roof on a flat surface.
-(2)The completed roof should be maintained in a spherical shape by air pressure.
-(3)The completed roof should be formed into a concave shape at deflation.

The condition (1) is essential for practical construction of membrane roofs. If the condition (2) is not satisfied, the characteristic of the shell cannot be produced. If the condition (3) is not met and the internal pressure becomes insufficient after completion (deflation), buckling or other troubles may be caused, resulting in damage to the segments. Sinoski's system introduced below is a metallic membrane roof which satisfies the three conditions shown above by the use of contraction joints. This paper describes the design procedure of stainless steel membrane roof, mainly membrane stresses and contraction joints referring to the Health Promotion Center at Nippon Steel's Muroran Works which was the first project completed using the stainless steel double membrane roof (hereinafter referred to as the "Muroran Project").

2.OUTLINE OF STAINLESS STEEL MEMBRANE ROOF

2.1 Structural element

Basically, the membrane roof is constructed by assembling and welding stainless steel sheets (of about 1.5mm in thickness for a span of 100m) into a very large sheet. The roof thus constructed is supported by air pressure from below. More specifically, this roof consists of the following members as shown in Figs. 1 and 2.
Compression ring (a): Member to support the tension applied to the segment
Trapezoidal segment (b): Segment are cut from stainless steel sheet and are welded at the plant and transported to the site.
Center segment (c): Same as segment (b)
Contraction joints (d and f): These joints are formed by pressing at the plant.
Closure joint (e): Polyurethane sheet or a material having the flexibility and durability equivalent to those of polyurethane

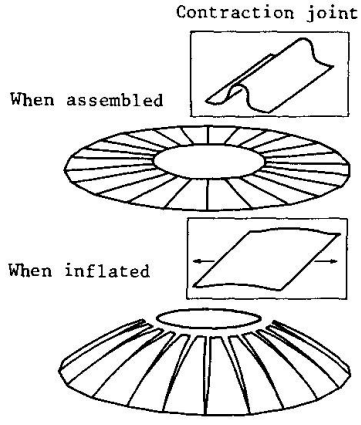

Fig. 1. System of stainless steel membrane roof

Basically, the segments are made of SUS304 and the contraction joints, SUS301 LHT (JIS). The membrane consists of six members (a) to (f) as described above. All members are joined mainly by welding. Spring members called "contraction joints" which can follow the expansion and contraction of the gap between the segments are used to ensure that the segments arranged on a flat surface can be formed into a spherical shape when the membrane is inflated (see Fig. 1). The roof can be inflated into a proper, stable dome by adjusting the spring characteristics, the amount of contraction and the arrangement of the contraction joints as appropriate.

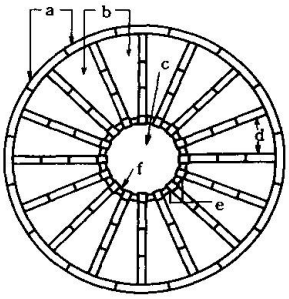

Fig. 2. Members of stainless steel membrane roof

3.DESIGN PROCEDURE

The flow chart for design of stainless steel membrane roofs is shown in Fig. 3. "Shape analysis" means the shape design of dome to be formed by inflation. In this design, the stable shape is determined in consideration of plan. "Structural analysis" means the analysis of membrane stress and compression ring stress which is undertaken using the above-mentioned shape. The details of this analysis are described in the following sub-chapter. The design of contraction joint is divided into two stages. In the first stage, the cross-sectional shape is designed to determine the arrangement and the amount of contraction of contraction joints which are necessary for developing the required dome shape. In the second stage, the spring characteristics of the contraction joint is analyzed in order to confirm that the specified dome shape can be developed when the membrane stresses calculated by structural analysis are applied, and to check the safety for the stresses to be caused in the contraction joints. (The details of this analysis are described in Chapter 3.)

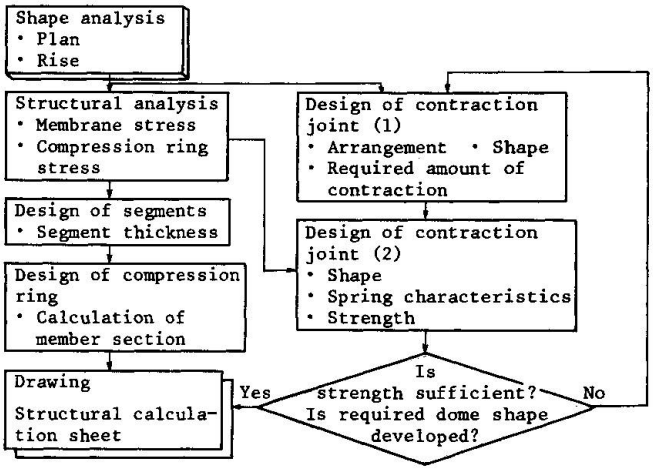

Fig. 3 Flow chart for design

3.1 Method for analysis of membrane stresses and compression ring stresses

The membrane and compression ring stresses are analyzed together according to the finite element method. The program and elements to be used for this analysis are shown below. In stress analysis, the shape obtained by fully extending the contraction joints is taken as the initial shape (it is assumed that the membrane is uniform and free from ondulations) and the stresses caused by internal pressures and other external forces are analyzed according to the small displacement theory. [A comparison of the stresses calculated by the small displacement theory with those obtained by the analysis in which the geometrical non-linearity is taken into account shows that the latter stresses are about 90% of the former stresses for this type of shape (in case where the internal pressure is 1.47kN/m^2).]

Program used: MARC
Elements used:
Segment: Three-dimensional thin-wall shell element
Compression ring: Three-dimensional beam element
As the two elements shown above have the same degree of freedom of node and boundary compatibility, they can be analyzed together.

3.2 Example of analysis of membrane stresses

3.2.1 Analytic model

An analytic model was assumed for the Muroran Project. This model is of such a shape, consisting of parts of sphere and cylinder with 30m in long side, 24m in short side and 1.1m in rise. The one-fourth model and element diagram for F.E.M. are shown in Fig. 4. The boundary conditions are such that the lines A and B are symmetrical and the nodes marked by ● which are the supporting points are free in the X and Y directions but constrained in the Z direction.

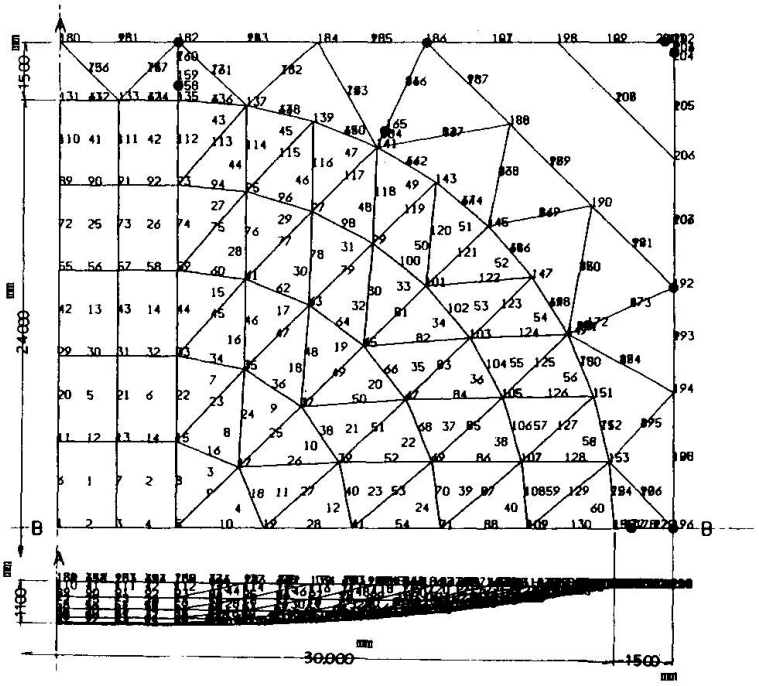

Fig. 4. Analytic model

3.2.2 Material constants

The material constants are as shown in Table 1.

Table 1 Material constants

	Stainless steel	SS41
Young's modulus	19,306 kN/cm^2	20,580 kN/cm^2
Poisson's ratio	0.3	0.3

3.2.3 Loads

Two kinds of loads are assumed. One is the load in the normal direction which corresponds to internal pressure and wind load. The other is the load in the vertical direction which corresponds to dead load and snow load. As the example of analysis being introduced here is for the double membrane roof, the stiffness of the compression rings of this model was evaluated by proportionally distributing the stiffness of the compression rings of the single membrane analysis model according to the ratio of loads applied to the upper and lower membranes so that the deformation of the upper membrane edge agrees with that of the lower membrane edge.

3.2.4 Results of analysis

Examples of the results of analysis are shown in Figs. 5 and 6. Figs. 5 shows the Mieses stress intensity at the center of the cross section and Fig. 6 shows the displacement in the X and Y directions at a magnification of 100. As these results of analysis show, the distribution of membrane stresses differs considerably from that according to the spherical and/or cylindrical shell theory. Particularly, the stress concentration to be caused at the end of the cylindrical

shell is excessive. It is considered that this stress concentration results from the shape instability and the difference in boundary conditions. As this stress concentration is very sensitive to the dome shape and the rigidity of compression rings, it should be given special attention in future design. On the other hand, the stresses to be caused in the compression rings are considerably smaller than those to be caused in case where the reaction force at the membrane edge which is calculated according to the membrane theory is applied to the rings as an external force. This may be due to the effect of plane rigidity of the stainless steel membrane. Namely, it may be because the deformation of the rings in the Y direction is constrained by the plane rigidity.

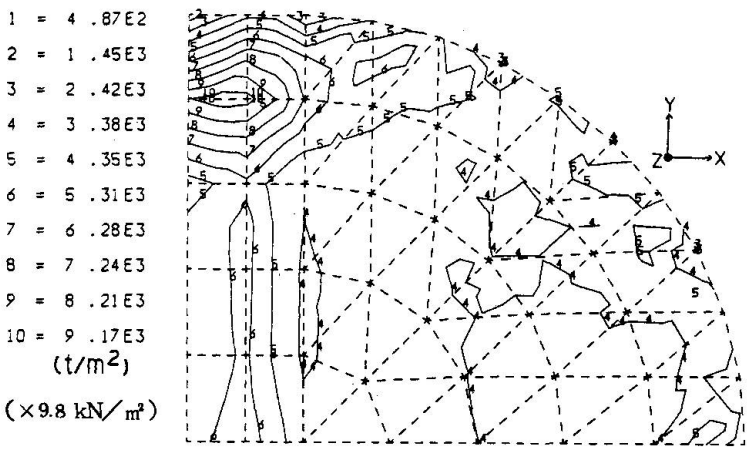

Fig. 5. Mieses stress

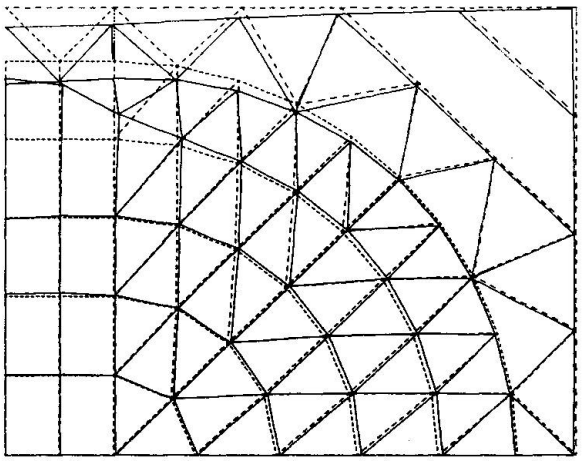

Fig. 6. Deformation diagram (x 100)

4.ANALYSIS OF THE MECHANICAL CHARACTERISTIC OF CONTRACTION JOINT

The contraction joint is the most important member of the stainless steel membrane roof. The designed curvature can be exactly produced and the development of undesirable stresses in the segments at the time of deflation can be prevented by arranging the contraction joints appropriately. The contraction joint is fabricated by cold-forming stainless steel sheet with high yield point. This joint expands nearly to a flat shape at the time of inflation but contracts nearly to its original shape at the time of deflation. In these cases, the residual stresses and strains developed within the contraction joint at the time of forming are changed in a complicated manner during the course of expansion and contraction. In Chapter 4, the structural safety of the contraction joint is studied by analyzing the behavior of this joint.

4.1 Analytic model of contraction joint

As shown in Fig. 7, the contraction joint can be expressed with the radius of curvature R and the angle θ as parameters. As the symmetry condition and the inflection point of bending moment are located close to the point Ⓠ, the analysis is conducted using the one-fourth model as shown in Fig. 8. In actual analysis, two radii of 20 and 30cm, θ of 30° and the sheet thickness of 0.15cm are used.

4.2 Analysis method

Analysis is conducted according to the finite element method in which material non-linearity (plasto-elasticity) and geometrical non-linearity (large deformation) are taken into consideration. For element division, the length between © and Ⓠ is divided into 100 elements and the cross section is divided into 20 layers. It is assumed that there is no stress change in each layer. The relation between the stress and strain is modelled as shown in Fig. 10 on the basis of the results of material test as shown in Fig. 9.

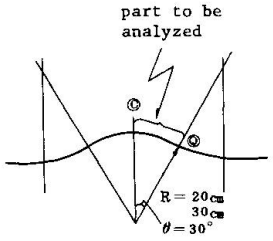

Fig. 7. Analytic model

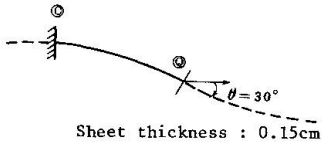

Fig. 8. Analytic model (1/4)

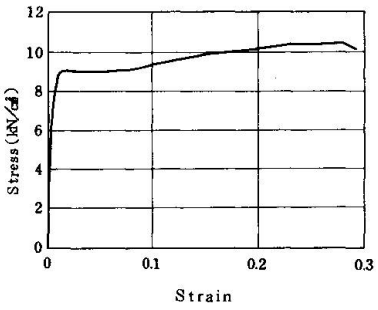

Fig. 9. Stress-strain relation

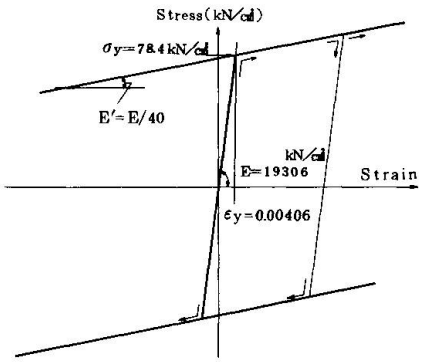

Fig. 10. Stress-strain relation (modeled)

4.3 Forming and contracting process

4.3.1 Forming process

An analysis for expressing the cold forming process, the bending moment (M) is given to the point Ⓠ as shown in Fig. 11 (processes O ⟶ A⟶B) until some of the layers yield . The desired shape is produced through residual deformation after the removal of the bending moment.

4.3.2 Expanding and contracting process

As an analysis for representing the expanding and contracting process, loading and unloading are repeated, the maximum load (P) being 117.6kN/m at which the average stress in the cross section becomes 7.84kN/cm^2 as shown by the processes B⟶C⟶D⟶E⟶F⇄G⇄H in Fig. 11.

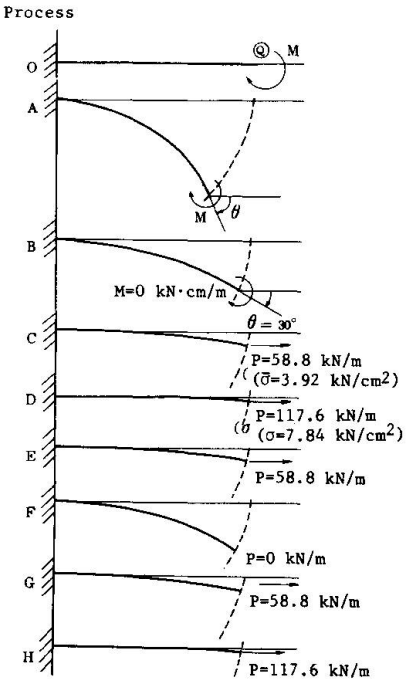

Fig. 11. Changes in deformation

4.4 Results of analysis

4.4.1 Relation between bending moment (M) and the angle of rotation (θ) (Fig. 12)

In the formation of a contraction joint with R of 20cm and θ of 30°, the desired shape can be produced by applying a bending moment of 42,111kN cm/m, rotating the point Ⓠ until θ becomes equal to 76.7° (process A), and removing the moment.

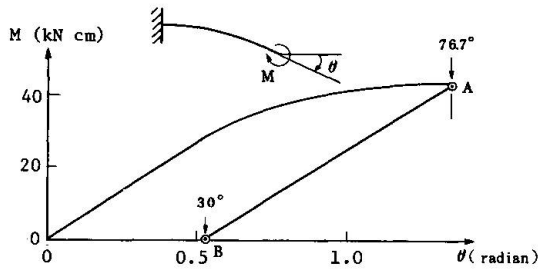

Fig. 12. M-θ relation

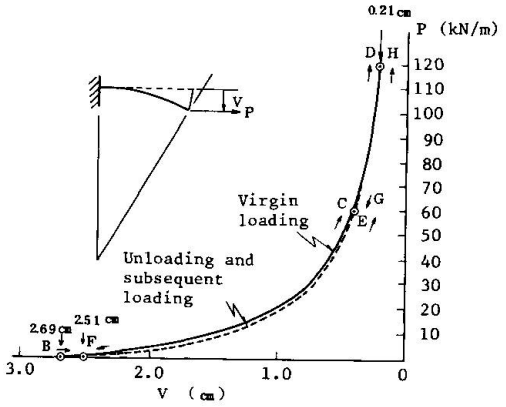

Fig. 13. P-V relation

4.4.2 Relation between load (P) and displacement (C) (Fig. 13)

When R is 20cm, the displacement V becomes 2.69cm at the end of forming (Process B). If virgin loading is done up to 118kN/m (process D), V becomes 0.21cm and the contraction joints extend nearly to a flat shape. The joints contract again if the load is removed. Even if the removal of load is completed (process F), however, V remains at 2.51cm and the contraction joints do not return to the originally formed shape. If the load is applied again, V becomes 0.21cm at the maximum load (process H). This V is the same as that obtained at the time of virgin loading (process D). Even if loading and unloading are repeated, the displacement in the respective processes does not vary.

4.4.3 Changes in stress and strain distributions at the fixed end (Fig. 14)

At the end of forming (process B), the residual stress and residual strain exist in the cross section. The strain is the largest under this condition but decreases as the load is removed. For the stress, the fiber stress reaches the yield level at P = 58.8kN/m (process C).

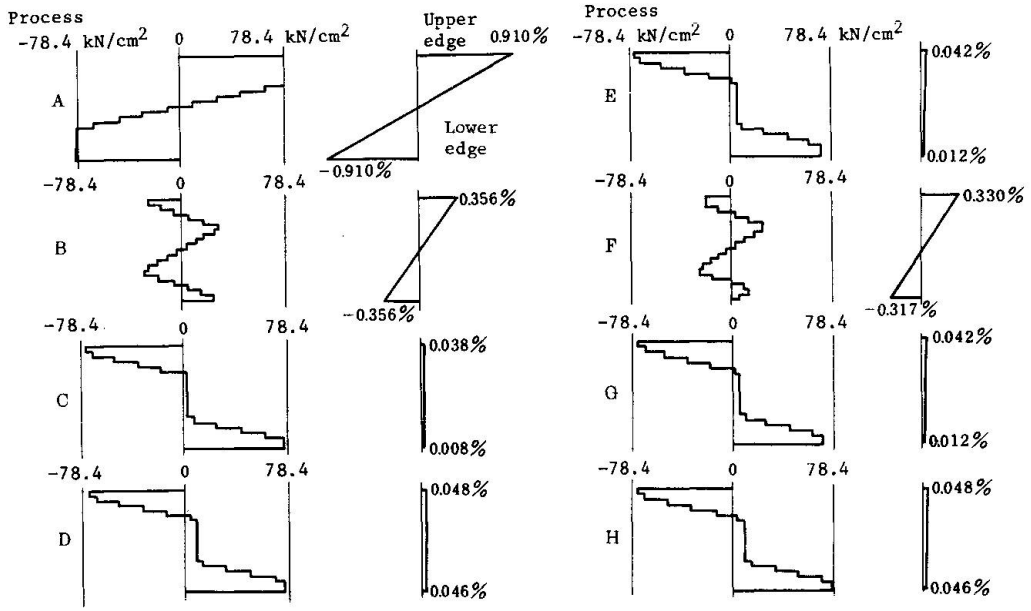

Fig. 14. Distribution of stress intensity at fixed end | Distribution of strain at fixed end | Distribution of stress intensity at fixed end | Distribution of strain at fixed end

4.4.4 Relation between fiber stress and strain at the fixed end (Fig. 15)

At the time of second and subsequent loading and unloading, the fiber stress and strain on surfaces change as the process proceeds from F through G to H and vice versa.

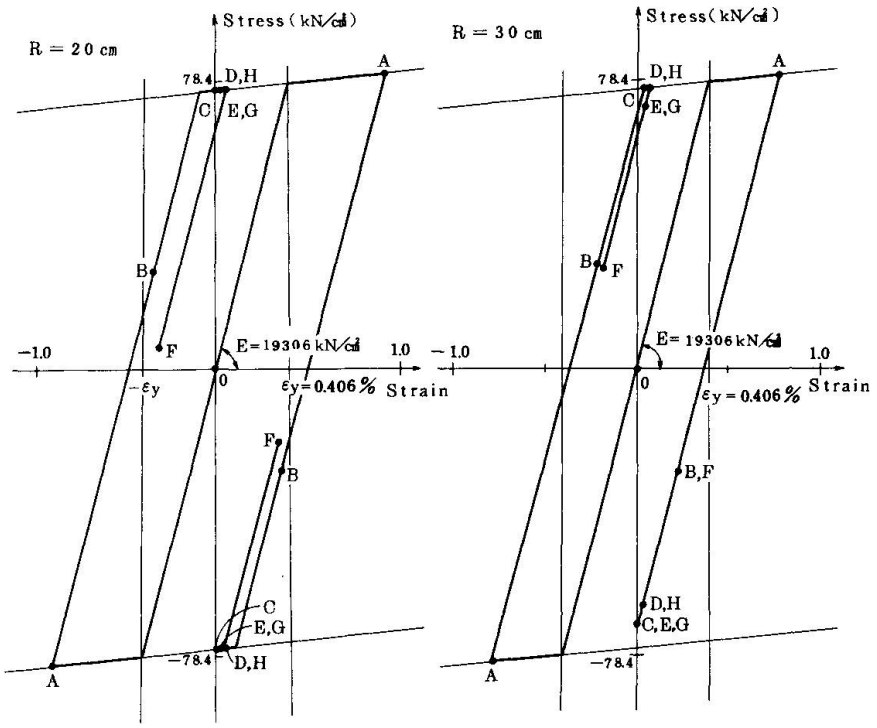

Fig. 15. Stress-strain relation of surface fiber stress

4.5 Study of structural safety

The study of the strain behavior of the contraction joint shows that the maximum strain is always below the yield strain and the maximum strain is caused under the no-load condition (process B or F). The study of stress behavior shows that the ratio of ultimate yield strength in the cross section to the integrated value of tensile stress in the cross section is higher than 4 as shown in Table 2, though there is such a case where yield occurs at the edge in the section when the maximum load is applied (process D or H). Based on these findings, it is said that the contraction joint is sufficiently high in structural safety.

Table 2

Classification	Ultimate yield strength in cross section (kN/cm) a	Integrated value of tensile stress in cross section (kN/cm) b	Ratio a/b
R = 20cm	11.76	2.94	4.0
R = 30cm	11.76	2.45	4.8

REFERENCE

1. FUJIMOTO, M. WADA, A. IWATA, M. Non-linear 3-dimensional analysis of Steel Frame Structure, A.I.J. No. 227, Jan. 1975.

Distortion and Warping of Profiled Metal Sheeting in Shear

Distorsion et gauchissement des plaques profilées en métal soumises au cisaillement

Verwindung und Verzerrung von Stahlprofilblechen unter Schubbeanspruchung

André v.d. BOGAARD
Struct. Engineer
University of Technology
Eindhoven, the Netherlands

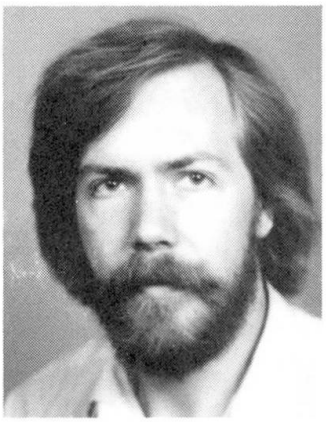

André van den Bogaard, born in 1953, received his structural engineering degree in 1983 at the Eindhoven University of Technology and is currently performing research work for a PhD at the same university.

SUMMARY

In this paper a mathematical basis is presented for the calculation of shear deformation of trapezoidally corrugated sheeting. Expressions are given for the calculation of shear strain and distortion both combined with warping of corrugations. Various boundary conditions along profiled edges can be treated. Explicit formulae are given for the two wavelengths, belonging to a profiled sheet with all corrugations equally attached. For shear diaphragms longer than wavelengths distortion is independent of the length: this can be simulated physically by discrete springs.

RÉSUMÉ

Dans cet article on présente une base mathématique pour le calcul de la déformation due au cisaillement de panneaux en tôle ondulée de forme trapézoïdale. On donne des expressions pour le calcul du glissement et de la distorsion, en combinaison avec le gauchissement. Des conditions aux limites différentes sur les bords des profilés peuvent être traîtées. On donne des formules explicites pour les deux longueurs d'onde attribuées à un panneau de tôle profilée fixé de façon égale dans chaque onde. Pour les panneaux plus longs que les longueurs d'onde, la distorsion est indépendante de la longueur; ceci peut être représenté physiquement par des ressorts ponctuels.

ZUSAMMENFASSUNG

In diesem Beitrag wird ein mathematisches Modell für die Berechnung der Schubverformung von Trapezblechscheiben präsentiert. Ausdrücke für die Berechnung von Schub- und Querschnittverformung werden gegeben, beide kombiniert mit Verwölbung. Verschiedene Bedingungen an den Querrändern können behandelt werden. Für Bleche, die gleichmässig in allen Rippentälern befestigt sind, werden Formeln für die Schubverformung mit zwei Beulwellen gegeben. Für Scheiben, welche länger als die Wellenlänge sind, ist die Querschnittverformung von der Blechlänge unabhängig: das kann physikalisch mit Einzelfedern simuliert werden.

1. SCOPE

Trapezoidally profiled metal sheeting in stressed-skin structures is capable of transferring considerable in-plane loads. For that purpose it must be connected to proper intermediate or edge members. Then normal forces or in-plane bending moments are basically taken by these members, where shear forces are transferred by the sheeting. In ECCS recommendations |1| this is called diaphragm action.
The application of shear diaphragms depends to a major extent on the resistance against in-plane deformation. Deformation of an individual diaphragm in its plane is generally caused by extension and deflection of the edge members in plane of the panel, by local deformation of fastenings and finally by shear deformation of profiled sheeting itself. In this paper attention will be paid to the latter only: shear deformation of profiled sheets.
Object of considerations will be sheeting with trapezoidally profiled cross section, that can be described with 5 relevant parameters (figure 1a). Few other interesting parameters then can be derived (figure 1b).

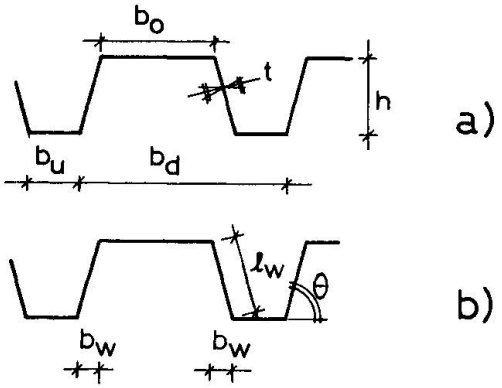

Figure 1: a) relevant parameters
b) derived parameters

For short notation following dimensionless shape factors are denoted:

$$\frac{b_o}{b_d} = \alpha_o \qquad (1)$$

$$\frac{2\,\ell_w}{b_d} = \alpha_w \qquad (2)$$

$$\frac{b_u}{b_d} = \alpha_u \qquad (3)$$

$$\frac{b_o + 2\,\ell_w + b_u}{b_d} = \alpha \qquad (4)$$

2. SHEAR DEFORMATION

2.1 Shear strain

For a global deformation only two independent displacements of a shear diaphragm are relevant: a displacement u in x-direction (perpendicular to foldlines) and a displacement v in y-direction (parallel to foldlines). In-plane rotation of a diaphragm as a rigid body is expressed by:

$$\frac{\partial u}{\partial y} + \frac{\partial v}{\partial x} = 0 \qquad (5)$$

If a profiled sheet is in stress, due to a constant shear force s per unit length, every strip will be strained to a magnitude of $\gamma = s/Gt$. Two parallel lines in y-direction with pitch b_d will translate with respect to each other, giving a parallel shift Δv:

$$\Delta v = \gamma(b_o + 2\ell_w + b_u) = \frac{s}{Gt}(\alpha b_d) \qquad (6)$$

Thus the parallel shift per unit width becomes:

$$\frac{\Delta v}{b_d} = \frac{\alpha s}{Gt} \quad \text{where} \quad \frac{\Delta}{b_d} = \frac{\partial}{\partial x} \qquad (7)$$

This is shear deformation merely as a result of shear strain. A top view of a strained element (figure 2) shows, that an originally plane cross section does not remain plane. This phenomenon is known as warping of a cross section.

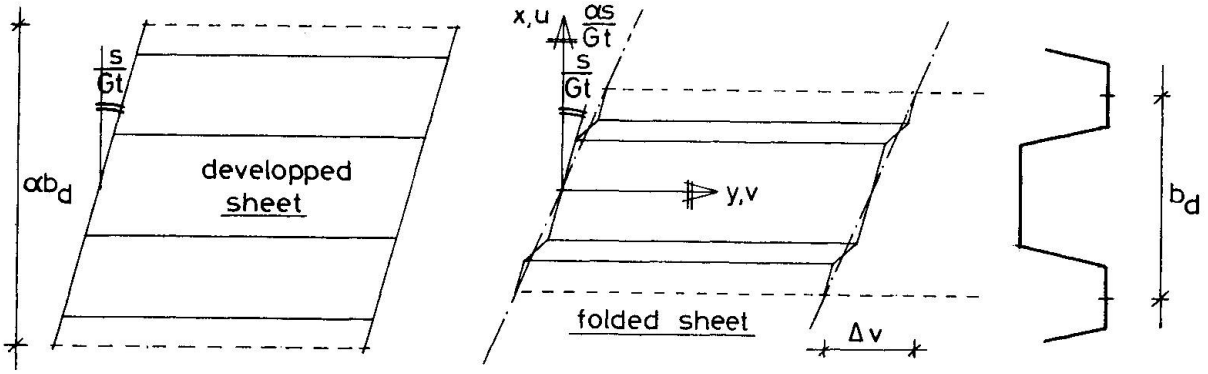

Figure 2: shift and warping due to shear strain

Combination of rigid body rotation and shear strain yields the kinematic condition:

$$\frac{\partial u}{\partial y} + \frac{\partial v}{\partial x} = \frac{\alpha s}{Gt} \qquad (8)$$

2.2 Distortion

A constant shear force per unit length can only exist if along the profiled sheet edges in every flange and web the shear force is transmitted to an edge member. This will hardly ever be possible in practice. Usually profiled sheeting is attached at one side to a supporting structure. In that situation the uniform distribution of shear stresses is disturbed, because the entire shear force over a cross section in the vicinity of fasteners is concentrated at one side of the sheet (figure 3). This causes distortion of the cross section, mainly due to inextensional bending.

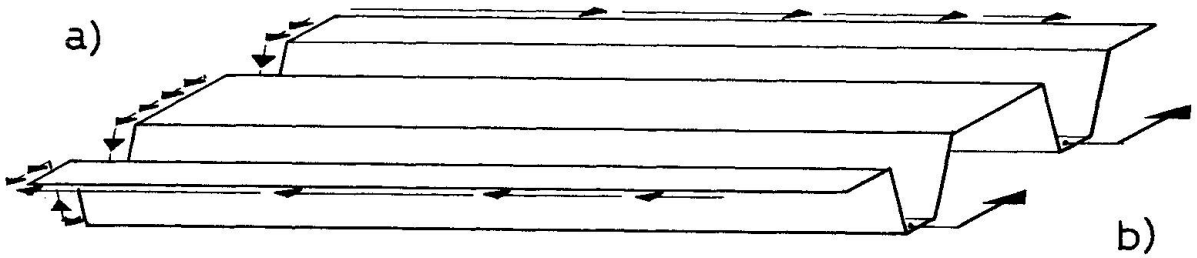

Figure 3: a) uniform shearforce
b) shearforce concentrated in bottom flanges

Further considerations will be confined to sheeting that is attached to supporting members identically in every corrugation, where distortion of all corrugations is equal. Distortion of a cross section now can be composed of two basic deformation modes (figure 4). Displacements in x-direction are denoted u_o for top flanges and u_u for bottom flanges, which means:

$$u_o + u_u = u_1 = 0 \quad \text{for basic mode 1 and}$$
$$u_o - u_u = u_2 = 0 \quad \text{for basic mode 2}$$

A top view of the deformed corrugation (figure 4) shows, that individual plate elements curve in their own plane. Initially plane cross sections do not remain plane and distortion always occurs simultaneously with warping.

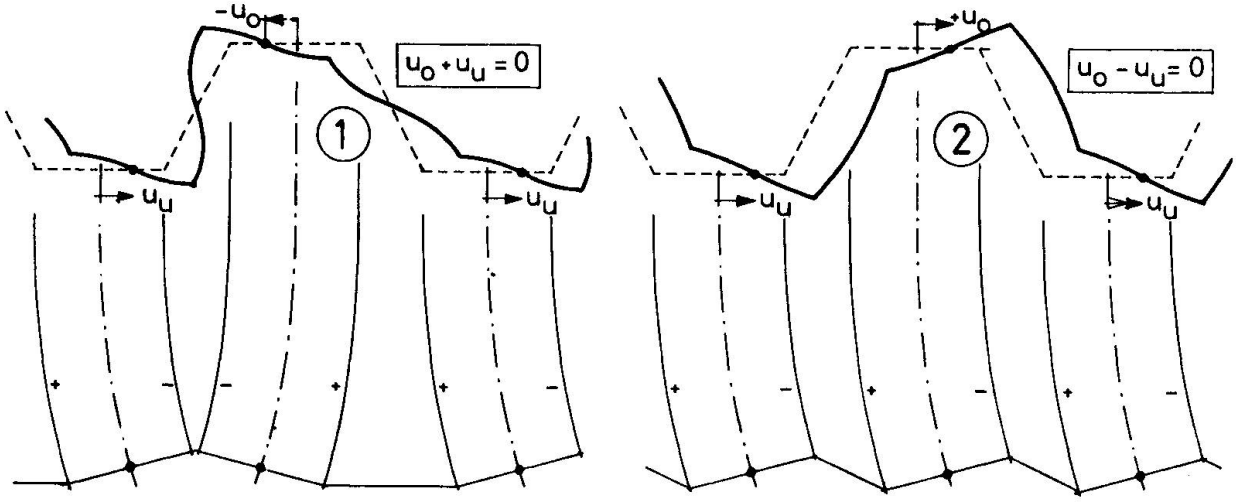

Figure 4: basic modes of distortion and warping

Distortion of corrugations can be exposed by a vector function $\underline{u}$, that contains two displacement functions of y:

$$\underline{u} = \begin{bmatrix} u_1 \\ u_2 \end{bmatrix} = \begin{bmatrix} 1 & 1 \\ 1 & -1 \end{bmatrix} \cdot \begin{bmatrix} u_o \\ u_u \end{bmatrix} \tag{9}$$

The relation between inextensional bending and warping of a cross section |2| leads to the following differential equations:

$$(K^{-1}J)(K^{-1}J)\ \underline{u}^{IV} + 4\beta^4\ \underline{u} = \underline{0} \tag{10}$$

where:

$$\underline{u}^{IV} = \frac{d^4}{dy^4}\,\underline{u} \quad , \quad \beta = \frac{1}{b_d}\sqrt{\frac{t}{h}}\sqrt{\frac{3}{1-\upsilon^2}} \tag{11}$$

$$K = \begin{bmatrix} k_{11} & k_{12} \\ k_{21} & k_{22} \end{bmatrix} = \begin{bmatrix} 0 & 1 \\ 1 & 2(\alpha_o - \alpha_u) \end{bmatrix} \tag{12}$$

$$J = \begin{bmatrix} j_{11} & j_{12} \\ j_{21} & j_{22} \end{bmatrix} = \begin{bmatrix} \frac{\eta_o + \eta_u}{2} & \frac{\eta_o - \eta_u}{2} \\ \frac{\theta_o - \theta_u}{2} & \frac{\theta_o + \theta_u}{2} \end{bmatrix} \tag{13}$$

Matrix J contains a number of non-linear combinations of dimensionless shape parameters:

$$\eta_o = \alpha_o^3 + \alpha_w\alpha_o^2 - \tfrac{1}{2}\alpha_o\alpha_w\alpha_u \qquad \eta_u = \alpha_u^3 + \alpha_w\alpha_u^2 - \tfrac{1}{2}\alpha_o\alpha_w\alpha_u \tag{14}$$

$$\theta_o = \alpha_o^3 + \alpha_w\alpha_o^2 + \tfrac{1}{2}\alpha_o\alpha_w\alpha_u \qquad \theta_u = \alpha_u^3 + \alpha_w\alpha_u^2 + \tfrac{1}{2}\alpha_o\alpha_w\alpha_u \tag{15}$$

Notice, that $(\eta_o - \eta_u) = (\theta_o - \theta_u)$ so that J is a symmetrical matrix. For corrugations with all flanges of equal width, where $(\alpha_o - \alpha_u) = 0$, also K is a symmetrical matrix.
The general solution for $\underline{u}$ of the differential problem can be written by means of two eigen vectors and two hyperbolic periodic functions:

$$\underline{u} = \begin{bmatrix} 1 \\ e_1 \end{bmatrix} f_1 + \begin{bmatrix} e_2 \\ 1 \end{bmatrix} f_2 = \begin{bmatrix} 1 & e_2 \\ e_1 & 1 \end{bmatrix} \cdot \begin{bmatrix} f_1 \\ f_2 \end{bmatrix} \tag{16}$$

where: $$f_1 = \cosh\frac{\pi y}{\ell_1}\left(A_1\cos\frac{\pi y}{\ell_1} + A_2\sin\frac{\pi y}{\ell_1}\right) + \sinh\frac{\pi y}{\ell_1}\left(A_3\cos\frac{\pi y}{\ell_1} + A_4\sin\frac{\pi y}{\ell_1}\right) \tag{17}$$

$$f_2 = \cosh\frac{\pi y}{\ell_2}\left(B_1\cos\frac{\pi y}{\ell_2} + B_2\sin\frac{\pi y}{\ell_2}\right) + \sinh\frac{\pi y}{\ell_2}\left(B_3\cos\frac{\pi y}{\ell_2} + B_4\sin\frac{\pi y}{\ell_2}\right) \tag{18}$$

$$\ell_1 = \frac{7}{3} b_d \sqrt{\frac{h}{t}} \sqrt[4]{\frac{\eta_b\theta_u + \eta_u\theta_o}{2}} \left(\zeta - \sqrt{\zeta^2 - 1}\right) \tag{19}$$

$$\ell_2 = \frac{7}{3} b_d \sqrt{\frac{h}{t}} \sqrt[4]{\frac{\eta_b\theta_u + \eta_u\theta_o}{2}} \left(\zeta + \sqrt{\zeta^2 - 1}\right) \tag{20}$$

$$\zeta = 1 + \frac{\{(\eta_b - \eta_u) - (\alpha_o - \alpha_u)(\eta_b + \eta_u)\}^2}{\eta_b\theta_u + \eta_u\theta_o} \tag{21}$$

$$e_1 = -e_2 \left\{\frac{(\eta_o + \eta_u)}{(\theta_o + \theta_u) - 2(\alpha_o - \alpha_u)(\theta_o - \theta_u)}\right\} \tag{22}$$

$$e_2 = -(\alpha_o - \alpha_u)\left\{1 - \sqrt{1 + \frac{(\theta_o + \theta_u) - 2(\alpha_o - \alpha_u)(\theta_o - \theta_u)}{(\alpha_o - \alpha_u)^2(\eta_o + \eta_u)}}\right\} \tag{23}$$

For corrugations with all flanges of equal width it is obvious that $\zeta = 1$ and $\ell_1 = \ell_2$; for all other kinds of profiled sheeting $\ell_1 < \ell_2$.
Hyperbolic functions f_1 and f_2 represent the fact, that distortion is caused locally and vanishes rapidly going along the foldlines. Characteristic lengths ℓ_1 and ℓ_2 indicate the area near fastening arrangements, where distortion and warping have impact. Beyond that range sheeting is not notably affected and a uniform distribution of shear stresses is achieved. The magnitude of distortion depends on the constants of integration, which can only be solved by considering profiled-edge conditions.

2.3 Boundary conditions at profiled edges

As a result of warping, according to figure 4, membrane stresses arise: longitudinal stresses linearly over each strip and transverse stresses parabolically over each strip (figure 5).

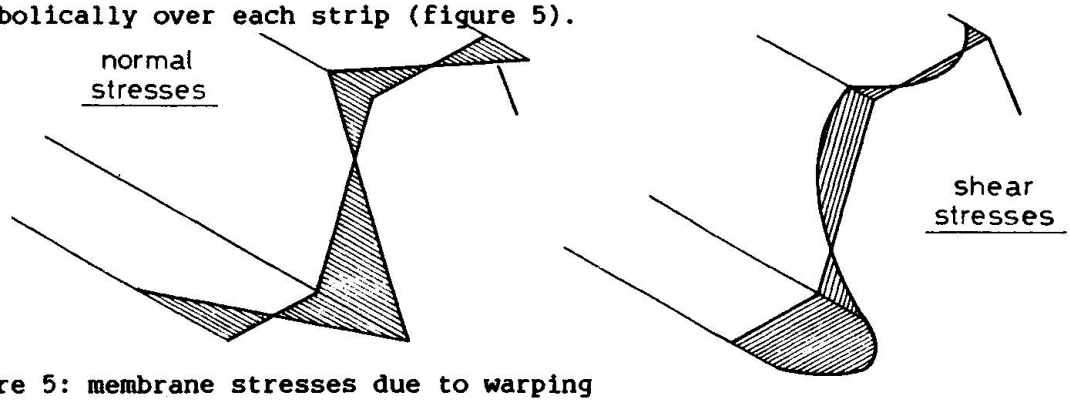

Figure 5: membrane stresses due to warping

Longitudinal stresses can be represented by longitudinal forces, concentrated in the foldlines |3|. Thus one pair of forces N_{ow} is found for every top flange, forming a bimoment $N_{ow}b_o$, and one pair of forces N_{uw} for every bottom flange, forming a bimoment $N_{uw}b_u$ (figure 6).

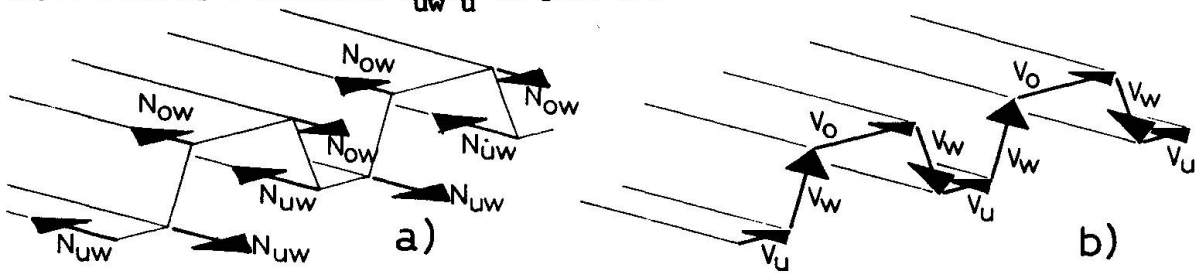

Figure 6: a) internal longitudinal forces concentrated in the foldlines
b) internal transverse forces concentrated in the strips

In a similar way transverse stresses can be represented by transverse forces V_o, V_w, V_u concentrated in topflanges, webs and bottom flanges respectively. The sum of transverse forces over one corrugation projected in-plane is constant and equal to the uniform shear force per pitch, hence:

$$V_o + 2V_w \cos\theta + V_u = s.b_d \tag{24}$$

The relation between concentrated forces and distortion is given by:

$$\underline{m} = -Et\,\frac{b_d^3}{12}\,J\,\underline{u}^{II} \tag{25}$$

$$\underline{q} = -Et\,\frac{b_d^3}{12}\,J\,\underline{u}^{III} = \underline{m}^{I} \tag{26}$$

where :

$$\underline{m} = \begin{bmatrix} m_1 \\ m_2 \end{bmatrix} = \begin{bmatrix} 1 & 1 \\ 1 & -1 \end{bmatrix} . \begin{bmatrix} N_{ow} \cdot b_o \\ N_{uw} \cdot b_u \end{bmatrix} \tag{27}$$

$$\underline{q} = \begin{bmatrix} q_1 \\ q_2 \end{bmatrix} = \begin{bmatrix} 1 & 1 \\ 1 & -1 \end{bmatrix} . \begin{bmatrix} V_o - b_o.V_w/\ell_w \\ V_u - b_u.V_w/\ell_w \end{bmatrix} \tag{28}$$

These expressions must be used in order to satisfy equilibrium at profiled edges. For example, at the very end of a diaphragm with overhang no longitudinal forces nor transverse forces are transmitted, which means mathematically: $\underline{m} = \underline{0}$, $\underline{q} = \underline{0}$ or rather $\underline{u}^{II} = \underline{0}$, $\underline{u}^{III} = \underline{0}$ at the end. Thus four constants of integration are solved per edge.
Along edges, where deformation is prevented, compatibility conditions must be satisfied. If distortion is prevented at the edge, the condition is mathematically: $\underline{u} = \underline{0}$.
Warping of a cross section is related to distortion on one hand and shear strain on the other hand; if the edge is forced to remain plane (edge welded to a beam), both modes of warping must compensate each other, mathematically formulated:

$$\underline{u}^{I} + \left(\frac{\alpha s}{Gt} - \frac{s}{Gt}\right).\begin{bmatrix}2\\0\end{bmatrix} = \underline{0} \text{ at the edge} \tag{29}$$

Compatibility conditions must also be used, when two diaphragms A and B are continuously connected to each other; over the connection line conditions are

for distortion: $\underline{u}_A = \underline{u}_B$ (30)

and warping: $\underline{u}^I_A + (\alpha-1)\frac{s}{Gt}\begin{bmatrix}2\\0\end{bmatrix}_A = \underline{u}^I_B + (\alpha-1)\frac{s}{Gt}\begin{bmatrix}2\\0\end{bmatrix}_B$ (31)

Warping related to distortion ($\underline{u}^I$) generally overwhelms warping related to shear strain. For cross sections, where distortion is not entirely prevented, the latter may therefore be simplified to:

for warping: $\underline{u}^I_A = \underline{u}^I_B$ (32)

2.3 Deformation of a shear diaphragm

As a result of distortion, supporting members translate in x-direction with respect to the sheeting. This translation, denoted by $\hat{u}$, is equal to the displacement u_u, if sheeting is fastened through bottom flanges, hence:

$$\hat{u} = u_u = [\,\tfrac{1}{2} \quad -\tfrac{1}{2}\,]\,\underline{u} \tag{33}$$

Two supporting members at the profiled edges with intermediate span b (figure 7) translate in opposite direction, showing a parallel shift $\Delta u = 2\,\hat{u}$. The parallel shift per unit length is:

$$\frac{\Delta u}{b} = \frac{2\,\hat{u}}{b} \quad \text{where} \quad \frac{\Delta}{b} = \frac{\partial}{\partial y} \tag{34}$$

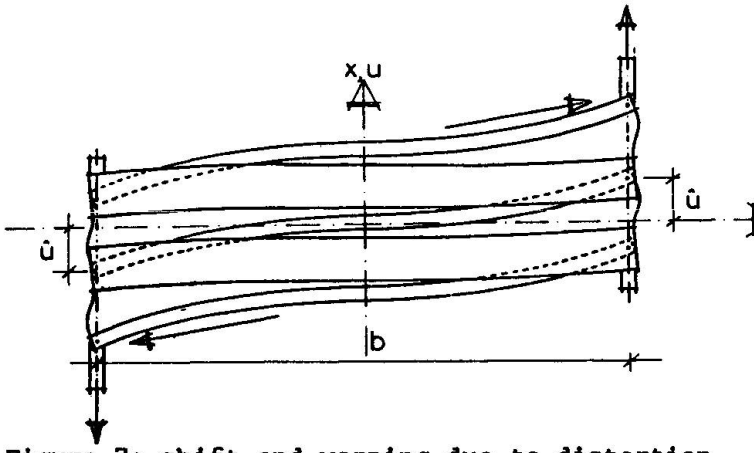

Figure 7: shift and warping due to distortion

This is shear deformation of a diaphragm due to distortion. The latter in combination with the previous result of 2.1 yields the complete kinematic condition for profiled sheeting in shear:

$$\frac{\partial u}{\partial y} + \frac{\partial v}{\partial x} = \frac{\alpha s}{Gt} + \frac{2\,\hat{u}}{b} \tag{35}$$

3. INFLUENCE OF WARPING RESTRAINT

Shear deformation $\Delta v/a$ of the diaphragm of figure 8 is found to be:

$$\frac{\Delta v}{a} = \frac{\alpha s}{Gt} + \frac{2\,\hat{u}}{b} \quad \text{where : } s = \frac{Q}{b} \tag{36}$$

$$\text{and} \quad \hat{u} = 6\,\frac{s b_d}{Et} \sum_{i=1,2} \left(\frac{\ell_i}{\pi b_d}\right)^3 F_i D_i W_i \tag{37}$$

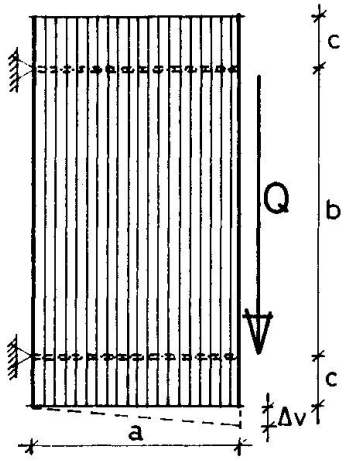

Figure 8: diaphragm with overhang

Sheeting is fastened to purlins through bottom flanges, therefore:

$$F_1 = \frac{1 - e_1}{1 - e_1 e_2} \frac{\theta_o + \eta_b e_2}{\eta_u \theta_o + \eta_o \theta_u} \qquad (38)$$

$$F_2 = \frac{1 - e_2}{1 - e_1 e_2} \frac{\eta_o + \theta_o e_1}{\eta_o \theta_u + \eta_u \theta_o} \qquad (39)$$

Distortional restraint is represented by the term D_i; For a type of fastening, where distortion is free $D_i = 1$, otherwise $D_i < 1$.

The influence of span b and overhang c (providing warping restraint) is expressed by the term W_i, in general form :

$$W_i = \frac{1}{4} \frac{(\cosh\frac{\pi b}{\ell_i} - \cos\frac{\pi b}{\ell_i})(2+\cosh\frac{2\pi c}{\ell_i} + \cos\frac{2\pi c}{\ell_i}) + (\sinh\frac{\pi b}{\ell_i} - \sin\frac{\pi b}{\ell_i})(\sinh\frac{2\pi c}{\ell_i} - \sin\frac{2\pi c}{\ell_i})}{(\cosh\frac{\pi b}{\ell_i} \sinh\frac{2\pi c}{\ell_i} + \cosh\frac{2\pi c}{\ell_i} \sinh\frac{\pi b}{\ell_i}) - (\cos\frac{\pi b}{\ell_i} \sin\frac{2\pi c}{\ell_i} + \cos\frac{2\pi c}{\ell_i} \sin\frac{\pi b}{\ell_i})} \qquad (40)$$

If b and $2c \ll \frac{\ell_i}{\pi}$: $W_i \simeq 3 \left(\frac{\ell_i}{\pi b_d}\right) \left(\frac{b_d}{b}\right) \left(\frac{b}{b + 2c}\right)^3$ (41)

If c is taken zero, Bryan's solution [4] for short diaphragms is found and (37) changes into:

$$\hat{u} = 18 \frac{s b_d}{E t} \frac{b_d}{b} \sum_{i=1,2} \left(\frac{\ell_i}{\pi b_d}\right)^4 F_i D_i \qquad (42)$$

In normal practice however, span b will be larger than both ℓ_1 and ℓ_2, and (40) can be reduced to :

$$W_i = \frac{1}{4} \left(1 + \frac{1 + \cos\frac{2\pi c}{\ell_i}}{e^{2\pi c/\ell_i}} + \frac{1 - \sin\frac{2\pi c}{\ell_i}}{e^{2\pi c/\ell_i}} \right) \qquad (43)$$

$W_i = 1$ for $c = 0$ (edge purlin) and $W_i = 0.25$ for $c \gg \ell_i$ (intermediate purlins). Obviously $\hat{u}$ is now independent of span b; the relation between displacement $\hat{u}$ and force per fastener $s b_d$ is constant for a given corrugation and a given overhang, which can be simulated by springs. Then rigidity of springs is proportional to $t^{2.5}$.

REFERENCES

1. ECCS, European recommendations for the stressed skin design of steel structures, Constrado, Croydon, England, March 1977
2. BOGAARD, A.W.A.M.J. v.d., Mathematical theory of stressed skin action in profiled sheeting with various edge conditions, report BKO/KO-85-14 Eindhoven University of Technology, Eindhoven, Holland, November 1985
3. VLASOV, V.Z., Thin-walled elastic beams (chapter IV), Israel program for Scientific Translations Ltd., 1961
4. BRYAN, E.R., The stressed-skin design of steel buildings, Constrado Monographs, Crosby Lockwood Staples, London, 1973.

Development of Thin Wall Cladding to Reduce Drift in Hi-Rise Buildings

Revêtement de façade à paroi mince réduisant le mouvement horizontal des immeubles multi-étagés

Dünnwandige Fassadenelemente zur Reduktion der Horizontalauslenkung von Hochhäusern

Richard L. TOMASETTI
Senior Vice President
Lev Zetlin Associates, Inc.
New York, NY, USA

Richard L. Tomasetti received a B. Sc. Degree from Manhattan College, New York, NY, a M. Sc. Degree from New York University, NY. He is the Sr. Vice President of LZA and is responsible for numerous projects. In addition, he acts as a special consultant to all staff members on critical structural design and analysis problems.

Abraham GUTMAN
Vice President
Lev Zetlin Associates, Inc.
New York, NY, USA

Abraham Gutman received a B. Civil Eng. and M. Civil Eng. Degrees at City College, New York, NY. As Vice President of LZA, he has overall responsibility for various large engineering projects. He is also recognized as an expert on special structures.

I. Paul LEW
Vice President
Lev Zetlin Associates, Inc.
New York, NY, USA

I. Paul Lew received a B. Civil Eng. Degree from Tulane University, New Orleans, a M. Cvil Eng. Degree from New York University, NY, Masters of Architecture from Columbia University, New York, NY. Mr. Lew's varied background in engineering, architecture and structural research provides a comprehensive technological overview for the firm's special engineering projects.

Leonard M. JOSEPH
Associate
Lev Zetlin Associates, Inc.
New York, NY, USA

Mr. Joseph received a B.Sc. Degree from Cornell University, NY, a M.Sc. Degree from Stanford University, CA and a Masters of Business Administration from Stanford University, CA. He has extensive experience in the analysis, design and review of a wide range of structures, working with a variety of materials.

SUMMARY

One Mellon Bank Center represents the first development of a thin wall metal facade panel (stress skin tube) to provide major stiffness for a hi-rise building. To achieve this results, a substantial analytical, design, detailing and testing program was undertaken. This paper reviews the program and presents the final product that was achieved.

RÉSUMÉ

Le «One Mellon Bank Center» est le premier bâtiment employant la technique des panneaux de façade en acier à paroi mince (structures en tube) qui renforcent la raideur d'un immeuble multi-étagé. Pour réaliser cela, un programme de calcul, d'essais et de conception des assemblages fut conduit. Cet article présente le programme ainsi que l'ouvrage réalisé.

ZUSAMMENFASSUNG

Das «One-Mellon-Bank-Zentrum» zeigt zum ersten Male die Entwicklung einer mitwirkenden dünnwandigen Fassaden-Verkleidung mit dem Ziel, eine grössere Steifigkeit des Hochhauses zu erreichen. Zu diesem Zweck wurde ein umfangreiches Programm für Berechung, Entwurf, konstruktive Details und Erprobung durchgeführt. Der Artikel beschreibt das Programm und die gewählte Lösung.

INTRODUCTION

One Mellon Bank Center, (OMBC), is a 54 story, 222 meters high office building in Pittsburgh, Pennsylvania (Fig. 1). It represents the first example of a stressed-skin tube using steel plate facade panels to provide major stiffness against building drift. The basic principle which makes the plate facade panels cost-effective is the separation of strength requirements from drift requirements. Since current U.S. building codes define required strength (wind pressure, seismic coefficients) but not wind drift, items provided only for wind drift need not be fireproofed. Thus, the facade panels have the structural plate face exposed, without the expense of fireproofing or flame shields.

STRUCTURAL FRAME

The building utilizes tube frame construction which consists of closely spaced perimeter columns and stiff spandrel beams. Columns 10 feet apart were architecturally desirable and no problem if kept narrow. However, to provide adequate stiffness in tube frames, spandrel beams are commonly made as deep 3-plate sections and located upset, so that about half the beam depth projects above the floor. This beam is usually concealed by an extra-deep windowsill, taking away valuable usable floor space. With plate stiffening this is not required and the spandrel can be placed below the floor, thus adding valuable usable floor space.

Since the panels cannot be counted upon for strength, a two-step analysis was performed. First, tower framing was modeled without facade panels. Several trials with condensed, simplified models aided in member selection for the first run. Approximately 3000 nodes and 6000 members were modeled using the EASE-2 computer program. The use of rigid diaphragms at each floor reduced the degrees of freedom to be solved to approximately 9,200. Loading consisted of code-required wind forces in the longitudinal, transverse and quartering direction. Code requirements were found to be more critical than the overall wind pressures determined in wind tunnel tests at Colorado State University.

The second model included tower framing plus façade panels (Fig. 2). To simulate the effect of the façade panels, equivalent uniform membrane elements were inserted in the model. The membrane stiffness required was established by using a separate model of each individual type of façade panel, using fine-mesh finite elements and racked using a 100N shear force. These models were later used for design of individual panels. The overall tower model showed that building drift with façade panels would be H/590, which was acceptable.

Panel membrane stresses were translated directly into panel shear forces on a panel-by-panel basis. From this a table similar to a column schedule was developed, and panel thicknesses and stiffener patterns were selected to meet the load requirements.

In addition, the change in shear force from panel to panel was determined. This was needed to establish the panel-to-column connection requirements, since only the change in force travels through this connection. The balance of shear travels through panel-to-panel connections.

STRUCTURAL FAÇADE PANEL

Description

The basic façade panel consists of a 300.7 cm. wide by 1107.4 cm. high panel covering three stories. The typical story height is 3.66 meters. There are six

window openings 133.3 cm. wide by 202.2 cm. high in a typical panel (see fig. 3). Stiffeners are required on the inside of the panel to prevent plate buckling and provide out-of-plane strength for wind. These stiffeners are placed on all sides of the windows and are continuous for the height and width of the panel.

Strength Analysis

The classical analysis approach to plates assumes that adequate stiffness would be provided from the panel stiffeners so that each subpanel could be analyzed as an independent plate simply supported at its longitudinal edges and loaded along its perpendicular edges, or width. The basic equation for plate buckling (Johnston, 1976) is:

Where:

$$fc = k \frac{\pi^2 E (\frac{t}{b})^2}{12 (1-\nu^2)} \qquad \text{(Eq. 1)}$$

fc = Critical Shear Stress

E = Modulus of Elasticity

b = Width of Subpanel

t = Thickness

ν = Poissons Ratio

a = Length of subpanel

α = a/b

k = Constant for each load

The critical stresses are valid in the elastic range. To adjust for the inelastic range, for compressive stresses, the elastic solution was used to determine an "equivalent column" slenderness ratio (KL/r). The equivalent slenderness ratio (Johnston, 1976), for ν =0.3, would be:

$$(KL/r) \text{ equivalent} = \frac{3.3 (b/t)}{\sqrt{k}} \qquad \text{(Eq. 2)}$$

This "equivalent column" slenderness ratio was used to determine allowable compressive stresses following AISC allowable compressive stress criteria.

Allowable shear stresses can be determined elastically and also by post-elastic-buckling analysis. Since visual buckling of the plate would not be desireable in the façade, only the elastic buckling solution was considered. The elastic buckling solution to web shear stress allowable has been adjusted by the AISC in their allowable shear stresses for inelastic behavior.

The actual state of stress in the panel is a combination of axial, bending and shear stress. The method of combining these stresses was based on the Column Research Council recommendations (Johnston, 1976). The following interaction equation was thus used:

$$(fa/Fa) + (fb/Fb)^2 + (fv/Fv)^2 \leq 1.0 \qquad \text{(Eq.3)}$$

Where subscripts a,b,v are axial, bending & shear respectively and f = actual stress, F = allowable stress.

The key to this classical analysis was the principle that the stiffeners were fully effective so that each subpanel defined by the stiffener grid could be

checked on an individual basis for buckling. To determine whether the stiffeners were effective, two analytical techniques were used.

First, the panel with its stiffeners is analogous to a cold formed structural steel member as a deep, relatively thin walled section. Therefore, the requirements of the AISI specification for the design of cold-formed steel for laterally unbraced beams were used as design criteria for the stiffeners (AISI, 1977).

As a second approach, the classical methods of analysis were confirmed by a state of the art computer analysis for plate buckling. The method applied was a finite element analysis for buckling, using the NASTRAN program. The goals were to verify that the subpanels would buckle before the stiffeners. In addition, the calculated stress at which the panels and stiffeners buckle was compared to classical solutions. A simulation of the computer buckling analysis used is shown in fig. 4.

Good agreement was found between the finite element buckling analysis and classical buckling analysis. It was therefore considered acceptable to use classical analysis to size the panels.

Stiffness and Stress Analysis

Once the buckling stresses for different thicknesses of panels and stiffener arrangements were determined, it was necessary to determine the state of stress in the panels and the deflection due to an arbitrary "unit" lateral force to be able to select the correct thickness and stiffener configuration for each actual load condition. To accomplish this, a fine mesh finite element analysis was performed (see Fig. 5). Resulting isolines for principal stress are shown in fig. 7.

The stresses in each subpanel were then broken up into axial, bending, and shear stresses for gradually increasing increments of force. This was then checked against the capacity of the panel using classical analysis.

The finite element analysis also provided the means of linking panel analysis to building frame analysis so that the force in the panels at each location of the building could be determined. This linkage was made by developing a solid panel "membrane" equivalent in shear stiffness to the actual perforated panel. The equivalent solid panel was then incorporated in the structural analysis of the overall building frame as an infill shear membrane. The effect of this equivalent infill membrane on the overall structure was then determined, the force induced in the infill panels was determined, and panel types were selected.

DESIGN AND DETAILING

The detailing of the panel to the structure was critical to the execution of the structural system. Each panel must act primarily as a shear diaphragm with respect to the structural frame and be relatively isolated against axial shortening of the frame. To accomplish this, two distinct groups of connections were necessary.

1. Panel-to-panel connections

2. Panel-to-frame connections

The top and bottom horizontal connections have three functions:
1. To pass horizontal shear between upper and lower panels.

2. To distribute a share of the horizontal wind shear from the frame into the

panels.

3. To relieve any vertical stress between panels due to frame shortening, thermal effects, etc.

These functions are achieved by continuous wide horizontal plates at the top and bottom edges of the panels, which are high-strength friction bolted to the top flange of the spandrel beam about 30.5 cm. away from the face. By having the shear plates span the 30.5 cm. distance they become flexible and act to form a stress relieving joint, (see fig. 6).

At the vertical edges, extensive analysis showed that the most effective connection between panels occurred adjacent to the window openings. This location tends to minimize the weakening effect of the window openings.

Since the panels in any one wall face act as a unit, there is little vertical shear transfer to or from the structural frame at vertical connections except at the ends of wall faces where the panels end and must unload their shear back into the structure frame. Therefore, at interior vertical joints it is necessary to connect to the structural frame only at approximately midheight of each panel, using small connection fins. (See fig. 8).

At the end panels a larger edge stiffener is used as a collector of the shear force so that, although a larger force has to be transferred to the frame, bolts can still be bunched together at a mid-height location. This mid-height connection greatly limits the zone in the panel affected by the frames axial shortening.

The connections for vertical shear consist of high-strength friction bolts in holes or slots punched in outstanding legs of angle edge stiffeners. At panel-to-frame locations (mid-height) a vertical shear plate or fin projecting from the column fits in the gap between two panels. Bolts clamp panel edge angles to the fin and to each other (See fig. 9). At panel-to-panel locations, the gap between panel edges is filled with finger shims. Bolts clamp panel-to-panel.

In addition to shear-transfer connections at panel edges, tiebacks are required to resist wind pressure and brace the stiffener grid against buckling. They must be stiff perpendicular to the facade, but not produce substantial restraint to frame shortening. The solution was to provide horizontal flexible tieback plates from the structural frame to the ends of horizontal stiffeners of the panels at each window head and sill.

TESTING

Testing of a full scale prototype was done at Lehigh University's Fritz Engineering Laboratory. American Bridge Division of U.S. Steel fabricated a 6mm thick test panel and a special test frame. To test for shear the panel and frame assembly was loaded diagonally. The heavy test frame surrounding the panel acted to break this force into components so the frame took axial load and the panel carried shear load.

The test panel was designed for a lateral load of 2.7×10^5 N which would correspond to a diagonal test load of 10^6 N. The panel showed non-visible signs of incipient buckling at about 1.89 times the design load. Visible signs of buckling occurred at 2.44 times the design load. At this point, the panel was exhibiting post-buckling strength. At about 3.33 times the design load the welds failed, but not the panel itself.

In general, the test showed that panel strength was in close agreement with

analytical predictions. It also indicated that there was substantial reserve post buckling strength in the panel. It further indicated that deflections were in the range anticipated and were acceptable both visually and structurally.

CONCLUSION

The successful testing of the prototype panel completed the development of an innovative structural system. The use of this panel allows for many positive structural benefits. The important benefits include:

1. Reducing deflections of the structural frame by half.
2. Allowing the structural frame to be designed for strength rather than deflection.
3. Improving the efficiency of the structural tube frame system.
4. Less costly, normal rolled sections are used in conjunction with the facade stiffening plate system.
5. Additional useable floor space is gained.

REFERENCES

GUIDE TO DESIGN CRITERIA FOR METAL STRUCTURES
3rd ed., Column Research Council, John Wiley and Sons, Inc., New York, pp. 86-109. Johnston, B.G., ed., 1976
AISC MANUAL OF STEEL CONSTRUCTION, 8th ed., American Institute of Steel Construction, New York, 1980
AISI COLD-FORMED STEEL DESIGN MANUAL, American Iron and Steel Institute, Washington D.C. 1977
STRUCTURAL STEEL DESIGN, 2nd ed., Ronald Press, New York, Tall, L. (Ed.), 1974

FIG. 1

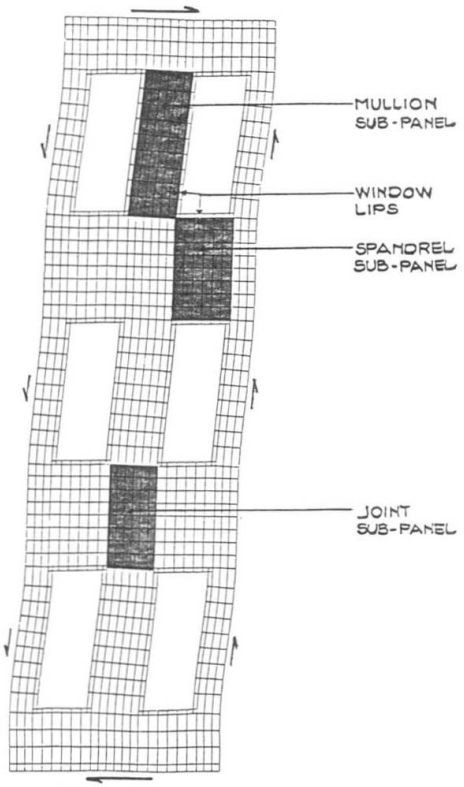

FIG. 2
RACKED PANEL (EXAGGERATED)

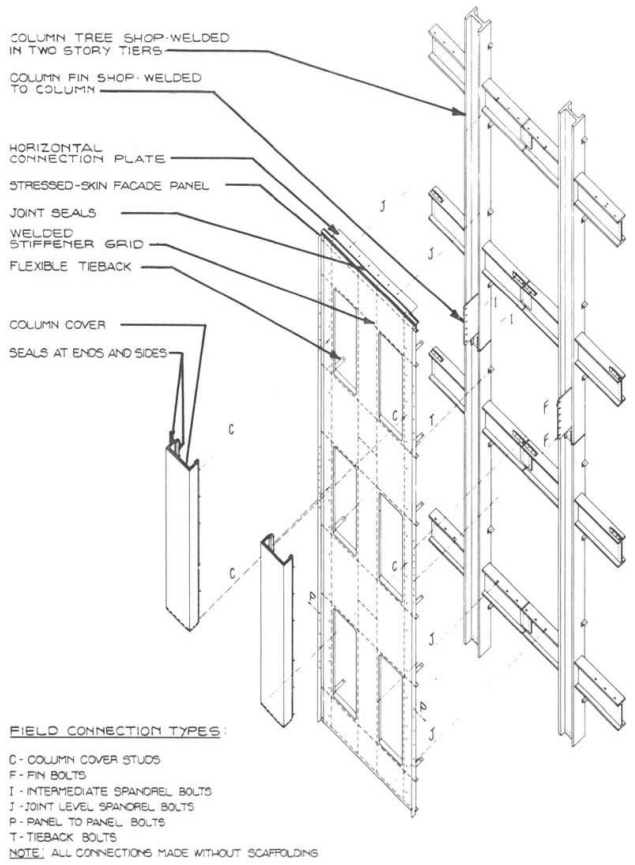

FIG. 3 ONE MELLON BANK CENTER: STRESSED SKIN - TUBE INTERFACE

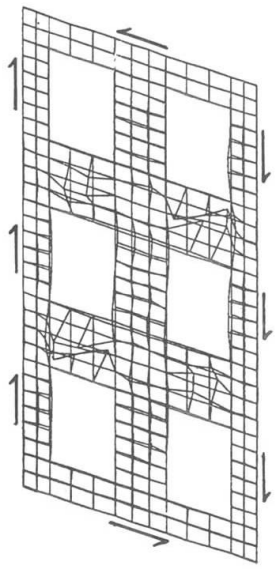

PANEL SPANDREL BUCKLING MODE UNDER SHEAR LOAD

FIG. 4

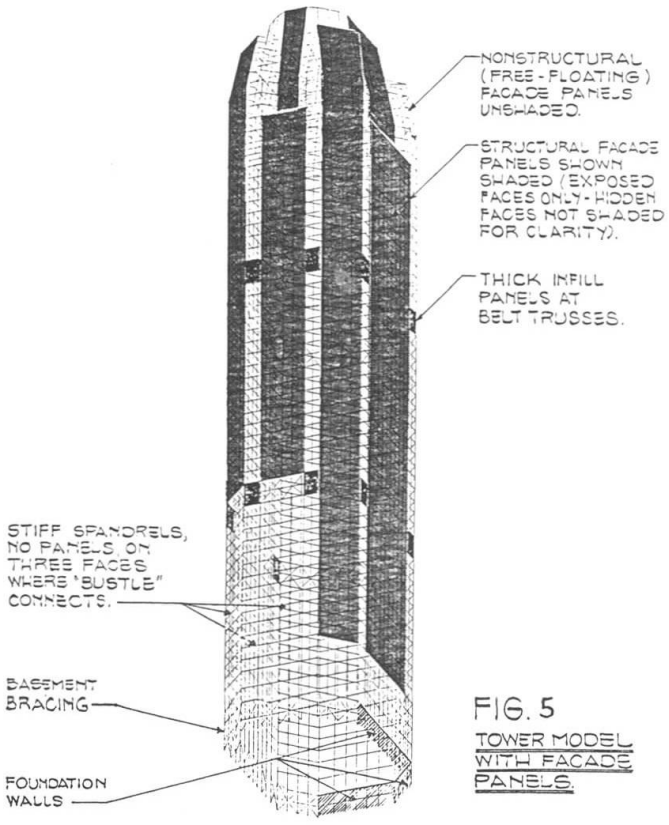

FIG. 5 TOWER MODEL WITH FACADE PANELS.

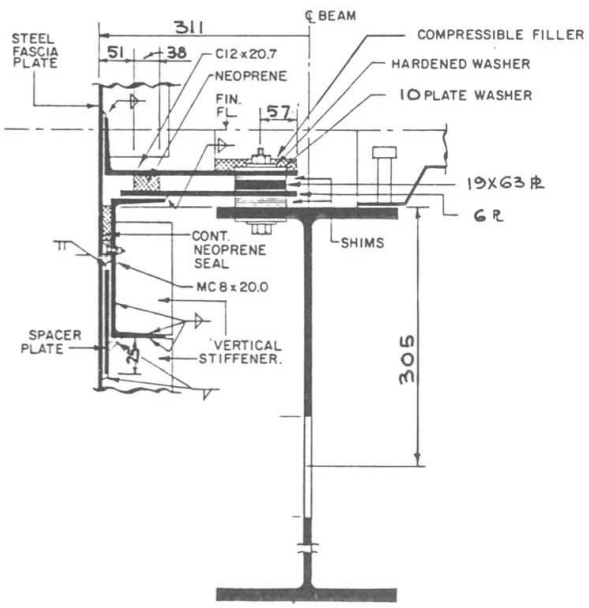

FIG. 6 HORIZONTAL JOINT

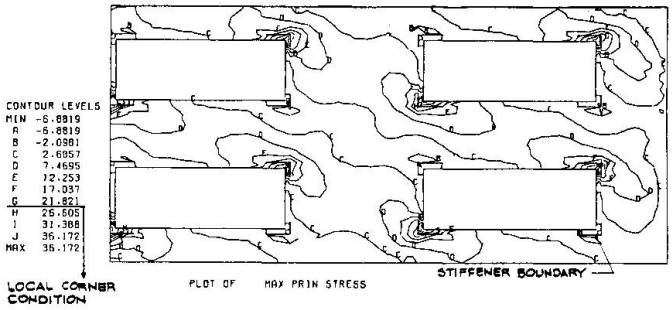

FIG. 7 σ_1 MAX. PRINCIPAL STRESS FOR 100 N HORIZONTAL SHEAR ON 8 MM PANEL

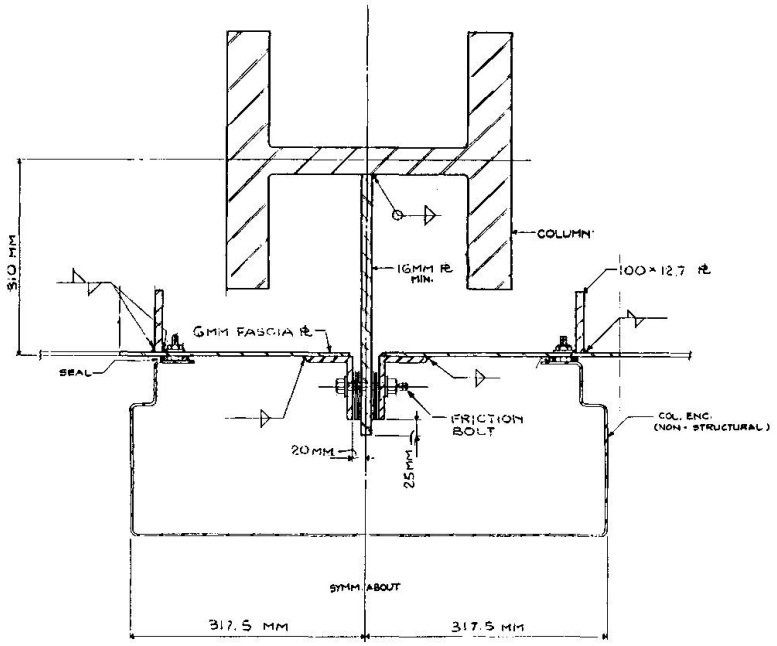

FIG. 8 PANELS-TO-COLUMN VERTICAL CONNECTION

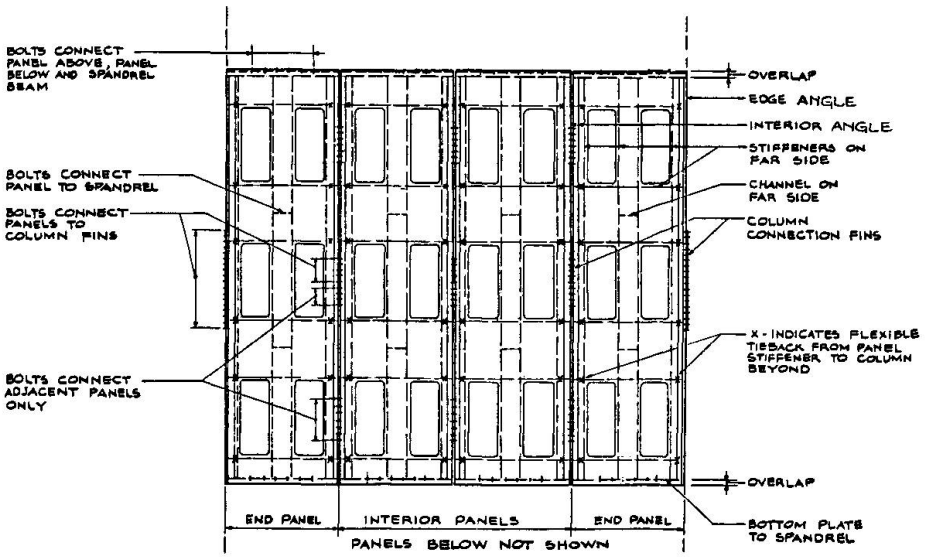

FIG. 9 TYPICAL ELEVATION

WITH COLUMN COVERS REMOVED - DIAGONAL FACE SHOWN

Diaphragm Action in Aluminium-Clad Timber-Framed Buildings

Effet de diaphragme dans les charpentes en bois revêtues de tôles d'aluminium

Membranwirkung in Gebäuden mit aluminiumverkleideter Holzkonstruktion

Richard N. WHITE
Professor of Struct. Eng.
Cornell University
Ithaca, NY, USA

Richard N. White, born 1933, received his undergraduate and graduate degrees from the University of Wisconsin, Madison, WI. He has been on the faculty at Cornell since 1961, teaching structures and doing research in concrete, metal, and timber structures, including nuclear reactors and effects of severe repeated loads on behavior. He has co-authored four books in structural engineering.

SUMMARY

The results of experiments on aluminium shear diaphragms fastened to timber framing are reported. The framing system is intended to be used on roof trusses in pole-type agricultural and commercial buildings. Variables studied include connector patterns, connector types (screws and adhesives), purling size and spacing, diaphragm length, and type of loading (unidirectional and reversing). The diaphragms were of sufficient strength and stiffness to be effective im medium size buildings. Cyclic loads up to 55% of single cycle load capacity did not reduce strength. Adhesive connections were highly beneficial.

RÉSUMÉ

Cette contribution présente les résultats d'essais sur des diaphragmes de cisaillement en aluminium fixés sur des charpentes en bois. Ces systèmes porteurs sont prévus pour les toitures à fermes en treillis en bois utilisées dans les bâtiments agricoles et commerciaux. Les paramètres étudiés concernent la disposition et le type d'assemblages (vis ou colles), la dimension et l'écartement des pannes, la longueur du diaphragme et le type de chargement (dans un seul sens ou dans les deux sens). Les diaphragmes se sont révélés suffisamment résistants et rigides pour être efficaces dans les bâtiments de taille moyenne. Des cycles de charges jusqu'à 55% de la capacité statique n'ont pas eu d'influence sur la résistance ultime. Les assemblages collés ont présentés un comportement très favorable.

ZUSAMMENFASSUNG

Resultate von Versuchen an schubbelasteten Aluminium-Membranen, die auf einer Holzkonstruktion befestigt sind, werden mitgeteilt. Das Membransystem soll auf den Dachbalken von auf Stützen ruhenden Landwirtschafts- und Lagergebäuden angebracht werden. Die untersuchten Variablen sind u.a. Grösse und Abstand der Pfetten, Membranlänge und Lasttyp (in einer Richtung oder wechselnd), sowie Befestigungsanordnung und Befestigungstyp (Schrauben oder Kleber). Die Membranen hatten hinreichende Stärke und Steifigkeit für die Anwendung in mittelgrossen Gebäuden. Wechselbelastungen bis zu 55% der Kapazität für einen einfachen Lastwechsel reduzierten die Tragfähigkeit nicht. Geklebte Verbindungen erwiesen sich als besonders wirksam.

1. INTRODUCTION AND SCOPE OF STUDY

Light gage aluminum roof and exterior wall systems have been used as covering materials for timber-framed agricultural and commercial buildings for many years. This type of structure normally has trusses spanning between timber pole columns, with knee braces running from the bottom chord of the truss to the columns to provide resistance against horizontal wind action. In-plane shear forces will tend to develop in the roof of this type of building when it is loaded by wind action. The shear stiffness of the roof will be mobilized and lateral wind forces will be transferred to the ends of the building, provided that the diaphragm is properly connected to the structural framing and that the framing itself is detailed and constructed to carry the substantial edge forces that develop. This so-called diaphragm action is well-documented for steel building construction and is used in current designs.

The purpose of this study is to evaluate the performance of aluminum panels on timber framing for use as shear diaphragms on buildings. Variables studied include truss spacing, purlin spacing and size, connector patterns, type of connector (several different screws, adhesives), diaphragm length, and type of loading (single load to failure, and cyclic reversing loads to simulate wind action). The most significant results are summarized and design recommendations are presented. Additional details are given in [1], [2], and [3].

2. SPECIMEN GEOMETRY AND MATERIALS

2.1 Geometry

Shear strength and stiffness were measured by testing cantilever-type shear diaphragms as shown in Fig. 1. The strength is expressed in terms of shear loading per meter of length, where the length of the diaphragm is measured parallel to the direction of the corrugations and the applied shear load. It is known from experiments on steel diaphragms that the strength per unit length is essentially independent of length. On the other hand, shear stiffness is dependent upon diaphragm length because much of the shear deformation is produced by imperfect connections of the shear diaphragm to the edge members, particularly at the ends of the sheets. As the diaphragm is made longer, the end deformations become a smaller fraction of the total deformation and the measured shear stiffness increases. Two diaphragm lengths (3.86 and 5.69 m) were tested.

Each diaphragm was made from ribbed ALCOA aluminum Super Temper Rib panels described in 2.2 below. Three panels, each covering a 0.914 m width, were used to make a 2.743 m wide diaphragm. Two building framing geometries were simulated: (a) trusses spaced 1.22 m on center, with 38 mm by 89 mm timber purlins spanning flatwise over the top chords of the trusses at one of three different spacings (0.61 m, 0.73 m, or 0.91 m), and (b) trusses spaced 2.44 m on center, with 38 mm by 190 mm timber purlins spanning on edge.

In each system the truss chords were simulated by 38 mm by 190 mm timber members loaded on edge. Purlins were fastened to the chords with two 12d pole barn nails at each intersection. The resulting bare frames had negligible shear stiffness. Most experiments utilized the closer truss spacing (1.22 m) because diaphragms built with the wider truss spacing and purlins on edge were extremely flexible in shear.

2.2 Aluminum Panels

The ALCOA Super Temper Rib panels had measured thicknesses of the patterned sheet (Fig. 2) ranging from 0.38 to 0.41 mm, with 19 mm deep major rib corrugations. Panel width was 0.956 m to cover a space of 0.914 m. The material had a 0.2% offset yield strength of 310 MPa, an ultimate tensile strength of 365 MPa, and an elongation at failure of 7% over a 51 mm gage length.

2.3 Timber Framing

All framing members were #1 and #2 Dense Southern Yellow Pine lumber furnished by Agway from their supply normally used for farm and commercial buildings.

2.4 Fasteners

Fastener notation is shown in Fig. 1. Fasteners around the perimeter of the diaphragm are called end frame fasteners and edge frame fasteners. Purlin fasteners are screws passing through the aluminum sheet directly into the purlins; purlin sidelap fasteners are similar connectors that pass through both panels at a sidelap. Sidelap stitch fasteners were used at the purlins in some specimens. Intermediate sidelap stitch fasteners are those connectors located at sidelaps and in between purlins (specimens 10, 19, 22, 31, 32, and 36).

Drill-Kwick self-drilling ALCOA aluminum screws were used in diaphragms 1-16, 23-35, and 37-39. These fasteners are #10 with an 8 mm hex-washer-head and an aluminum/neoprene composite bonded washer for weather tightness. 25 mm long screws were used through the flat portion of the sheet and 50 mm screws were used through the high corrugated ribs; the longer screws proved to be ineffective and were not used in later specimens.

Buildex Hi-Thread TEKS screws (designation #10-16 by 25 mm hex washer head TEKS 2 Alu TRU-GRIP/h.t.) were used in diaphragms 11-22 and 36. The screw features a larger diameter thread under the head of a 16 mm across-flats hex two piece Twin-Seal washer head.

Adhesive connections were utilized in the sidelap seams in diaphragms 25, 28-30, 34, and 39. The adhesive consisted of a 6 mm diameter bead of B.F. Goodrich PL-400 construction adhesive. One specimen, #40, had continuous adhesive connections between the purlins and the sheeting, in addition to adhesive connections at the sidelap seams.

3. TEST PROCEDURES AND DEFINITIONS

The cantilever test method described in [4] was used to evaluate shear strength and stiffness of each diaphragm. Shearing force was applied with a hand-operated mechanical jack in increments of 445 N. The net shearing deformation used in calculating shear stiffness was corrected for support movements in accordance with the method suggested in [4]. Another very important deformation measured in each test was the sidelap seam slip; it is an excellent indicator of shear stiffness as well as a good signal of impending difficulties in maintaining strength as load is increased since the full shear load in the diaphragm must be transmitted from one panel to the next across each of the two sidelap seams in the three-panel diaphragm.

The effective shear stiffness G for use in design is defined as $G' =$ the load P at 40% of P_{ult} divided by Δ'_s, where Δ'_s is the deflection measured at a load of $0.4P_{ult}$ minus the calculated bending deflection at the free end of the cantilever diaphragm, as specified in [4]. The bending deflection is factored out to eliminate the dependence of test results on the properties (plan dimensions, perimeter member areas and modulus) of the cantilever test specimen.

4. EXPERIMENTAL RESULTS

4.1 Introduction

Many connector combinations were used in the overall test program to find the optimal arrangement of connectors; hence many test results are not significant. Details of all tests are given in [1], [2], and [3]. Results here are limited to three diaphragms loaded unidirectionally to failure and one diaphragm loaded with reversing shear to simulate wind effects. Comparisons between various tests and

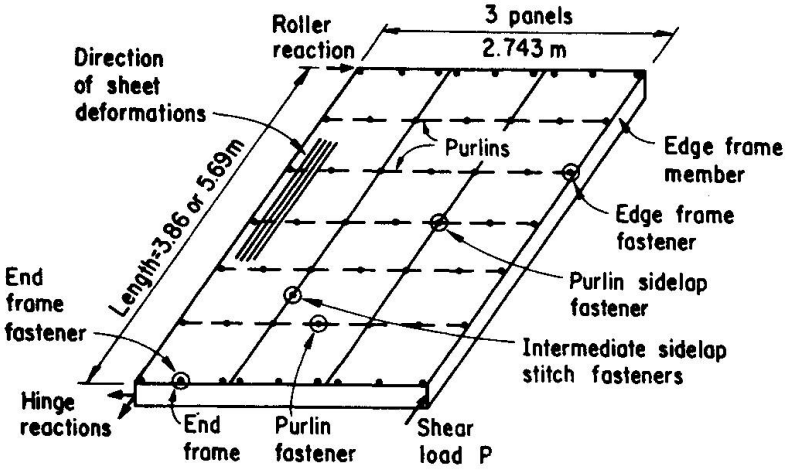

Fig. 1 — Diaphragm Geometry and Connector Geometry

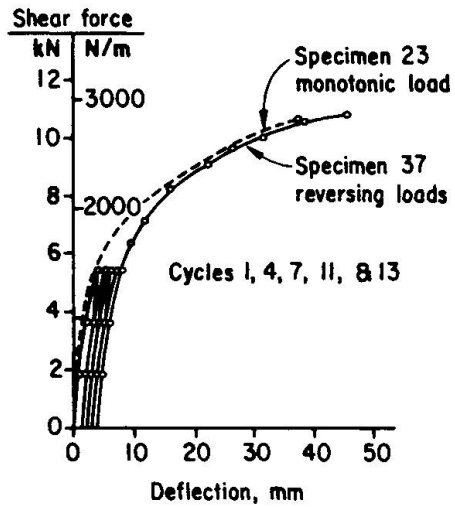

Fig. 4 — Effect of Reversing Loads

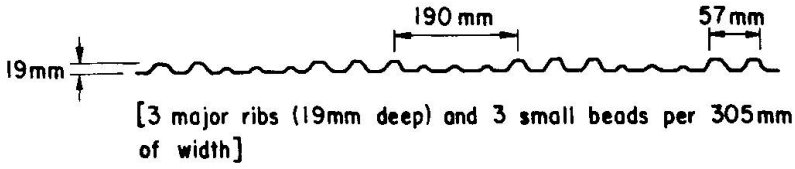

Fig. 2 — Panel Dimensions

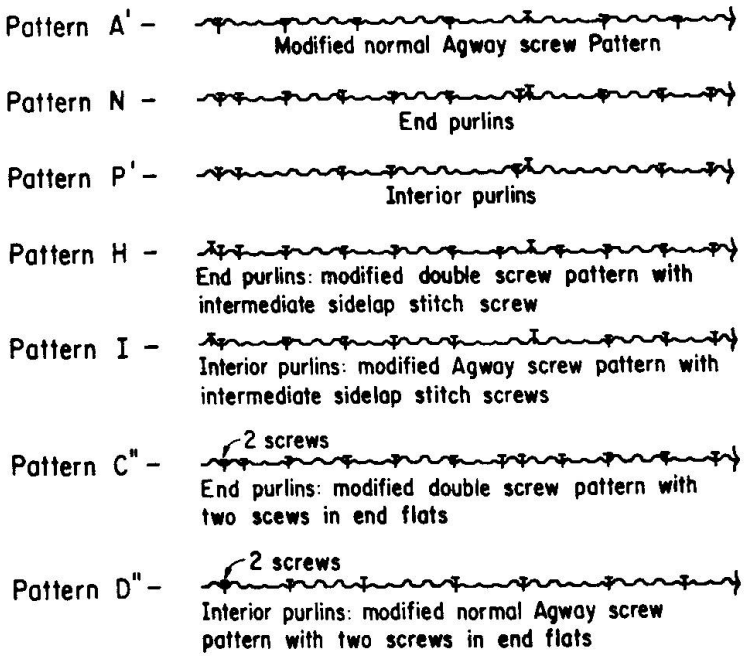

Fig. 5 — Screw Patterns for Recommended Designs

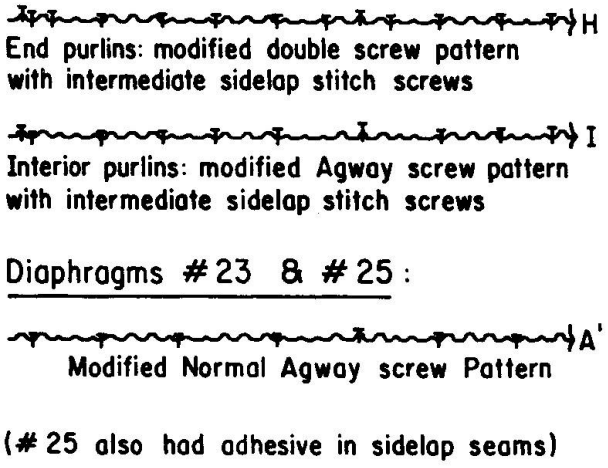

(a) Connector patterns

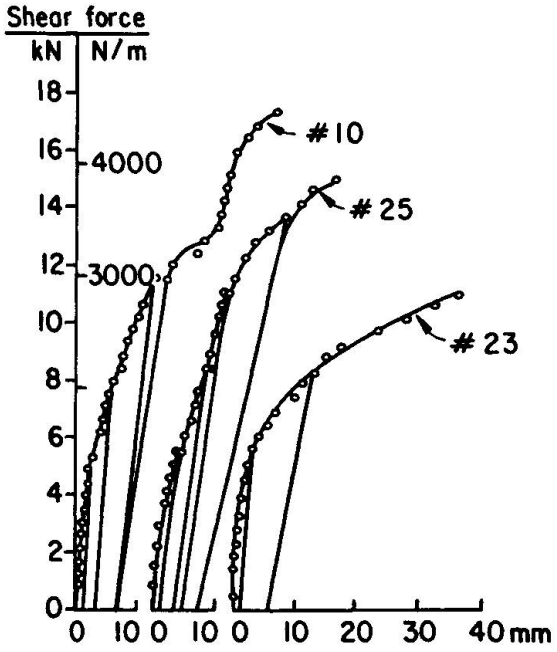

(b) Shear vs. deflection

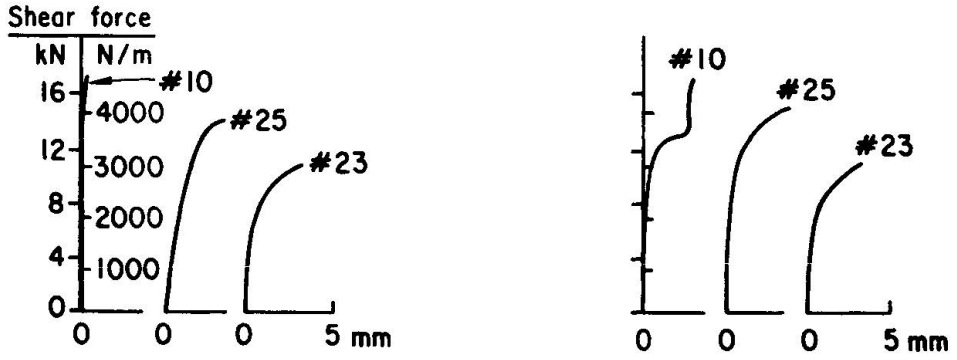

(c) Net slip along loaded edge member, mm

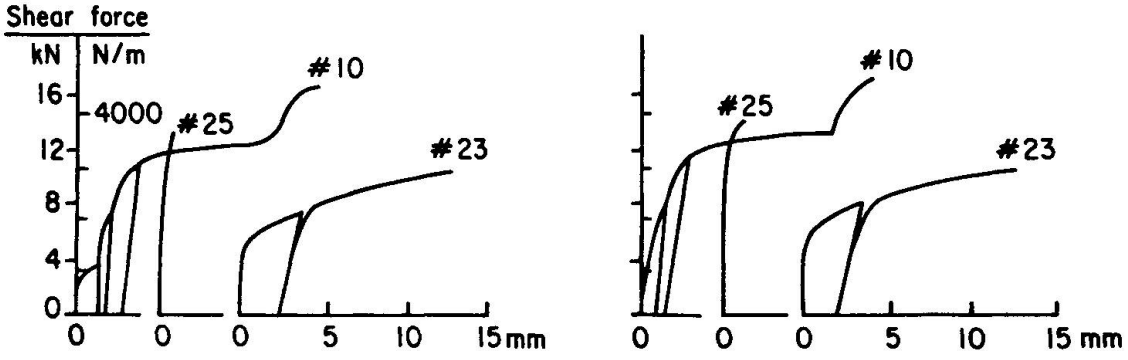

(d) Sidelap seam slip, mm

Fig. 3 – Performance of Typical Diaphragms

evaluation of the influence of test parameters are given in Chapter 5.

4.2 Diaphragms Loaded to Failure with a Single Load

Typical results are given for three specimens with capacities suitable for design shears of 1680, 2260, 2700 N/m, respectively. These design shear capacities are appropriate for small to medium size buildings. Each of these diaphragms had a truss spacing = 1.22 m and a purlin spacing = 0.61 m.

4.2.1 Minimal Screw Pattern (Specimen 23)

This diaphragm had 91 screws with all edge screws placed in the valley between ribs as shown in Fig. 3a. The diaphragm exhibited buckling-type deformations in the central flat areas of the panels, along with twisting of the adjacent ribs, at a load of 1600 N/m. Net deflection, slip along the loaded edge member, and sidelap seam slip are plotted in Figs. 3b, 3c, and 3d, respectively. Failure was initiated by tipping of the sidelap seam screws of up to 45° with associated sheet tearing around the screws. The specimen failed at 2760 N/m by fracture of several sidelap seam screws at the purlins; G′ was 1.20 kN/mm.

The diaphragm exhibited nearly elastic behavior up to a load of about 1170 N/m with less than 2.5 mm residual deflection upon unloading from 1460 N/m; there was virtually no sidelap seam slip at 1460 N/m shear load. Sidelap seam slip increased rather sharply at higher loads and residual seam slip was nearly 6 mm after unloading from 2190 N/m, as shown in Fig. 3b. Interior panel deformations were completely elastic and fully recoverable up to loads of 2190 N/m.

A duplicate specimen showed essentially identical behavior. As confirmed by other tests, the only way to reduce the sidelap seam lip at higher load levels was to either add intermediate stitch screws in the sidelap seams or to place adhesive in the sidelap seams.

4.2.2 Minimal Screw Pattern Plus Adhesive in Sidelap Seams (Specimen 25)

This diaphragm was identical to Specimen 23 discussed in 4.2.1 above except for the addition of a 6 mm continuous bead of BFG PL-400 construction adhesive in the sidelap seams. The adhesive eliminated the sidelap seam as the critical link in strength and stiffness of the diaphragm. As shown in Fig. 3d, sidelap seam slip was an order of magnitude smaller than in the previous specimen and residual slips remained low even when unloading from load levels up to 2800 N/m.

The diaphragm showed buckling-type deformations in the central flats of each panel at a load of approximately 1600 N/m. It failed at 3810 N/m as a result of severe distortion of the panels and resultant runaway deflections. The shear stiffness G′ was 0.74 kN/mm, lower than for Specimen 23. This apparent anomoly is attributed to great increase in load capacity of the diaphragm and hence the proportionally larger displacement at 40% of the ultimate load.

4.2.3 Additional Screws at Purlins Plus Intermediate Stitch Screws (Specimen 10)

This diaphragm used 150 screws in the patterns shown in Fig. 3a. End purlins had double screw patterns in the flats to help control deformations at the ends of the panels. Intermediate stitch screws were used between the purlins in both sidelap seams. As shown in Fig. 3b, this diaphragm design had an extremely high initial stiffness and a high shear stiffness G′ (1.08 kN/mm). The presence of the intermediate stitch screws forced the failure to occur by shear-off of the edge frame screws at a load of 4490 N/m. The observed sharp arresting of sidelap seam slip at a load of 3650 N/m (Fig. 3d) suggests that the stitch screws became effective only at high load levels. As ultimate load was approached, the stitch screws tilted and eventually broke the seal between the panel and the neoprene washer under the screw head.

4.3 Diaphragms Subjected to Reversing Shear Loads

Four diaphragms (Specimens 16, 37, 38, and 39) were subjected to reversing

shear load tests to better simulate the actual loading history that a roof diaphragm will encounter during its lifetime. The objective of these experiments was to study potential degradation in stiffness and strength from the cyclic loading. Behavior of Specimen 37, which was identical in design to Specimen 23 discussed in 4.2.1 above, is summarized in Fig. 4. Load-deflection behavior is plotted for loads in one direction only for selected cycles. It is apparent that there is substantial cumulative gain in diaphragm deflection. However, the tangent stiffness at any load level does not change significantly from the monotonically loaded specimen, and strength after cycling is unchanged. Other specimens confirm this behavior.

5. INFLUENCE OF MAIN DESIGN PARAMETERS ON DIAPHRAGM PERFORMANCE

The influence of the main design parameters on diaphragm performance is evaluated in the chapter. Included are: purlin spacing, truss spacing, use of adhesive in sidelap seams, reversing loads, connector patterns, and length effect.

5.1 Purlin Spacing

Three specimens (26,33,11) made without adhesives showed that increasing the purlin spacing from 0.61 m to 0.73 m reduced strength by 10%, and that a further increase to 0.91 m reduced strength an additional 8%. Shear-slip response up to loads of nearly 1500 N/m was not affected by purlin spacing, nor was G . Three specimens (29,30,34) with adhesive in sidelap seams showed that strength was essentially independent of purlin spacing because failure was in the panel rather than in the connectors.

5.2 Truss Spacing

Decreasing the truss spacing from 1.22 m (Spec. 23,24) to 0.81 m (Spec. 35) had little effect on strength and produced a small increase in stiffness.

5.3 Use of Adhesive in Sidelap Seams

In addition to Specimens 23 and 25, three other pairs of diaphragms (26 and 29, 33 and 34, 38 and 39) were built with and without adhesive in the sidelap seams. The sidelap seam adhesive connection produced the most dramatic change in behavior of any of the parameters studied. It drastically reduced the sidelap seam slip at high load levels (see Fig. 3d), eliminating the sidelap seam as a failure path in the diaphragm, and increasing strength from 20% to 40%. The strength of a 6 mm bead of this adhesive stabilized at 20 N/mm after 7 days of curing at room temperature.

5.4 Reversing Loads

Three pairs of tests (23 and 37, 26 and 38, 29 and 39), in which the second specimen of each pair was subjected to 13 cycles of reversing loads, showed that the behavior during the last cycle of loading was very similar to that of the monotonically loaded specimen except for the residual deflections of 2.5 to 5 mm that existed after 13 cycles of load. Secant stiffnesses based on total deflections at $0.4P_{ult}$ indicated that the cycled specimens without adhesive sidelap seams were about 1/3 as stiff as uncycled specimens; Specimen 39 made with adhesive sidelap seams retained about 60% of the secant stiffness of the uncycled diaphragm.

5.5 Connector Patterns

Fastener patterns for several different levels of strength are given for a truss spacing of 1.22 m with purlins spaced at 0.61 m and nailed flat against the top chord of the trusses. Permissible design loads are taken as 60% of the ultimate load capacity for design conditions controlled by wind loading. Connector patterns are summarized in Fig. 5.

Shear capacity N/m	Connector pattern	No. of screws	Adhesive	Stiffness G′ kN/mm
1680	A′	91	No	0.89 kN/mm
2260	N′,P′ + S.S.*	123	No	0.88 k
2700	H,I + S.S.*	150	No	1.07
2260	A′	91	Yes	0.74
2550	C′′, D′′	123	Yes	1.05

*S.S. = stitch screws

Higher capacities could be achieved in diphragms made with adhesives by using more screws, and substantially higher capacities (certainly up to 3700 N/m) could be reached by using adhesives to fasten the panels to the purlins. Research is needed to assess performance of adhesives over the lifetime of a structure, where they would be subjected to thermal effects and aging.

5.6 Length Effect

The use of the length effect equation given in [4] was verified with two pairs of specimens of different lengths. Use of this equation requires experimental determination of the factor K_2, which depends upon the diaphragm cross-sectional shape and the end fastener configuration.

6. CONCLUSIONS

Diaphragms made of aluminum panels and timber framing have sufficient strength and stiffness for use as roof shear diaphragms in medium size farm and industrial buildings, provided the timber framing is designed to carry the tensile forces developed by diaphragm action. Sidelap seams are critical in determining response to shear loads, and it is necessary to use either intermediate stitch screws at an average spacing of about 0.3 m, or adhesives. Screws at the ends of purlins should be located in the low flat areas of the panels rather than being placed through the high ribs. Purlin spacing had little effect on performance, provided sufficient intermediate stitch screws were used. Shear stiffness G′ varied little with different connector patterns, being quite close to 0.9 kN/mm for 4 m long diaphragms. Reversing loads of about 55% of single cycle strength can be carried safely.

7. ACKNOWLEDGEMENTS

This investigation was supported by Agway, Inc., the ALCOA Foundation, and the Buildex Division of the Illinois Tool Works, Inc. Advice and counsel was provided by Lyle Hovland of ALCOA, Clifford Mellor and Erle Stoddard of Agway, and John Patterson and Craig Hindman of Buildex. Participating graduate students included Charles Warshaw, John Hart, and Anthony Tocci.

8. REFERENCES

1. WARSHAW, C., Performance of Aluminum Diaphragms, M.S. Thesis, Cornell University, January 1979.
2. WHITE, R.N. and TOCCI, A., "Diaphragm Action in Aluminum-Clad Timber Framing Systems," Department of Structural Engineering Report No. 78-3, Cornell University, Ithaca, N.Y., June 1978.
3. WHITE, R.N., WARSHAW, C., and HART, J., "Shear Strength and Stiffness of Aluminum Diaphragms in Timber-Framed Buildings," Department of Structural Engineering Report No. 370, Cornell University, Ithaca, N.Y., June 1977.
4. Design of Light Gage Steel Diaphragms, American Iron and Steel Institute, 1967.

Tests on Full-Scale Cold Formed Steel Roofing Systems

Essais en vraie grandeur de systèmes de toiture en acier formé à froid

Versuche an kaltverformten Stahldachbelagssystemen

David MOORE
Senior Scientific Officer
Building Research Establishment
Garston, Watford, UK

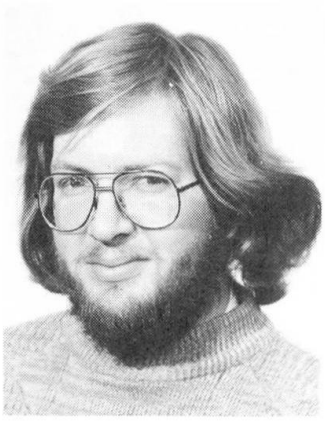

David Moore, born 1956, obtained his civil engineering degree at the Univ. of Bradford and joined the Building Research Establishment in 1981. He is engaged in steelwork research and is currently investigating the stability of thin-walled members and the behaviour of beam-column connections.

Paul SIMS
Senior Scientific Officer
Building Research Establishment
Garston, Watford, UK

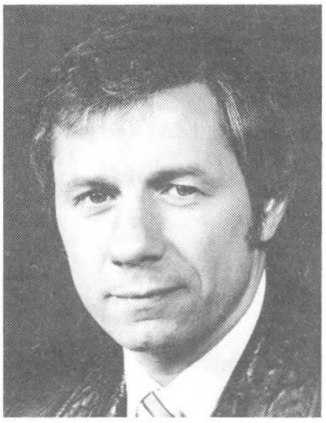

Paul Sims, born 1948, obtained his degree in mathematics at Queen Mary College London and joined the Building Research Establishment in 1974. He is head of a research team investigating the stability of thin-walled members and the behaviour of beam-column connections.

SUMMARY

An experimental investigation was undertaken on three representative British cold formed steel roofing systems to assess the effect of drifting snow. Details of this investigation are presented here. Comparisons are made between variably distributed loading and equivalent uniformly distributed loading. Differences in response are identified and the implication for design discussed.

RÉSUMÉ

Une étude expérimentale a été effectuée sur trois systèmes de toiture d'acier formés à froid, typiques de ceux fabriqués au Royaume-Uni, afin d'évaluer les effets d'un amoncellement de neige. Des détails de ce programme sont présentés ainsi que des comparaisons entre les charges réparties variables, simulant un amoncellement de neige, et les charges équivalentes uniformément réparties. Une discussion s'ensuit, concernant l'écart entre les résultats obtenus et leurs conséquences pour la conception de telles structures.

ZUSAMMENFASSUNG

Vollmassstäbliche Versuche wurden an drei typischen kaltverformten Stahldachbelagssystemen, wie sie in Grossbritannien hergestellt werden, durchgeführt, um die Auswirkungen von Schneeablagerungen zu beurteilen. Das Versuchsprogramm wird ausführlich beschrieben. Beliebig verteilte Lasten sind mit gleichmässig verteilten Belastungen verglichen worden. Unterschiede zwischen den Ergebnissen werden festgestellt und ihre Bedeutung in Bezug auf die Konstruktion diskutiert.

1. INTRODUCTION

During the winter of 1981/1982 heavy falls of snow accompanied by strong winds resulted in damage to a number of light-gauge steel roofs within the United Kingdom(U.K). A review of these failures indicated that in many cases the snow load on some parts of the roof, particularly those areas close to parapets, was considerably higher and of a different distribution than is currently specified in the British Standard code of practice for loading[1]. This review also indicated that although the failures were principally due to excessive snow load, the stability of light-gauge steel roofs was questionable under the loading distributions observed.

Consequently the Building Research Establishment(BRE) in collaboration with the Cold Rolled Sections Association(CRSA) started a programme of research to investigate the performance of light-gauge steel roofing systems. Although there are many different systems available the double span sleeve system with any one of the zed, zeta and sigma purlins is commonly used within the U.K. Trapezoidal profiled sheeting and a 10° roof pitch are also commonly used with these systems. The test roofs incorporated all these features.

A general layout of the roofs tested is shown in Figure 1. For each of three roof systems tested the purlins and sheeting were selected using the manufacturer's safe load tables. The size of the purlin and sheeting chosen for each system and their corresponding working and design loads are given in Table 1.

SECTION TYPE	SIZE (D*B*T)	WORKING LOAD(kN/m^2)	DESIGN LOAD(kN/m^2)
SIGMA	140*70*1.6	1.40	2.38
ZETA	125*60*1.6	1.02	1.73
ZED	140*50*1.6	1.16	1.97
SHEETING	A1000[2]	3.28	5.58

TABLE 1 Dimensions and loading for each roof

This paper briefly describes the tests carried out on part of these three typical cold formed steel roofing systems. A more detailed description is contained in reference [3]. The test programme included loading each roof with uniformly and variably distributed loads. The performance of each roof under the different load distributions is compared and recommendations for their design subject to variably distributed loading, proposed.

2. LOADING AND INSTRUMENTATION

Dead weight applied at forty-eight independent points was used to load each roof. With this scheme it is possible to simulate uniformly and variably distributed loads, varying in either the longitudinal or the transverse directions. The load was applied in available combinations of

weights(5.5kg, 9.5kg, 19kg and 45.5kg) to each hanger and transferred to the sheeting by a 380*380*25mm thick plywood spreader board.

The translations and rotations of each purlin were measured at mid-span; the former in both parallel and perpendicular directions to the roof slope. Transducers capable of measuring displacements upto 100mm with an accuracy of 0.01mm were used to record the translations. To prevent the transducers being damaged, they were positioned away from the purlin and the movements of the purlin transferred to them via a steel bar rigidly connected to the purlin. Contact between the transducers and steel bar over the full range of displacements was maintained by fitting an aluminium bar bent at right angles to each transducer. Details of this arrangement are shown in Figure 2. Accelerometers, rigidly mounted on the web of each purlin, were used to detect rotation. These instruments can measure angles upto 90deg with an accuracy of 0.01deg. For some tests the movements of the purlin supporting cleats were monitored using dial gauges.

The readings from each transducer and accelerometer were recorded by a data logging system and stored on magnetic tape. The logger was also programmed to display the readings of particular interest so the performance of the roof could be monitored as the test proceeded.

3. TEST PROGRAMME

Traditionally manufacturer's safe load tables are used to select cold formed steel roofing systems and in most cases these are based on either test data or the simplified design rules given in BS 449 Addendum No.1[4]. Both these methods assume the load is uniformly distributed over the roof. In practice, however, snow can build-up behind parapets and in valleys, loading roofs with variably distributed loads. It is therefore pertinent to investigate the performance of traditionally designed systems when subject to these loading conditions. Using BRE Digest 290[5] as a guide the following practical loading distributions were identified:

a) Uniformly distributed load(u.d.l) over the complete structure.

b) Transverse variably distributed load(v.d.l) over the complete structure.

c) Uniformly distributed load(u.d.l) over the end-bay only.

d) Longitudinal variably distributed load(v.d.l) over the end-bay only.

Load case (b) simulates the build-up of snow either behind a parapet at the eaves or in the valley between multi-bay pitched roofs, while (d) simulates the build-up of snow behind a gable end parapet. The uniformly distributed loads (a) and (c) are included as a standard against which the performance of the roof subject to loads (b) and (d) can be compared.

The test programme consisted of working load tests, design load tests, long-term tests and a test to failure. Only the following two phases are discussed here;

the remainder are detailed in reference [3].

phase 1:- working load tests

At this stage it was considered essential to keep the loads within the working load of the roof so that any comparison between distributions would not include the non-linearities resulting from yielding or buckling of the structure.

The four loading cases identified above were applied to each roof and in each case the load was incremented until working load (as defined by the manufacturer's safe load tables) was attained. After each load increment the displacements and rotations of each purlin were recorded.

phase 2:- design load tests

The purpose of these tests was to determine the strength of each roofing system under different loading distributions and identify the most critical loading distribution.

For the zed and zeta systems loading cases (a),(c) and (d) were applied to the roof and in each case the load was incremented until design load was attained.

4. DISCUSSION OF RESULTS

4.1 Working load tests

4.1.1 Comparison of u.d.l with transverse v.d.l.

Figure 3 shows typical load-displacement characteristics for the sigma, zed and zeta roofing systems respectively subject to load cases (a) and (b). Also shown in Figure 3 is the purlin identification nomenclature. The response is seen to vary in an approximately linear fashion upto working load indicating that for both load cases the behaviour of each roof was completely elastic. As expected for each roof the displacements of purlins a-d and i-l for load case (a) are similar while for load case (b) those of purlin a-d are approximately one quarter those of purlin i-l. Furthermore for both load cases the maximum displacements occur in purlin g-h and are of similar magnitude. From this observation it is tentatively suggested that a reasonable estimation of the maximum displacement at working load for a transverse variably distributed load can be obtained by considering the roof to be loaded with an equivalent uniformly distributed load.

4.1.2 Comparison of u.d.l. with longitudinal v.d.l.

Figure 4 shows the load displacement characteristics for the sigma, zed and zeta roofing systems respectively for load cases (c) and (d). Once again all the

displacements are seen to vary in a linear manner upto working load; moreover, the magnitude and distribution of these displacements are similar for both load cases. Again this suggests that a reasonable estimate for both the size and distribution of displacement for load case (d) can be obtained be replacing the longitudinal v.d.l. with the same total load distributed uniformly. In making this recommendation, it is appreciated that the transducers were not positioned at the point of maximum displacement for load case (d). However, the difference between the true maximum and the measured maximum is small and will not invalidate this recommendation.

4.2 Design load tests

4.2.1 Comparison of u.d.l with transverse v.d.l.

The load-displacement characteristics from working load to design load (1.7*working load) for each roof are shown in Figure 3. Just after working load has been applied curling of the compression flange at an internal support occurred for both the zed and zeta roof systems. On increasing the load both structures exhibited pseudo-plastic behaviour but continued to carry the load in a stable manner.

4.2.2 Comparison of u.d.l. with longitudinal v.d.l.

Figure 4 shows the load displacement characteristics for each roof up to design load. After working load these displacements continue to demonstrate linear behaviour indicating that the behaviour of each roof is completely elastic up to full design load. Again there is little difference between the displacements for either load case. These observations reinforce the supposition that there is little difference between the performance of each roof subject to load case (c) and (d). Furthermore, under these load conditions no local buckling or distress of any roof was observed. Thus it is concluded that the strength of each roof should be derived from the performance of each roof under either load case (a) or (b). However, load cases (c) and (d) give the largest deflections at working load , so if the deflections at serviceability are important they should be determined using these load cases.

4.3 Comparison with continuous beam theory

Figures 3 and 4 also show the theoretical displacements of the centre purlin These were calculated using continuous beam theory with the following three assumptions:

(a) The load on the centre purlin can be determined from the method described in reference [6].
(b) The sleeved connection are continuous and have the same flexural rigidity as the purlin.
(c) Each purlin bends about an axis parallel to the roof slope.

From the figures it is evident that the theory gives different degrees of

accuracy for the different roofing systems; overestimating the displacements of the sigma system, accurately predicting those of the zed system and underestimating those of the zeta system. This probably results from assumption (b). Assuming continuous connections both increases the load and reduces the deflections of the centre purlin, while assuming the sleeve to have the same flexural rigidity as the purlin, results in an overestimation of deflection. Without detailed knowledge of the behaviour of sleeved connections it is difficult to quantify the effect of these assumptions. However, it is speculated that the difference between experiment and theory for the sigma system is due mainly to the underestimation of the connection's flexural rigidity. This view is supported by observing that the sleeve for this system penetrates further into the span than the sleeves for the other systems thus having a more pronounced effect on the displacements at mid-span. The performance of these connections is currently being investigated at the Building Research Establishment.

5. CONCLUSIONS AND RECOMMENDATIONS

Loading tests have been carried out on three full-scale cold-formed steel roofing systems. Each roof was clad with trapezoidal profile sheet and had a 10° pitch. The test programme included the application of both uniformly and variably distributed loads up to working load and design load. The v.d.l's were representative of drifting snow on roofs. The conclusions and recommendations are summarised as follows:

(a) For the determination of the maximum displacement normal to the roof a variably distributed load can be replaced by an equivalent uniformly distributed load.

(b) A longitudinal v.d.l should be used to determine the displacements at serviceability while a transverse v.d.l should be used to determine strength.

(c) The performance of sleeved connections need to be established if a more accurate theoretical model is to be made.

ACKNOWLEDGEMENTS

The tests were carried out as part of the research programme of the Building Research Establishment and this paper is published by permission of the Director. The authors would like to thank all their colleagues who provided assistance during the tests. Thanks are also extended to the Cold Rolled Sections Association and Buildex Ltd. for their support and advice.

REFERENCES

1. Design loading for buildings BS6399:Part 1, Code of practice for dead and imposed loads,1984, British Standards Institution.

2. Wards Building Components.,The Moduclad Handbook Components, Ward Building Components,Sherburn North Yorks, U.K. 1985.

3. D.B.MOORE and P.A.C.SIMS.,Full-scale tests on light-gauge steel roofs. Series of B.R.E. reports.In press.

4. Specification for the use of cold formed steel sections in building, Addendum No.1 to BS449: part 2,British Standards Institution, 1969

5. Loads on roofs from snow drifting against vertical obstructions and in valleys, BRE Digest 290,Building Research Establishment,1984.

6. J.RHODES,W.KING,J.M.HARVEY and K.JAMES.,Tests on a continuous purlin roofing system. Recent research and developments in cold-formed steel structures,vol.1,pp253-282,June 1978.

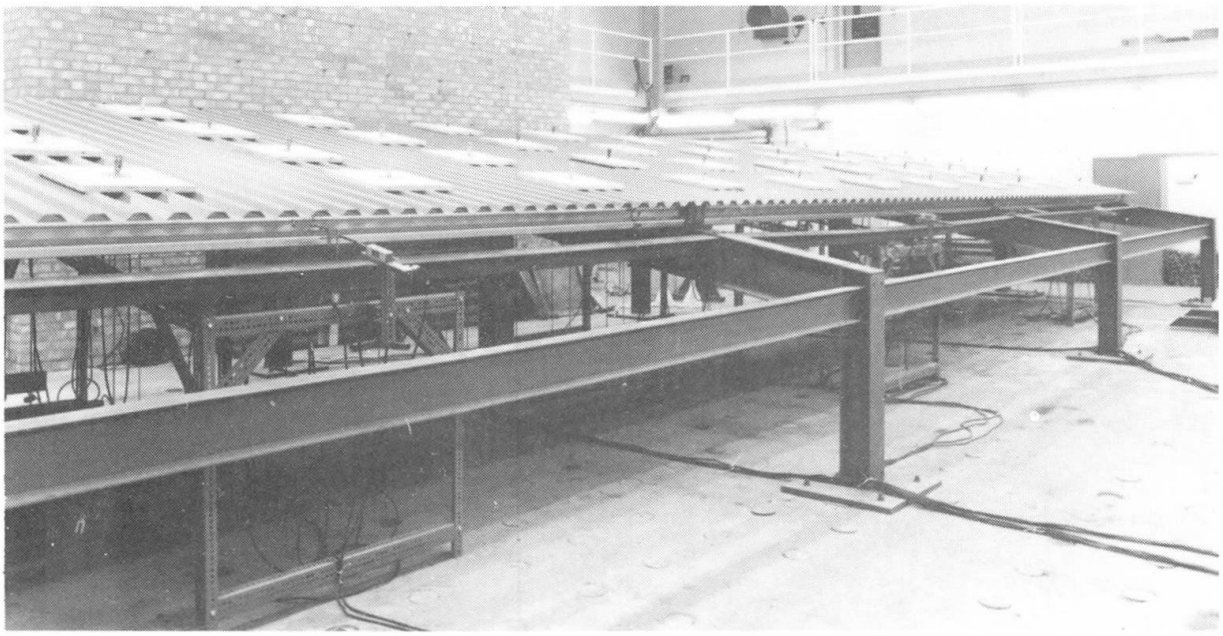

Fig. 1 General view of test roof

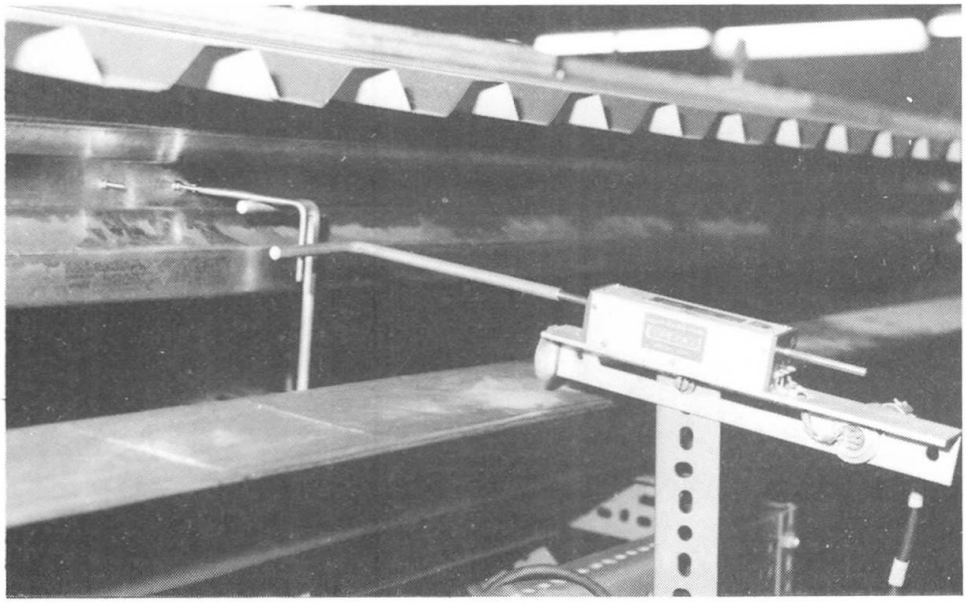

Fig. 2 Measurements of purlin displacements

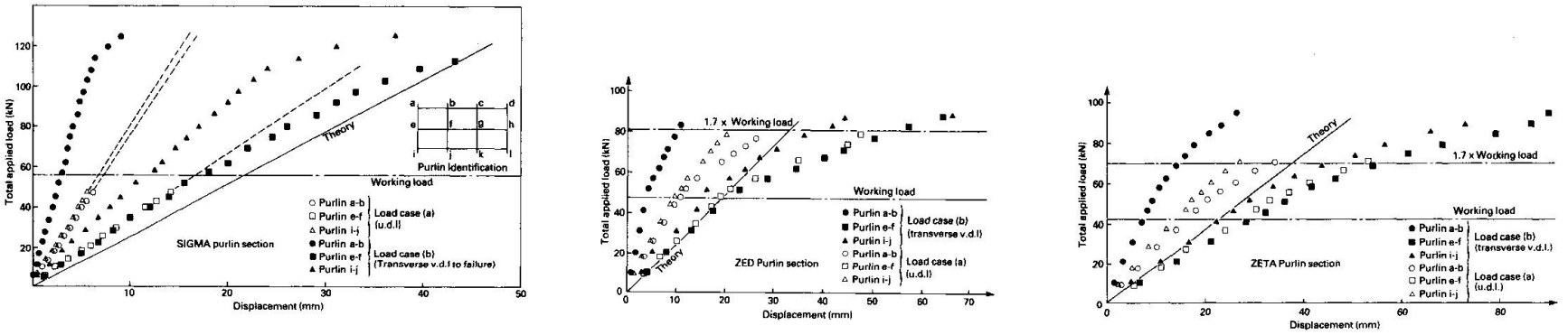

Fig. 3 Load displacements for u.d.l and transverse v.d.l

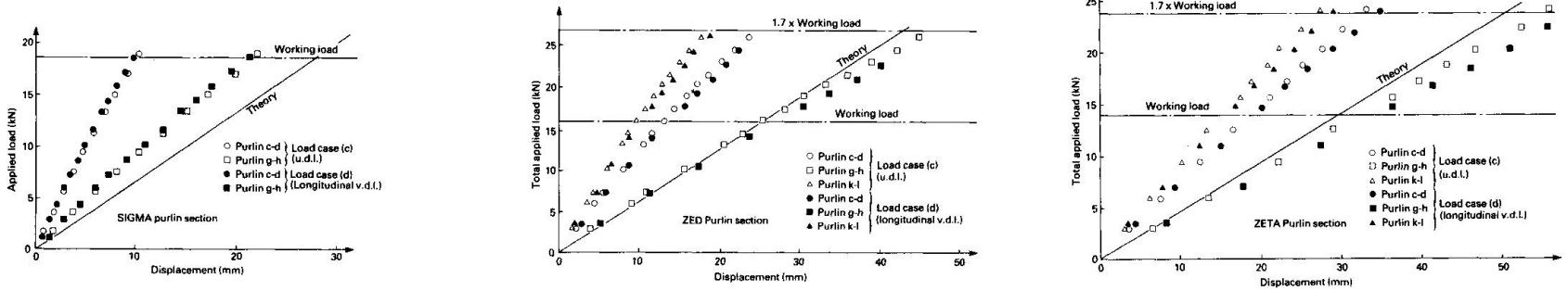

Fig. 4 Load displacements for u.d.l and longitudinal v.d.l

Half-Barrel Shells Composed of Cold-Formed Profiles

Coques hémicylindriques réalisées à l'aide de profilés minces formés à froid

Halbzylindrische Schalen aus dünnen kaltgeformten Profilen

Fausto BENUSSI
Assoc. Professor
University of Trieste
Trieste, Italy

Fausto Benussi, born 1951, received his civil engineering degree at the University of Trieste, Italy. Author of papers on stability of steel structures and tensile structures, he is now Associate Professor of Steel Construction in the Faculty of Engineering at the University of Trieste.

Antonio MAURO
Full Professor
University of Trieste
Trieste, Italy

Antonio Mauro, born 1938, received his civil engineering degree at the University of Bari, Italy. Author of papers on thin shells and tensile structures, he is presently full professor of Strength of Materials at the Faculty of Engineering, University of Trieste.

SUMMARY

This paper reports the first stage of a research programme on static problems of half-barrel shells of cold formed thin profiles. The construction system consists of panels jointed together with a self-propelled sealing machine. The numerical and experimental study of the instability of the compressed «wings» of stiffening ribs is discussed.

RÉSUMÉ

Cette contribution concerne la première phase d'une recherche consacrée aux problèmes statiques posés par les coques hémicylindriques en profilés minces. Le système de construction consiste en des panneaux assemblés entre eux par sertissage à l'aide d'une machine automotrice. L'étude numérique et expérimentale de l'instabilité des ailes comprimées des raidisseurs y est présentée.

ZUSAMMENFASSUNG

Der Aufsatz berichtet über die erste Phase einer Forschungsarbeit betreffend statische Probleme von halbzylindrischen Schalen aus dünnen kaltgeformten Profilen. Das konstruktive System ist aus Blechen zusammengesetzt, die mittels einer selbstfahrenden Falzmaschine verbunden werden. Ein numerisches und experimentelles Studium der Instabilität von gedrückten Flanschen mit Versteifungsrippen wird präsentiert.

1. INTRODUCTION

Over the past several years, thanks to technological developments in industrial processes, cold formed steel sections have increasingly been employed in buildings as a material for integral solutions, and not only as an accessory material to be used for simple coating or cladding. One field of remarkable interest for the application of cold formed profiles is that of self-supporting cover structures for industrial buildings even of considerable span such as are employed, e.g. for industrial or agricultural storage, military hangars and temporary shelters. In these applications, the simplest and most widespread type is the half-barrel shell made of galvanized and prevarnished corrugated steel sheets (Fig. 1a).

The applications in building date back to the turn of the century (first patent 1896 in the USA) and have been extensively developed especially in America. The most currently used system is based on strips of arch-curved, transversally corrugated sheet, with wave depth depending on the different static requirements (Fig. 1b,c); the transverse connection is usually accomplished by bolts, screws or rivets.

In the system considered in the present work the arched panels are connected transversely by a self propelled machine which folds and seals the edges of the panels in a continuous way along the whole length of the arch (Fig. 2a,b).

The result is a semi-cylindrical shell with almost smooth internal surface and regularly spaced transverse external ribs, which consist of a web composed of two adjoining sheets and a folded and sealed wing three times thicker than the component sheet (Figs. 2b and 3). In effect, the need to slightly corrugate the webs of the ribs in the panel curving operation causes the two sheets of the web to be slightly divergent (Fig. 2c).

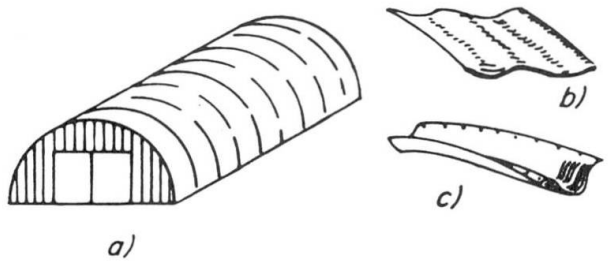

Fig. 1

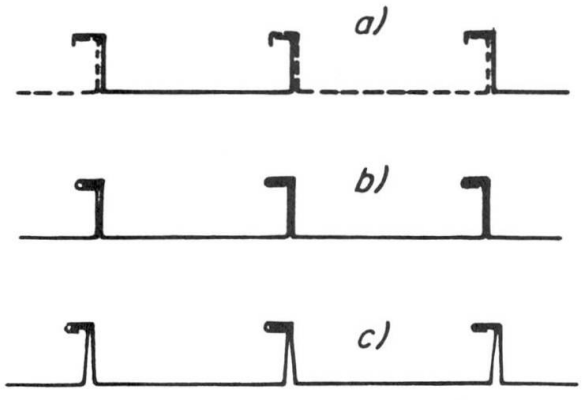

Fig. 2

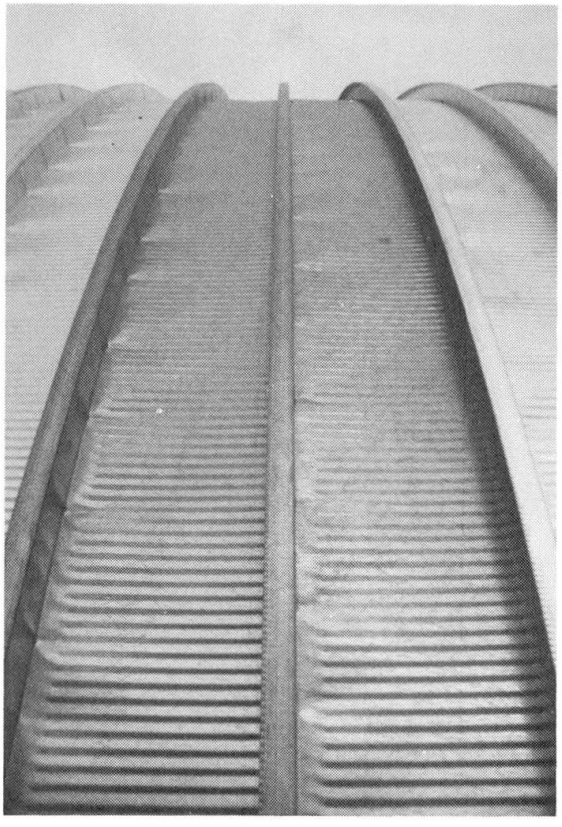

Fig. 3

The building system described above requires fairly short assembling times and, as the drilling of the sheets is avoided, ensures a perfectly watertight cover. With sheets less than 1mm thick and stiffener dimensions of the same order as those indicated in Fig. 5, arches with span of about 15-20 m can be obtained. The present paper reports on the early stages of a research aimed at ascertaining the effective strength of the structure under the usual snow and wind loads and defining with accuracy the maximum spans compatible with the geometry and thickness used.

2. STRUCTURAL ANALYSIS AND OUTLINE OF THE RESEARCH

The analysis of a semicylindrical structure of the type indicated in the preceding section should be performed by theoretical models which take into account the orthotropic behaviour of the shell [1,2,3,4]. The distribution of the loads is generally uniform along the longitudinal direction, and the ratio of length to span of the sheds is often very high, so that in the central zones the disturbance due to end diaphragms - if present - can be considered negligible; it seems therefore sufficiently correct - at least in an early stage of the analysis - to calculate the individual unit module transverse arches as if they were extracted from an infinite series of adjoining modules. In the specific case studied, this simplification appears even more justified in view of the high ratio of transverse to longitudinal stiffness of the sheet.
The distribution of variable loads, determined according to the usual assumptions of the most updated Codes, leads to load distributions such as are illustrated in Figure 4. With reference to the static scheme of the clamped arch, Figure 4 presents the bending moment diagram due to snow and wind loading.
The bending moment, which is associated with axial actions along the length of the arch, is the most important characteristic for the dimensioning of the structure. However, since the structural scheme is hyperstatic, the bending moment is - though to a small extent - a function of the tensional level, which in turn affects the width of the sheet area effective with the stiffener and, hence, the moment of inertia of the section.
The small thicknesses involved make it necessary that the complex stability problems on which the strength of the structure is dependent be analyzed with the utmost accuracy.
A first general problem is to determine the collapse due to the overall buckling of the compressed and bent arch and to check that this phenomenon is not too strongly affected by the progressive and high local deformations.
A second problem is to verify the zones of the arch subjected to the bending moment which compresses the internal fibres, i.e. the flat part of the sheet between the ribs. This is one of the classic issues in the analysis of cold formed profiles with extensive flat zones in their sections; it has been the object of vast theoretical and experimental investigations and has by now been defined and incorporated in the Codes of several countries. The usual approaches to the analysis of the behaviour of the compressed parts adjacent to stiffenings aim at the definition of"an effective width" or a "stress reduction factor" [5,6].

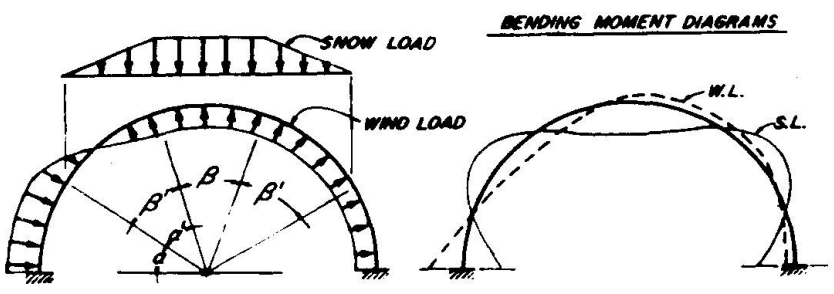

Fig. 4

The research under way will include experimental flexural tests to check the validity of these approaches and evaluate the influence of the slight transverse corrugations originated in the flat parts of the panels as a result of the curving operation.

The main problem tackled in the first stage of the research is the instabilization of the stiffener in those zones where the sign of the bending moment is such that the external fibres become compressed [7]. The study of this problem is similar to that of the behaviour of purlins for which the section (at I,Z,C) can no longer rotate torsionally in a free way because of the continuous connection between the upper flange and the roof sheet [8,9,10]. In the case under study, the problem is further complicated by the presence of the axial action associated with bending action (both of them being variable) and by the curvature of the structural elements.
The main purpose of the first stage of this research is to develop a numerical model based on the use of shell-type finite elements, in a geometrically non-linear field. The reliability of the model is verified through a series of tests on models of different span subjected to different distributions of the bending action. A numerical model taking into account also the hypothesis of non-linearity of the material seemed unnecessary because of the extremely limited capability of plastic redistribution in the structure. To facilitate the development of the above mentioned numerical approach, the first experiments were carried out on models with rectilinear axis obtained by using the panels before the curving operation.

3. EXPERIMENTAL ANALYSIS

The sheets used for the tests were 0.75 mm thick, without considering galvanizing and prevarnishing. The yielding stress, ultimate tensile stress and strain at fracture of the material were 305 N/mm^2, 370 N/mm^2 and 21%, respectively. Prior to the tests, the effectiveness of the transverse sealing of the sheet modules was verified: slip occured at a force about 1.05 kN per length of 100 mm.

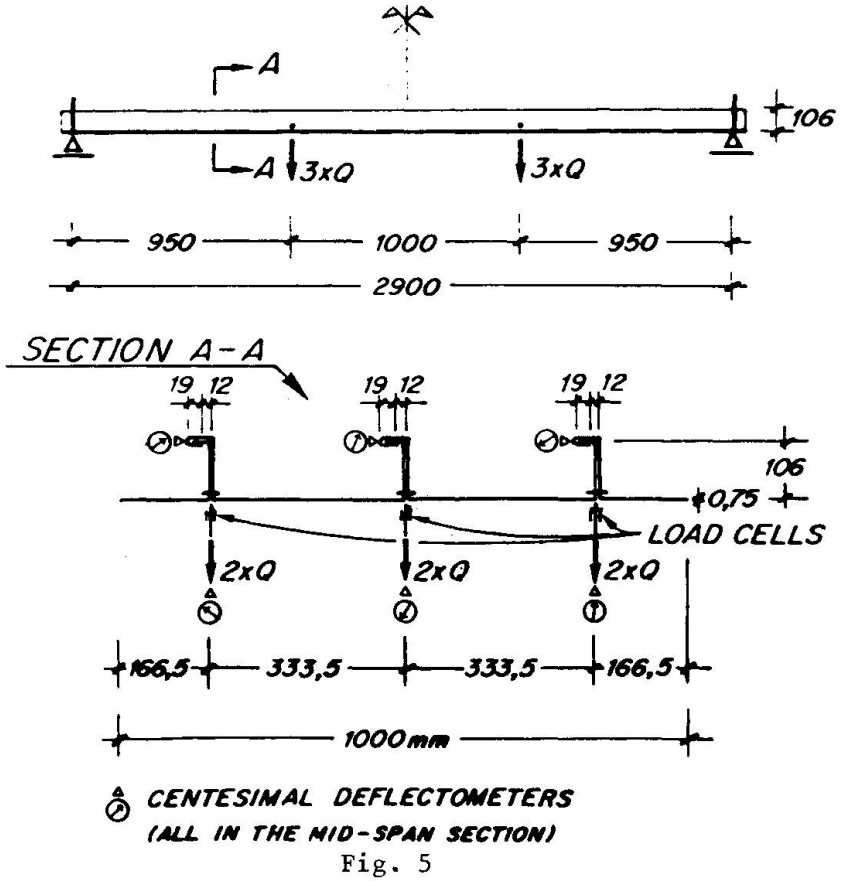

Fig. 5

The first models tested, were simply supported and consisted of three sheet modules, connected transversely but without edge supports, suitable to ensure the real structural continuity (Fig.5). In this way the tests were easier to perform, but the response was obviously characterized by more pronounced deflections (Fig. 6b), different than would have occured in an indefinite succession of modules (Fig. 6a). The ultimate load was, of course, much less than the value corresponding to the real situation.
In the tests, with deformation control, the load was applied progressively by means of pins, placed at the base of the webs, in

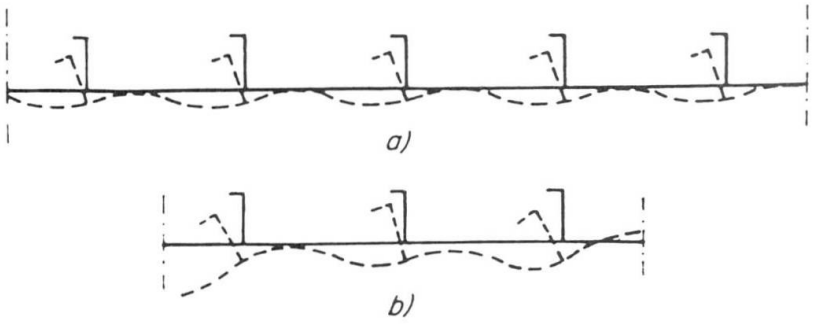

Fig. 6

two sections near the thirds of the span, and was nearly the same for the three stiffeners. The loading device was obtained through a particular system of pulleys, suitable to subdivide the total load into six equal parts. Load cells were located at each of the six points where the loads were applied. A series of centesimal deflectometers (Fig. 5) and of electrical strain gauges (Fig. 7) were placed in the midspan section.
Failure occured under a total load of 9.5 kN; yielding occured at the web-wing bend of one of the lateral stiffeners (Fig. 8) where the compression stresses due to both vertical and horizontal deflections add together.
The lateral deflection is much more marked in the lateral stiffeners, since the torsional rotation of the webs is strongly affected by the rotational stiffness of the tensile flange, which in the model is considerably lower at the edges.
The tests performed so far have confirmed the repeatibility of the phenomenon and the good accuracy of the theoretical model adopted to define the main features of the response of the structure.
The behaviour of the system is characterized by a sufficiently moderate and gradual geometric non-linearity, so that it can be easily followed through a non-linear numerical model based on the usual solving procedures which combine incremental methods with iterative techniques.

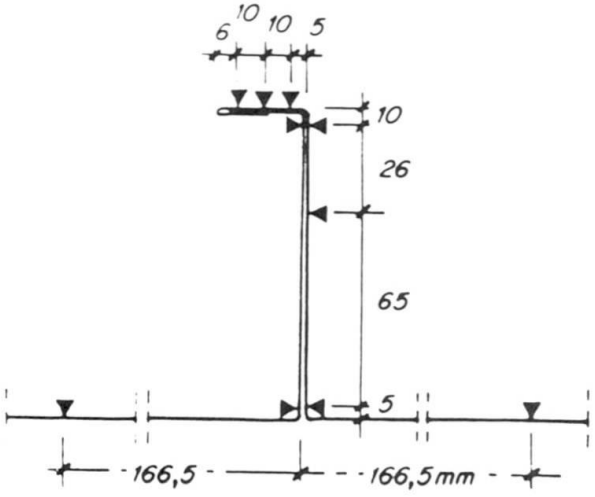

Fig. 7

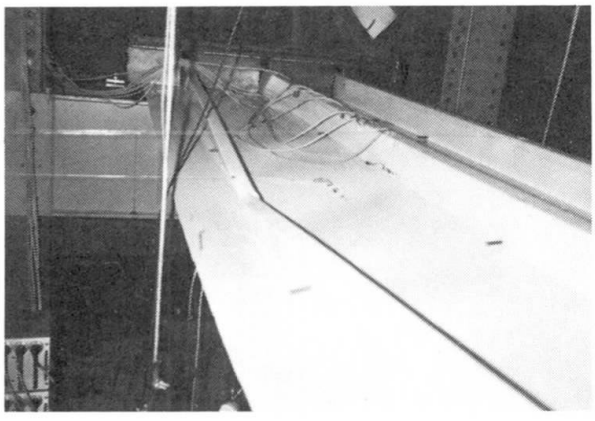

Fig. 8

REFERENCES

1. ABDEL-SAYED G., Critical Shear Loading of Curved Panels of Corrugated Sheets, Journal of Engineering Mechanics Division, ASCE, EM 6, December 1970.

2. ABDEL-SAYED G., EL-ATROUZY M.N., Cylindrical Shells Made of Corrugated Sheets, IABSE Congress Report, Amsterdam, 1972.

3. MARZOUK O.A., ABDEL-SAYED G., Linear Theory of Orthotropic Cylindrical Shells, Journal of the Structural Division, ASCE, ST 11, November 1973.

4. MARZOUK O.A., ABDEL-SAYED G., Stability of Half-Barrel Orthotropic Shells, Journal of Structural Division, ASCE, ST 7, July 1975.

5. RHODES I., Effective Widths in Plate Buckling, Developments in Thin-Walled Structures -1, Ed. I. Rhodes and A.C. Walker, Applied Science Publishers,1982.

6. RHODES I., Some Thoughts on Future Cold Formed Steel Design Rules. Behaviour of Thin-Walled Structures, Ed. I. Rhodes and I. Spence, Elsevier Applied Science Publishers, 1984.

7. YU W., Cold-Formed Steel Structures, McGraw-Hill, 1973, pgg. 152-166.

8. PEKOZ T., Diaphragm-Braced Thin Walled Channel and Z-Section Beams. Beams and Beam Columns, Stability and Strength, Ed. R. Narayanan, Applied Science Publishers, 1983.

9. TRAHAIR N.S., NETHERCOT D.A., Bracing Requirements in Thin-Walled Structures, Deevelopments in Thin-Walled Structures -2, Ed. I. Rhodes and A.C. Walker,Applied Science Publishers, 1984.

10. INGS N.L., TRAHAIR N.S., Lateral Buckling of Restrained Roof Purlins, Thin--Walled Structures, N.4, 1984.

Use of Cold-Formed Steel in the Building Industry of China

Application de l'acier formé à froid dans l'industrie chinoise de la construction

Anwendung des kaltgeformten Stahls im Baugewerbe in China

Zhong-Quan ZHANG
Structural Engineer
Hubei Ind. Building Design Inst.
Wuchang, Hubei, China

Zhong-Quan Zhang, born 1942, graduated from the Departement of Mechanics, Tongzhi Univ. in 1964. He is one of the chief editors of the 1975 and subsequent editions of the specification «Design of Cold – Formed Steel Structures» in China.

SUMMARY

This paper mainly describes the use of cold-formed steel in the building industry of China with some engineering examples. A brief review is presented of the state-of-the-art in design specification and the current situation.

RÉSUMÉ

Cet article donne une vue générale concernant l'application de l'acier formé à froid dans l'industrie chinoise de la construction illustrée par quelques exemples. Un bref survol de l'état des connaissances et du développement des règles de construction ainsi que des recherches en cours est présenté.

ZUSAMMENFASSUNG

Der Bericht behandelt vorwiegend die allgemeine Anwendung des kaltgeformten Stahls im Baugewerbe der Volksrepublik China. Als Beispiele werden einige Bauwerke vorgestellt. Die Entwicklung in Bezug auf Normierung und die Forschungsarbeit in diesem Bereich werden kurz erläutert.

In the People's Republic of China, cold-formed steel products were for the first time produced in the mid 1950's. Cold-formed steel structural members have begun to be widely used in the building industry only since the last two decades. Since the mid 1960's, a series of cold-formed steel constructions have been successively built up throughout our country such as Shanghai, Beijing and Guangdong, Shanxi, Hubei provinces, etc. According to incomplete statistics, the construction area of civil and industrial buildings using cold -formed steel have far exceeded 1,000,000m^2.

1. MATERIALS

In China, Cold-formed sections are shaped from low cabon or high strength low-alloy steel sheets, strips or plates. The following steel have been used as their virgin materials: A3, 16Mn, 15MnV, 15MnVNi, 09PV, 10PCuRe and 12MnPV, etc. among which the most poular ones are A3 and 16Mn, their yield strength being 240MPa and 35MPa, and their ratio of specified ultimate tension strength to yield strength being about 1.58 and 1.48 respectively.

2. SHAPES

Usually, cold-formed steel sections used in the building industry can be divided into two categories: framing members and surface members.

2.1 Framing members

The depth of such sections ranges from a few centimeters up to 30cm or more. Their thickness varies from 2 to 6mm. Among these shapes, the most popular ones are square or rectangular tubes, cold-rolled circular tubes, channel sections, hat sections, C - sections, Z- sections, angle sections and some other built-up sections (as shown in Fig. 1).

2.2 Surface members

The depth of profiled steelsheetings ranges generally from 12 to 173mm, their thickness varies from 0.5 to 1.6mm, their ribs space at 90 to 230mm.

The typical sheetings are shown in Fig. 2.

Fig. 1 framing member

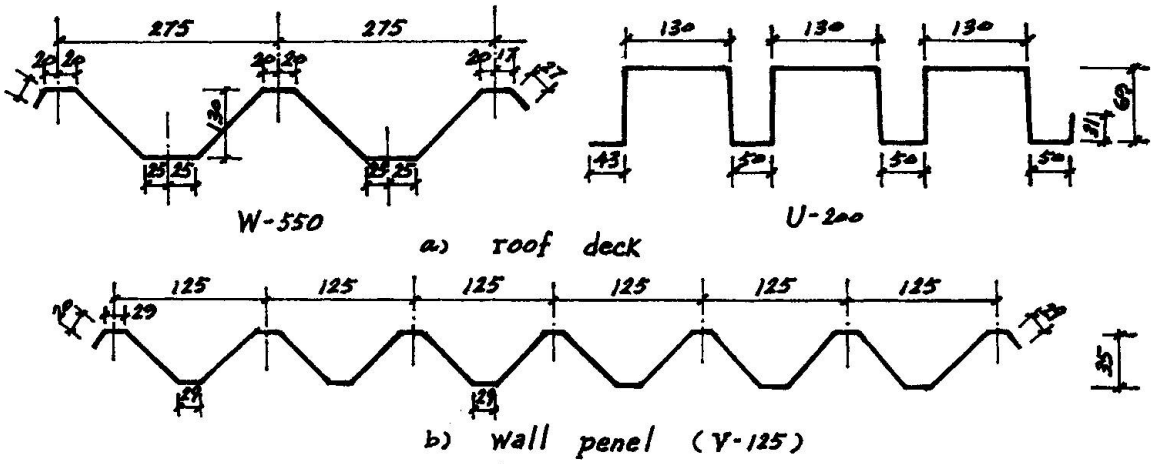

Fig. 2 surface member

3. APPLICATION AND EXAMPLES

In the building constructions of our country, cold-formed steel sections are mainly used as gable frames, space grids, trusses, columns ,beams, purlins, studs, wall girders, skylight frames, keels, vessels and railings, window frames, bridgings, bracings, etc. The profiled steel sheetings are generally used as roof decks, wall panels and cellular panels. In recent years, various pre-engineered one-story or two-story buildings, hothouses, Mongolia tents and high-rise rack structures, etc., which are made of cold-formed sections, have been designed and built. The importance of these sections is growing with days to come.

The portal frames made of cold-formed sections are now in common use, their forms are different from each other, including columns and/or beams or lattice members, of which the cross sections are variable or uniform, connected by either welding or bolt or high strength bolt, subjected to dead load only or to dynamic load on the columns or beams in addition. The spans of frames are from about 8 to 30m, for examples, the lattice gable frames with 29m span were made of cold-rolled circular tubes and built at Shanghai Exhibition Hall in 1967, and the gable frames with 18m span were made of Γ- sections and built at Shaoguan Plastic Factory in 1966.

Among the various cold-formed section structures, the most popular ones are the roof structures (including roof trusses, purlins, skylight frames, bracigs or space grids and framed domes, etc.) which are used in civil buildings (such as halls and exhibition center, etc.) and workhouses or warehouses, they are also used not only in light workhouses without cranes, but also in heavy workhouses with bridge cranes of lifting capacity up to 125 tons and " flexible workshops " of large column spacing with hanging-crane facilities. Usually the range of purlin span is 4 to 6m or 12m, including solid ($\sqsubset$ - sections and $\llcorner$ - sections), open web and lattice purlins. The roof truss span varies from 9 to 30m, including triangular, trapezoidal, shuttle and parallel chord trusses. They are made of closed square or rectangular tubes or cold-rolled circular tubes and also of full open sections, such as the trapezoidal roof trusses, with 30m span, were made of cold-formed square tubes and built at Baotou Iron and Steel Plant in 1968; the triangular roof trusses, made of square tubes and installed with hanging-crane facitities of lifting capacity equal to 2.5 tons at any bottom chord joint (see Fig. 3) were used with spans of 12 and 15m in The Second Automobile Works P.R.C. at Shiyie in early 1970's.

The space grids, made of cold-rolled circular tubes or other sections with welding balls or screwed cast balls,began to be widely used both in civil (such as halls and gymnasiums, etc.) and industrial buildings in the last two decades. Among these structures, the most popular ones are planar grids (consisted of an intersecting system of lattice beams or trusses) and space trusses (consisted of pyramids). Up to now, the completed space grids have amounted to several tens. Among those, there are some examples as following: a planar grid consisted of an inclined intersecting system of lattice beams (40m long $\times$ 40m wide) made of cold-rolled circular tubes was built at Beijing International Club in the mid 1970's; an inclined pyramid grid (35m long $\times$ 35m wide), also made of circular tubes with welding balls, was built at Shanghai Gymnasium for Practice in 1966.

Since the mid 1970's, the high-rise rack structures, made of cold-formed sections, have been built and mainly used in warehouses or libraries such as a high-rise rack structure (6.3m wide $\times$ 50.7m long $\times$ 15m high), made of square tubes and other sections and connected with high strength bolts(see Fig. 4), was built at Beijing Automobile Manufactory in 1977, and so on.

In recent years, the use of profiled steel sheetings has been increasing gradually in building constructions. According to incompleted statistics, the buildings using these materials as roof decks and wall panels have far exceeded 1,000,000m^2 up to now, among these 'are Shanghai Baoshan Iron and Steel General Plant, Shanxi Shentou Power Station, Shenzhen Dock Warehouse and Guangzhou Container Plant , etc.

Fig. 3 roof trusses with hanging-crane

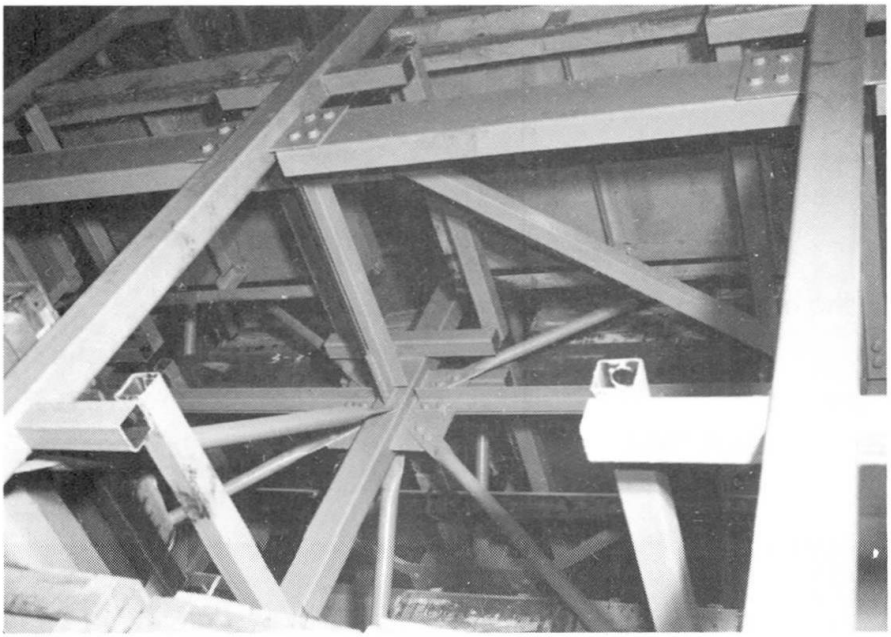

Fig. 4 rack structure

4. ECONOMICAL ANALYSIS

According to incompleted statistics ,the steel consumption (per unit area) of several popular types of cold-formed steel structures (members) is shown as follows:

-Roof systems made of cold-formed sections (including roof trusses, purlins , skylight frames and bracing members only):
with span ≤ 18m and roof load ≤ 10KN/m²: about 12kg/m²;

-Planar grid (consisted of an inclined intersecting system of lattice beams) made of cold-rolled circular tubes of 16Mn steel with 40m long × 40m wide: about 25kg/m²;

-Purlins:
lattice purlins: about 2-4kg/m²;
solid ℒ - shapes purlins: about 4-6kg/m²;

-Roof trusses with span ≤ 24m and roof load ≤ 15KN/m²:
about 2-5kg/m²;

-Gable frames with span ≤ 30m and roof load ≤ 6KN/m²,
wind load ≤ 10KN/m²: about 3-12kg/m²;

-Profiled steel sheetings (their thickness varies from 0.5 up 1.6mm): about 5-20kg/m².

5. DEVELOPMENTS IN SPECIFICATION

In China, the first edition of the Specification for the Design of Cold-Formed Steel Structures was published in 1969. Since then, based on the findings of research works and accumulated practical experiences, the Specification was revised and issued as a second edition in 1975. The new one is now in being compiled and is to be published next year.

In recent years, to improve the problems existing in analysis,structural design, antirust measures and developments of new technique, there have been fourteen research projects carried out since 1976. Some valuable achievments were gained and mostly adopted in the new edition of the Specification. In comparison with the existing Specification, the new edition has some different striking aspects as following:

-Limit state design method based on the probablistic approach (level 2) was introduced to take the place of the traditional allowable stress criteria;

-The provision permitting to take into account the possible beneficial effects of cold work is supplemented in the new Specification;

-The equations and relative coefficients to compute stability of the centrally loaded columns, beams and beam-columns are revised and adjusted;

-The computation method for considering the local buckling of flat compression elements is partly revised and adjusted;

-The provisions for dealing with the electric resistence spot welding, high-strength minor diameter bolt connections and design of profiled steel sheetings are added respectively in the new edition;

-The provisions concerning antirust are revised and replaced.

6. ACKNOWLEDGEMENTS

The auther wishes to express his thanks to his colleagues, Mr. Xu Zhong Yao and Chen Xue Ting, Ms. Li Hua and Zhu Wa Li, for their helps in accomplishing this paper.

Leere Seite
Blank page
Page vide